BEHAVIOUR OF PILES IN LIQUEFIABLE DEPOSITS DURING STRONG EARTHQUAKES

By

Hayden James Bowen

Supervised by

Dr Misko Cubrinovski

A thesis submitted in partial fulfilment of the requirements for the
Degree of Master of Engineering in Civil Engineering
in the University of Canterbury

Department of Civil Engineering
University of Canterbury
Christchurch, New Zealand

August 2007

Abstract

Soil liquefaction has caused major damage to pile foundations in many previous earthquakes. Pile foundations are relatively vulnerable to lateral loads such as those from earthquake shaking; during liquefaction this vulnerability is particularly pronounced due to a loss of strength and stiffness in the liquefied soil. In this research seismic assessment methods for piles in liquefied soil are studied; a simplified approach and a detailed dynamic analysis are applied to a case study of a bridge founded on pile foundations in liquefiable soils. The likely effects of liquefaction, lateral spreading and soil-structure interaction on the bridge during a predicted future earthquake are examined.

In the simplified approach, a pseudo-static beam-spring method is used; this analysis can be performed using common site investigation data such as SPT blow count, yet it captures the basic mechanism of pile behaviour. However, the phenomenon of soil liquefaction is complex and predictions of the seismic response are subject to a high level of aleatoric uncertainty. Therefore in the simplified analysis the key input parameters are varied parametrically to identify key features of the response. The effects of varying key parameters are evaluated and summarised to provide guidance to designers on the choice of these parameters.

The advanced analysis was based on the effective stress principle and used an advanced constitutive model for soil based on a state concept interpretation of sand behaviour. The analysis results give detailed information on the free field ground response, soil-structure interaction and pile performance. The modelling technique is described in detail to provide guidance on the practical application of the effective stress methodology and to illustrate its advantages and disadvantages when compared to simplified analysis.

Finally, a two-layer finite element modelling technique was developed to overcome the limitations conventional two-dimensional (2-D) models have when modelling three-dimensional (3-D) effects. The technique, where two 2-D finite element meshes are overlapped and linked by appropriate boundary conditions, was successful in modelling 3-D characteristics of both deep-soil-mixing walls for liquefaction remediation and pile groups in laterally spreading soil. In both cases the new two-layer model was able to model features of the response that conventional one-layer models cannot; for cases where such aspects are important to the overall response of the foundation, this method is an alternative to the exhaustive demands of full 3-D analysis.

Acknowledgments

I wish to acknowledge the help and guidance of my supervisor, Dr Misko Cubrinovski, his experience and expertise was extremely valuable throughout my research.

Financial support was gratefully received from the Earthquake Commission, the William Georgetti Scholarship Fund, the Todd Foundation and the University of Canterbury.

The site investigation data for the case study was made available through cooperation with Tonkin and Taylor and the Christchurch City Council, their assistance is greatly appreciated.

Table of Contents

List of Figures

List of Tables

1. Introduction

1.1 Liquefaction and piles

Pile foundations are primarily designed to transfer vertical loads from the superstructure to the bearing stratum. For this reason, piles are relatively vulnerable to lateral loads such as those imposed by ground shaking during strong earthquakes. In the case of soil liquefaction, this vulnerability is particularly pronounced since the loss of strength and stiffness in the liquefied soil results in a near complete loss of lateral support for the embedded piles.

It is known from previous earthquakes that liquefaction can cause very large loads on pile foundations, both from inertial loads from the superstructure and from lateral displacements of liquefied soil. The extensive damage and failure of piles have affected numerous bridges, buildings and storage tanks in the past.

1.2 Previous research

During recent strong earthquakes, a large number of pile foundations of modern structures have been severely damaged or collapsed in liquefied soils. In the 1995 Kobe earthquake, for example, massive liquefaction of reclaimed fills caused damage to numerous pile foundations of multi-storey buildings, storage tanks and bridge piers. The unprecedented level of damage to foundations of modern structures instigated a great number of research studies in order to better understand soil-pile interaction in liquefied soils and to improve the seismic performance of pile foundations.

In the initial stages of these studies, detailed field investigations of the damage to piles, *in-situ* soil conditions and permanent ground displacements were carried out. These investigations were then followed by detailed experimental studies aiming to clarify the mechanism of damage by means of seismic centrifuge tests and 1-g shake table tests including benchmark experiments on full-size piles. Based on these studies, new concepts and analysis procedures have been proposed in an effort to explore design based methodologies for piles in liquefied soils. A number of outstanding issues have been investigated including:

- Behaviour of piles based on full-size tests and back analyses from well documented case histories
- Mechanism of damage to piles caused by lateral ground displacements
- Stiffness and strength characteristics of liquefied soils undergoing lateral spreading

- Effects of unliquefied crust layer on the pile response
- Relative contributions of inertial loads from the superstructure and kinematic loads due to lateral ground movement in the overall pile response
- Effects of pile groups
- Development of simplified psuedo-static methods for design of piles
- Development of advanced methods for the analysis of important structures on pile foundations

1.3 Thesis objectives

The objective of this research is firstly to investigate and summarise the seismic performance of pile foundations in liquefiable soil, and then to contribute to the improvement both of simplified and advanced design methodologies.

The behaviour of pile foundations in liquefiable soil observed in (a) case histories from previous earthquakes; (b) experimental tests using 1-g shake tables and centrifuge models and (c) analytical studies is summarised. This is to provide evidence of the performance of pile foundations and to identify key issues and damage characteristics. The capabilities and performance of existing analytical methods are also summarised.

With regard to these key issues and considering the large uncertainties present in simplified, design-orientated analysis a case study of a bridge is presented. The bridge was analysed using a simplified pseudo-static method and the key parameters were varied in a parametric study. This was for two reasons, firstly to present a rational method for dealing with uncertainties in design and secondly to identify key features and trends in the soil-pile interaction during liquefaction, with the ultimate goal of improving design orientated methods for analysing pile foundations in liquefiable soil.

An advanced time history analysis was performed on the same bridge, with the objective of applying such an analysis to a New Zealand case study. The effectiveness and applicability of the advanced analysis is demonstrated by its ability to model the response of the free field soil and the soil-pile-structure interaction in great detail. Finally, a modelling concept is presented which aims to modify existing two dimensional advanced modelling methods to incorporate three dimensional effects. The effectiveness of this modified method is demonstrated through simulation of (a) simplified models; (b) deep-soil-mixing walls (a liquefaction remediation technique) and (c) large scale shake table experiments of pile groups in liquefied soil.

1.4 Thesis organisation

Pile behaviour subject to soil liquefaction is summarised in Chapter 2 through a literature review of case histories, experimental tests and analytical methods. In Chapter 3 a pseudo static beam-spring analysis method is applied to a case study of a bridge foundation. The key design issues and parameters are identified, and a parametric study is conducted to assess how the variation of parameters affects the analytical results. The application of an advanced time history analysis to the same case study is presented in Chapter 4. Here the computed response is discussed, and issues regarding the relevance and application of advanced modelling are examined through a comparison with the pseudo static analysis. Chapter 5 describes a modelling concept where conventional 2-D advanced analysis is extended to account for the 3-D behaviour of foundations in liquefiable soil.

2. Literature Review

2.1 Introduction

The loading of piles in liquefiable soils during earthquake shaking is a complex phenomenon involving interaction between the soil, pile and superstructure. Figure 2.1 shows this interaction during and after the earthquake. At the beginning of the shaking, only inertial loads from the superstructure are significant (Case I in Figure 2.1). With the development of excess pore water pressure during the shaking, large cyclic shear strains develop, resulting in large cyclic ground displacement (Case II). At this stage kinematic forces from these ground displacements are acting in addition to the inertial forces from the superstructure. Near the end of the shaking, a residual component of the shear strain may accumulate, producing a permanent horizontal ground displacement (Case III). The inertial forces at this stage are very small or zero; the kinematic forces due to soil movement are dominant. In the case of piles embedded near a free face (such as a riverbank or quay wall) or in gently sloping ground the residual deformations can be quite large (Case III-b), whereas in level ground they are generally less than the maximum cyclic displacement (Case III-a).

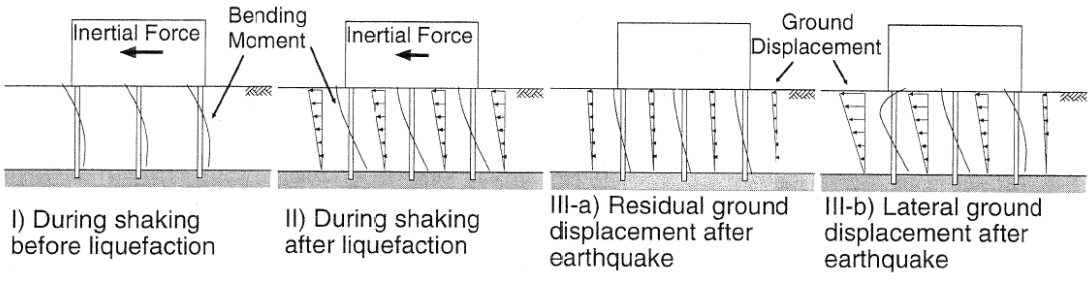

Figure 2.1 Schematic figure showing soil-pile interaction in liquefiable soils (Tokimatsu and Asaka 1998). The inertial force and ground displacement acting on piles at different stages of the loading are shown, with the resulting pile bending moments.

The pile behaviour can thus be divided into two distinct phases, the *cyclic phase* and *lateral spreading*. During the cyclic phase the piles are subjected to cyclic horizontal loads from both the ground displacements and the inertial loads. At this stage the soil may not be fully liquefied and retains some of its stiffness and strength. By contrast, lateral spreading is a post liquefaction phenomenon; here the soil stiffness is very low and the pile experiences large unilateral soil movements and relatively small inertial loads. For both cases, key factors influencing the response of piles were studied by considering observations from case histories and experimental tests.

2.2 Case histories

Case histories represent a real basis for assessing the effects of an earthquake. Through observing damaged sustained in past earthquakes, a baseline level of performance can be established for engineering structures. Here observations of pile performance in liquefied soil during several earthquakes are presented to determine the key factors that influence the behaviour of pile foundations in liquefiable soil.

2.2.1 Cyclic phase

During the 1995 Kobe earthquake, widespread liquefaction in reclaimed fill deposits caused severe damage to the concrete piles of many buildings and structures. As described in Tokimatsu and Asaka (1998) many piles in level ground not subjected to large permanent horizontal ground displacements suffered damage which often caused excessive tilting and settlement of their superstructures. Piles often failed at the pile head, and severe damage was observed near the bottom of the liquefied layer, at the interface with the unliquefied base soil layer.

Oh-Oka *et al*. (1997) and Fujii *et al*. (1998) studied a two storey reinforced concrete building founded on prestressed concrete piles during the Kobe earthquake. A 15-20m thick layer of soil liquefied, and the cyclic ground displacements were large, in the order of 300-400mm. As shown in Figure 2.2, the piles failed at the interface between the unliquefied crust layer and the liquefied layer. Large cracks were also observed at the middle of the liquefied layer and at the interface with the base layer. The pile heads moved 300 – 450mm, and the building suffered severe titling and was unserviceable after the earthquake. In contrast, a nearby building with steel encased concrete piles for the top 8m of length suffered no damage or inclination (Fujii et al. 1998). This can be attributed to the enhanced strength and ductility of the piles.

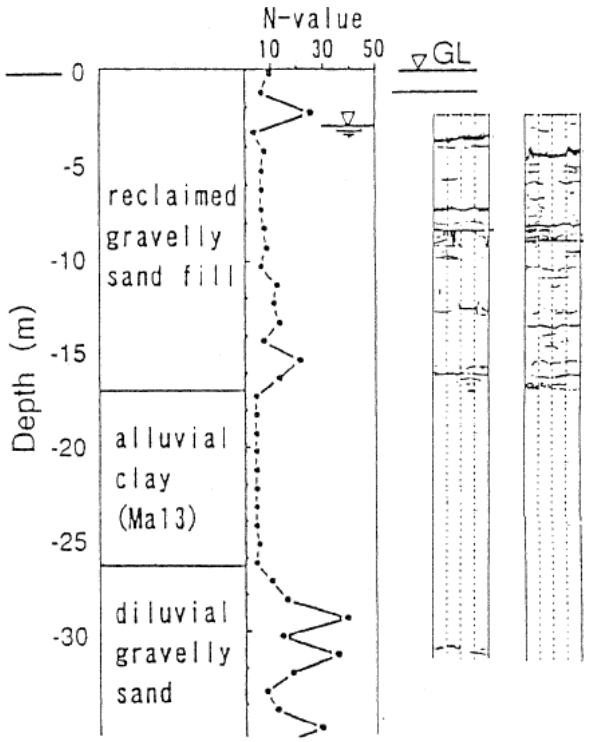

Figure 2.2 Damage to piles due to cyclic phase in the 1995 Kobe earthquake (Oh-Oka et al. 1997). The building suffered severe tilting and was unserviceable after the earthquake.

Horikoshi *et al*. (2000) studied the damage to 111 piles subjected to liquefaction during the Kobe earthquake. All piles were slender piles and located 350m away from any quay walls, so no large permanent ground displacements due to lateral spreading occurred. At the time of the earthquake there were no superstructure or footing above the piles, hence the damage was due solely to the effects of cyclic ground displacements. The piles experienced major cracks at a depth corresponding to boundary between the liquefied and non-liquefied layers and residual displacements of 250 – 420mm were observed at the pile heads.

2.2.2 Lateral spreading phase

Evidence of damage to piles due to large permanent ground displacements has been observed in many earthquakes. In the 1964 Niigata earthquake, lateral spreading caused the failure of the Showa Bridge, when a 10m layer of liquefied soil moved towards the Shinano River. The spans of the simply supported bridge fell into the river, as shown in Figure 2.3a. This failure was explained through observations of the pile deformation after the event; large rotations were observed at the interface between the liquefied and base soil layers as shown in Figure 2.3b (Abdoun et al. 2005; Finn and Fujita 2002; Hamada and O'Rourke 1992). In addition, the bridge collapsed some time after the shaking ceased (Hamada and O'Rourke 1992), indicating

that the large horizontal ground displacements and subsequent pile rotations were a post shaking and post liquefaction phenomenon. Other researchers (Bhattacharya et al. 2004) suggest that the bridge failure was caused by pile buckling.

The Yachiyo Bridge did not collapse like the nearby Showa Bridge; however the abutments and piers suffered damage as shown in Figure 2.4a. Permanent ground displacements of 4-6m were recorded on both banks of the river, whereas a permanent displacement of 1.1m was observed between the top and bottom of a bridge pier. The foundation piles were severely destroyed at the interface between the liquefied medium sand and the non-liquefied fine sand, at a depth of 8m. Horizontal cracks, indicating large bending moments, were found throughout the piles. The large ground movement pushed the foundations of the piers toward the river; however the tops of the piers were restrained by the stiffness of the bridge girders. The pile head displacement was in the order of one metre, which was resisted by the non-liquefied base layer. This caused large stress concentrations at the interface between the liquefied layer and the non-liquefied base layer, explaining the severe pile damage observed. The difference between the foundation deformation (~1m) and the free field deformation (4-6m) is due to the longitudinal stiffness of the bridge and foundation.

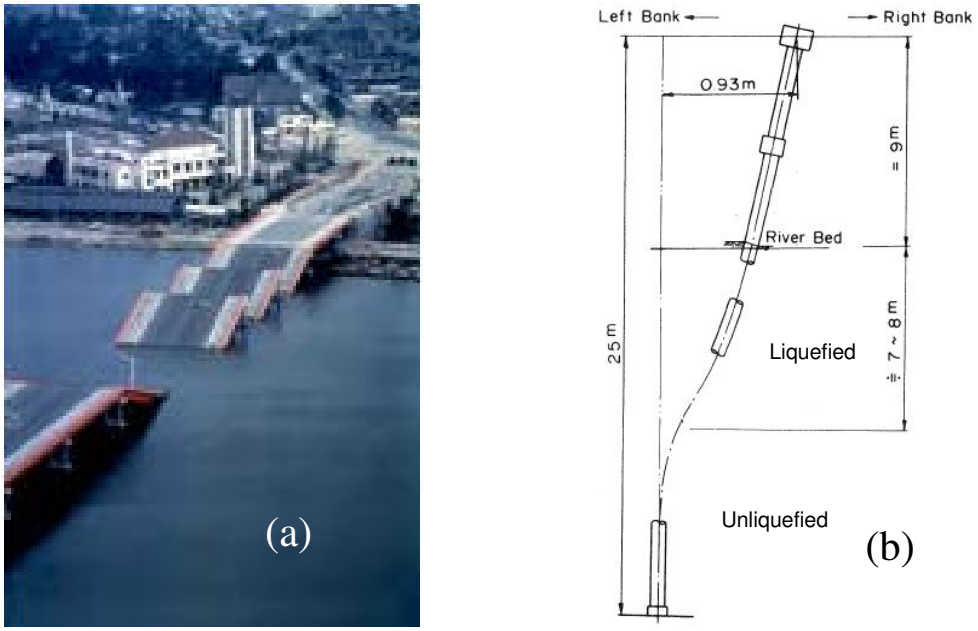

Figure 2.3 Collapse of Showa bridge due to lateral spreading: (a) collapsed bridge (Abdoun et al. 2005), (b) deformed pile extracted after the earthquake (Hamada and O'Rourke 1992)

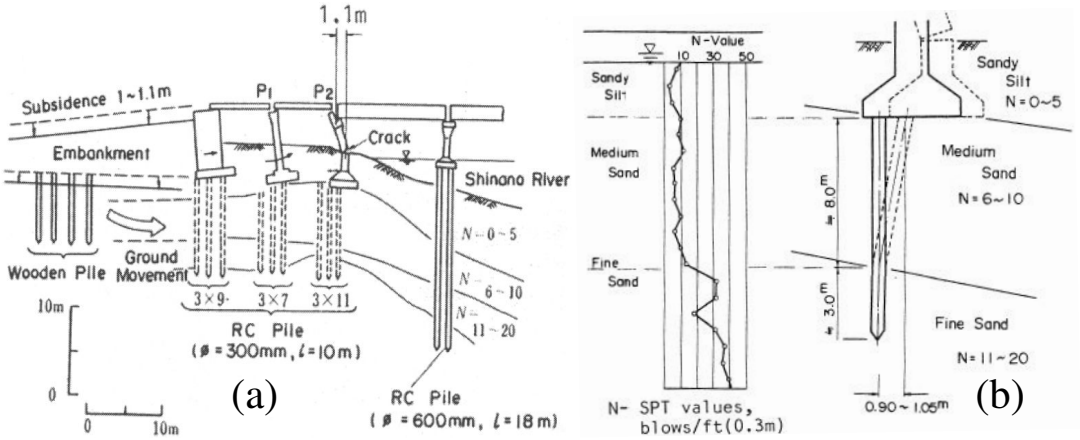

Figure 2.4 Damage to Yachiyo Bridge due to lateral spreading: (a) damage to abutment and piers, (b) SPT profile and pile damage (Hamada and O'Rourke 1992). The damage was similar on the opposite bank.

The piles of buildings suffered many instances of heavy damage and failure due to lateral spreading in the Niigata earthquake. The piles of the Niigata Family Court House Building (NFCH) suffered extensive damage (Abdoun and Dobry 2002; O'Rourke et al. 1994; Yoshida and Hamada 1991). At the site a 6m thick layer of soil liquefied and a permanent ground displacement in the order of one metre occurred (Hamada and O'Rourke 1992). Two piles that failed due to the liquefaction induced ground displacement were studied. The pile failures resulted in a building inclination of 1°.

As Figure 2.5 shows, one pile (Pile No. 1) is a floating pile whereas the other (Pile No. 2) extends to the firm, non-liquefied base layer. A comparison between the behaviour of the two gives insight into the mechanism of damage to piles in undergoing lateral spreading. Pile No. 1 had many cracks at the level of the water table, showing that the largest bending moments were induced at the interface between the non-liquefied crust layer and the liquefied layer. Tensile cracks were observed on one side and compression failure was observed on the other. This indicates that the predominant load on the pile was a monotonically increasing load caused by lateral spreading, as opposed to loads from cyclic ground displacements or inertial loads from the superstructure. There was little damage to the pile at the pile tip. Pile No. 2 also shows damage typical of lateral spreading, however the damage was much heavier and significant damage occurred near the base of the pile at the interface between the liquefied and base layers.. The double curvature of Pile No. 2 shown in Figure 2.5 shows that the non-

liquefied crust layer pushes the pile, and that the non-liquefied base layer resists this action. The damage to the two piles show that lateral spreading of the ground imposes a pseudo-static loading on the pile, which is only indirectly related to the earthquake shaking.

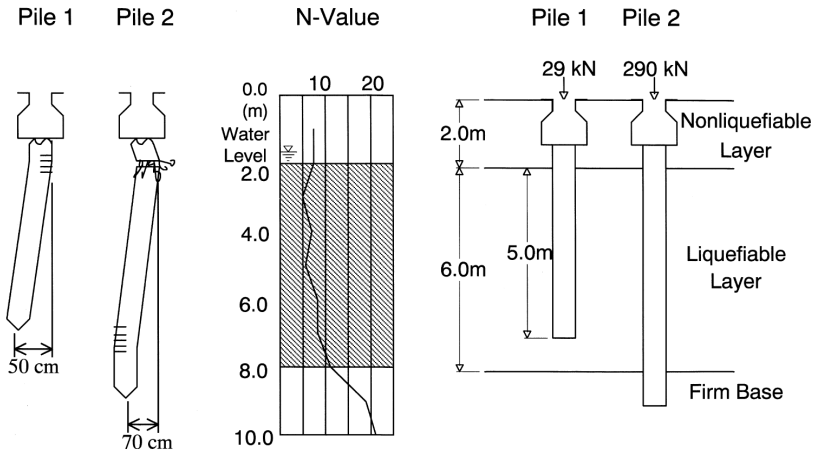

Figure 2.5 *Piles of NFCH building, showing damage, SPT profile and location relative to the liquefied layer (Abdoun and Dobry 2002)*

The concentration of damage at the interface between liquefied layers and the crust and base layers above and below was also seen at the NHK Building (Figure 2.6), which suffered pile failure due to a ground movement of 1-1.2m (Hamada and O'Rourke 1992). The pile failed at the interfaces at the top and bottom of the liquefied layer. However the nearby Hokuriku Building suffered no damage, despite having nearly identical soil conditions and ground displacement. The larger Hokuriku Building had a much stiffer foundation with more piles; the building also had a one storey basement, which extended to 6m below the ground surface. Additionally, temporary piles used during excavation of the basement were not removed. The stiffened foundation resisted the large ground displacement and the basement reduced effects from the unliquefied crust layer. Also, the large number of piles had a great effect on the densification of the soil, perhaps preventing liquefaction.

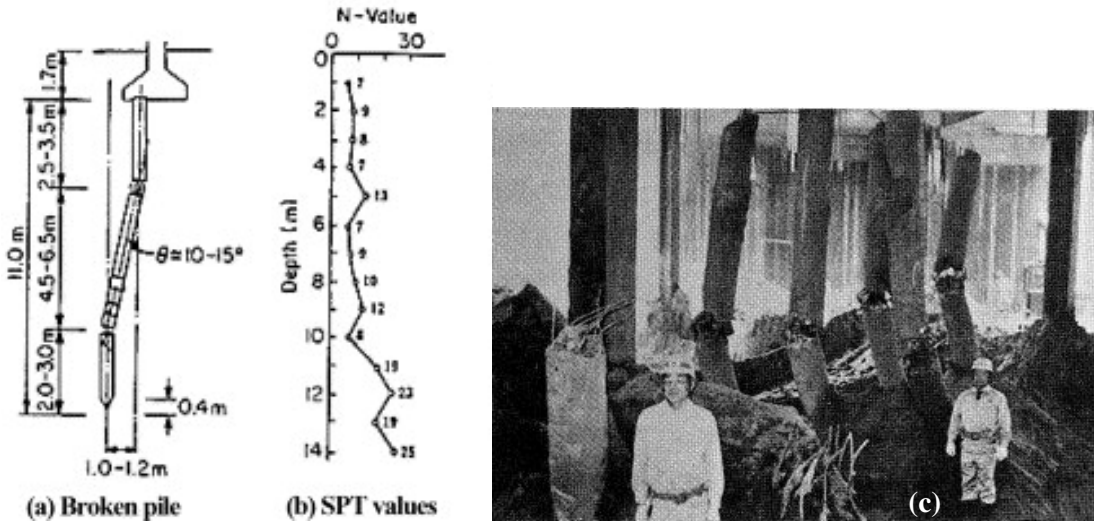

Figure 2.6 *Damage to piles of NHK Building: (a) schematic, (b) SPT profile, (c) photo of piles after excavation (Hamada and O'Rourke 1992)*

Observation of the damaged piles of the Hotel Niigata building and the East Railway overbridge in the Niigata earthquake (Hamada and O'Rourke 1992), and at the large diameter piles of the Hanshin Expressway in the Kobe earthquake (Ishihara and Cubrinovski 1998) also show concentration of damage at the interfaces between the non-liquefied and liquefied soil layers. For the Hotel Niigata building a lateral ground displacement of 4m occurred, causing a bending failure of the piles. The East Railway overbridge showed cracks on one side of the pile only, indicating a monotonically increasing load caused by lateral spreading. A permanent horizontal ground displacement of 1m occurred at Pier 211 of the Hanshin Expressway, most of the damage was at the interface of the liquefied soil and the non-liquefied base soil as shown in Figure 2.7. Some cracks were also observed at the pile head.

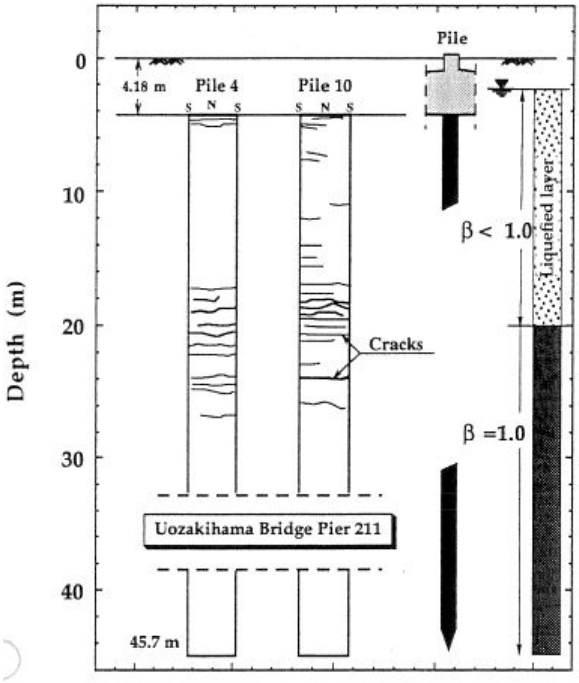

Figure 2.7 *Crack distribution to the large diameter bored piles of Pier 211 (Ishihara and Cubrinovski 1998)*

Immediately after the 1987 Edgecumbe earthquake in New Zealand, lateral spreading occurred at the Landing Road Bridge in Whakatane. A 4m thick layer of soil liquefied and moved 1.5 – 2m towards the Whakatane River. Investigations by Berrill *et al.* (2001) showed mounding of soil on the landward side of the bridge piers, and gaps of up to 600mm on the river side. It was found that mounding was evident for about 2.5m back from the pier, and a shear surface was clearly seen in the sandy silt near the ground surface. This shows clear evidence of passive failure in the unliquefied crust overlying the liquefied sand layer. The passive load from the crust layer was estimated to be about 1MN per pier, whereas the drag force from the liquefied soil was estimated to be about 50kN. The loads imposed on the bridge were very close the collapse load of the substructure. This case study shows that piles passing through liquefied soil to firm ground can attract large forces from lateral spreading. Overlying unliquefied layers can impose large forces, in the limit corresponding to passive failure in the soil, and these forces are much larger than drag forces from the liquefied soil.

Another example of pile failure occurred in the 1990 Luzon earthquake in the Philippines (Hamada and O'Rourke 1992; Yasuda and Berrill 2000). The 7-span RC Magsaysay Bridge collapsed during the earthquake. Ground flow occurred towards the centre of the river; the ground moved 6m on the west side of the bridge, and 5m on the east. Four girders fell down

during the earthquake, as shown in Figure 2.8. When the piles of piers No. 4 and 5 were removed during reconstruction, it was found that they were fractured 10m below the ground surface, coincident with the boundary between the liquefied and non-liquefied layers. The tops of the piles were bent towards the centre of the river. This evidence suggests the loose sand layer liquefied and flowed towards the centre of the channel, bending the piles and causing large displacements of the piers which unseated the girders. Again the damage was concentrated at the interface between liquefied and non-liquefied soil.

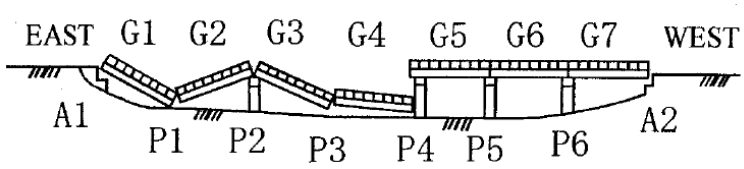

Figure 2.8 *Sketch of damage to the Magusaysay Bridge in the 1990 Luzon Earthquake (Yasuda and Berrill 2000)*

During the 1995 Kobe earthquake a three storey RC building studied by Tokimatsu *et al*. (1997) inclined by 5° due to pile damage caused by lateral spreading, as shown in Figure 2.9. The permanent horizontal ground displacement was 2m at the quay wall and decreased rapidly with distance inland. The displacement of the pile heads was estimated to be 0.8m. As shown in Figure 2.10, contrasting deformation and damage was observed between the seaward piles and the landward piles, despite the piles having the same pile head displacement. The seaward piles had a change in slope at 5m depth, and suffered large horizontal and diagonal cracks in three places; at a depth of 5m, near the pile head and the interface between the fill and the natural deposit. The landward pile had similar cracks at the pile head and interface with the base soil but no damage or change in slope was observed at 5m depth. The differences can be explained by the different ground displacements on the seaward and landward sides; on the seaward side the soil is pushing the pile, whereas on the landward side the pile pushes the soil. In the same study (Tokimatsu et al. 1997) similar observations were made with an eleven storey RC building during the same earthquake.

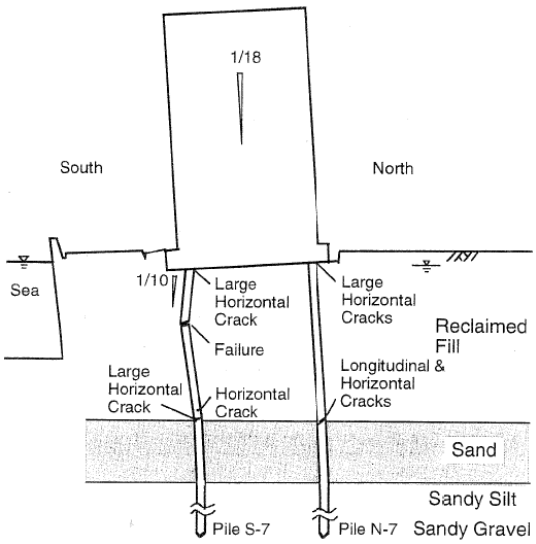

Figure 2.9 *Failure pattern of piles due to liquefaction induced lateral spreading (Tokimatsu et al. 1997)*

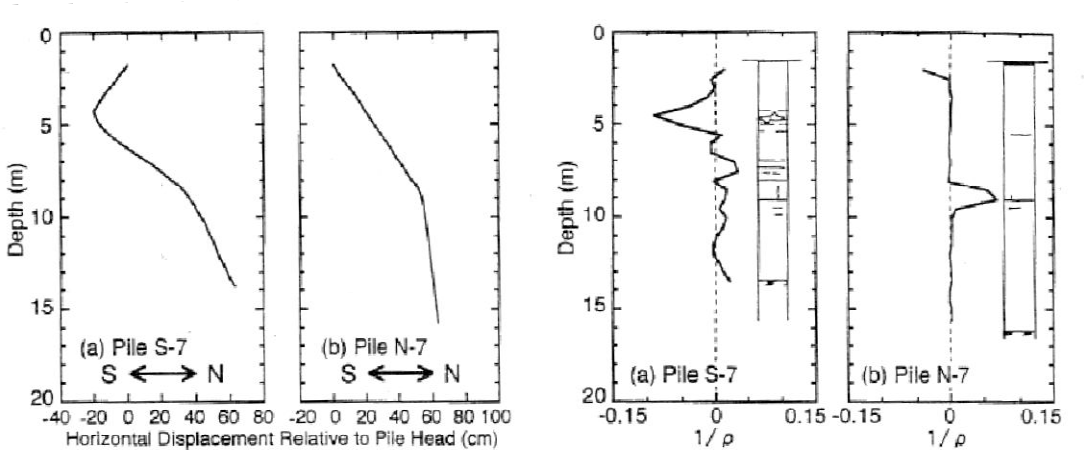

Figure 2.10 *(a) Deformation patterns of the seaward (S-7) and landward (N-7) piles; (b) Variation of curvature in piles (Tokimatsu et al. 1997)*

A similar deformation pattern was observed for the piles of a storage tank during the Kobe earthquake (Ishihara and Cubrinovski 2004). Here the ground moved approximately 55cm on the seaward side of the tank and 35cm on the landward side. Again, the damage was most pronounced at the interface between the liquefied layer and the base layer. The previous two case studies show that different lateral spreading displacements can cause different lateral loads on the piles connected to the same pile cap. The effect of these differences, along with interaction forces at the pile head, results in distinct deformational features of each pile depending on its place within the pile group.

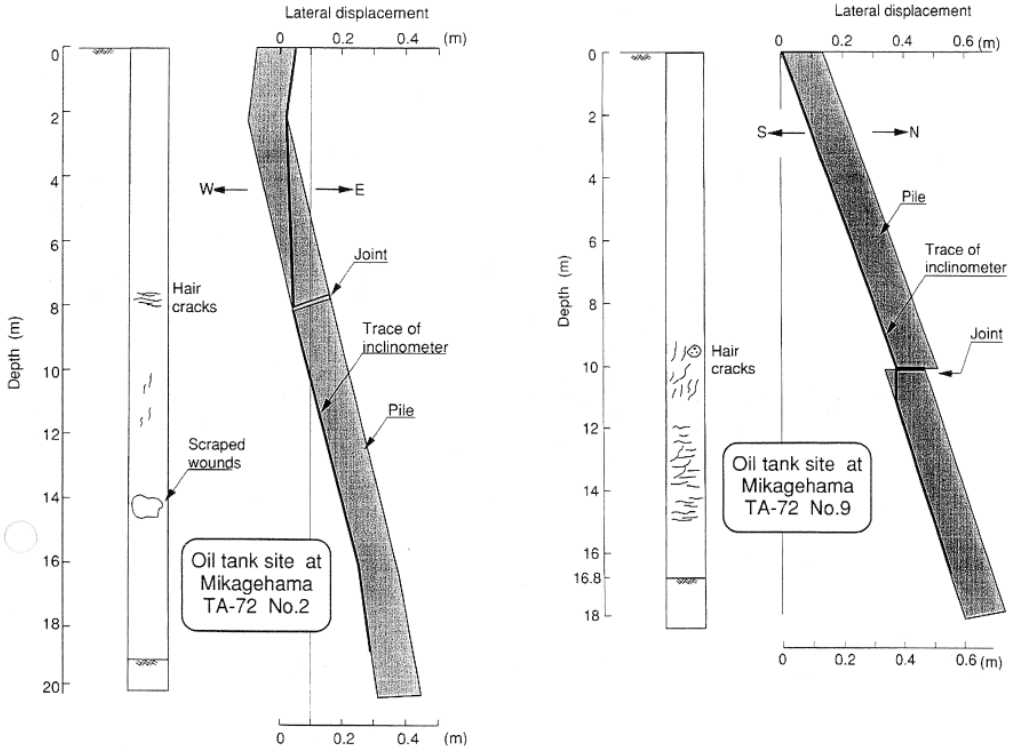

Figure 2.11 Lateral displacement and observed cracks on the inside of the seaward (No. 2) and landward (No. 9) piles (Ishihara and Cubrinovski 2004)

2.3 Experimental studies

Experiments provide a tool for investigating specific features of pile response. By controlling experimental conditions, researchers can accurately observe and measure pile behaviour as it occurs. Soil conditions are more uniform, the input motion is known and the response can be recorded accurately, making experiments valuable in verifying methods of analysis. While experiments can never fully capture the features of real life structures and earthquakes, they remain a vital instrument in understanding of the behaviour of pile foundations subjected to liquefaction.

2.3.1 Cyclic phase

A full-scale shaking table test described in Cubrinovski *et al*. (1999) was designed to investigate the cyclic phase of soil-structure interaction and provides insight into the importance of both pile head fixity and the magnitude of cyclic lateral ground displacements. Two piles, one fixed head and one free, were embedded in uniform sand inside a laminar box, 3.5 x 12m in plan and 6m high. Two sinusoidal type shaking events were applied to the model; Test 1 had a peak ground acceleration of 0.084g, compared with 0.21g in Test 2. Complete liquefaction occurred in both tests; however the cyclic lateral ground displacements were about 50% larger in Test 2. This was reflected in the observed pile bending moments, the piles sustained much higher bending moments and subsequent damage during Test 2 for both the free and fixed head piles. This suggests that the magnitude of the cyclic ground displacements is the key parameter in the response of the piles, not the extent of liquefaction. The damage to the piles was inspected after the experiment; the fixed head piles reached the yielding level at the pile tip and cracks were observed at the pile head whereas the free head pile only suffered damage at the pile tip.

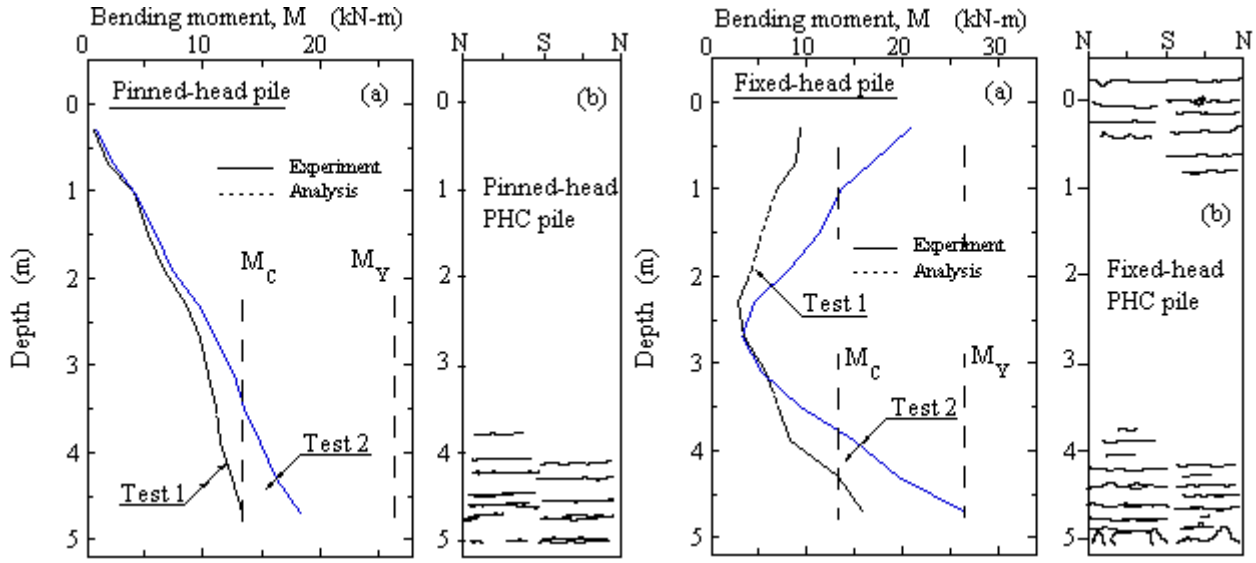

Figure 2.12 Measured bending moments and observed cracks for the free and fixed head piles (Cubrinovski et al. 1999)

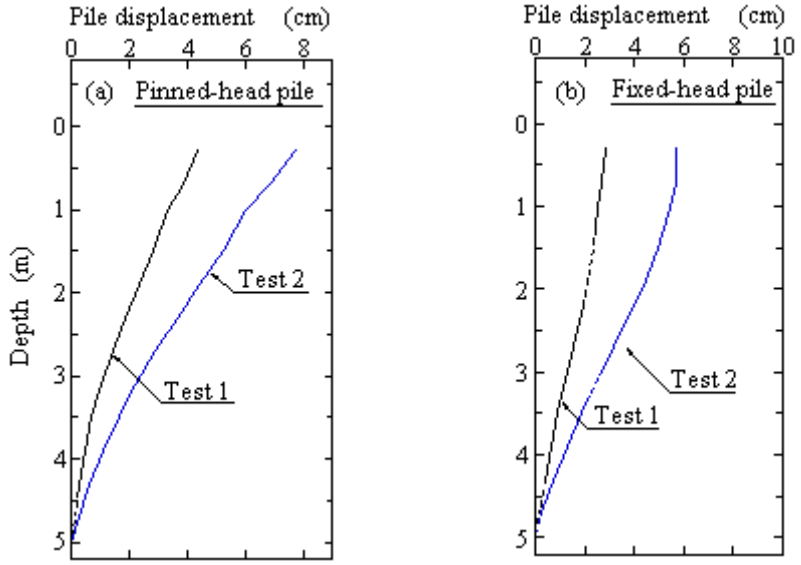

Figure 2.13 Maximum lateral displacements of piles: (a) free head pile, (b) fixed head pile (Cubrinovski et al. 1999)

Yasuda *et al*. (2000) describe two large-scale shake table tests investigating pile foundations in liquefied soil. The first test was on piles in level ground and the second on piles in sloping ground. Both models were subjected to a sinusoidal input acceleration and liquefaction was induced throughout the model. The results of the first test are shown in Figure 2.14 for Foundation B, with a pinned connection at the pile head, and for Foundation A, where the pile head is rigidly connected to the footing. The fixed head pile shows damage at both the pile head and at the pile tip, whereas the free head pile shows damage only at the pile tip.

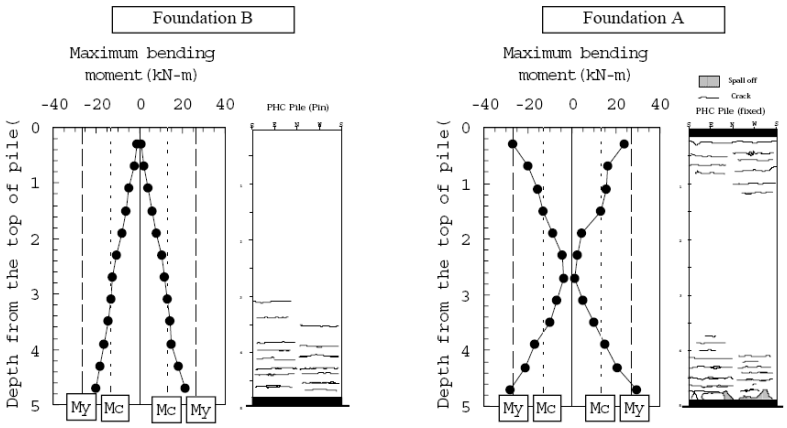

Figure 2.14 Measured maximum moments and observed crack patterns during the cyclic phase experiment on level ground for the free head pile (Foundation B) and the fixed head pile (Foundation A) (Yasuda et al. 2000)

The second test is shown in Figure 2.15; here three piles are embedded in saturated sand with a sloping ground surface of 14%. The three piles are all PHC piles and fixed at the base and pinned at the head. From the way the piles are embedded it can be seen that Pile No.1 will experience the most lateral spreading whilst Pile No. 3 will experience relatively little. Figure 2.16 shows the measured bending moments and observed cracks throughout the length of all three piles. The damage at the base of the piles is expected due to the fixity at the base, but it is interesting to note that Pile No. 1 has cracks on one side only; the downslope side of the pile shows little damage. This is consistent with a monotonically increasing load from the laterally spreading ground. Pile No. 3, however, has cracks on both sides. Thus the damage to Pile No. 1 is due primarily to lateral spreading and the damage to Pile No. 3 is due primarily to the cyclic phase of the response.

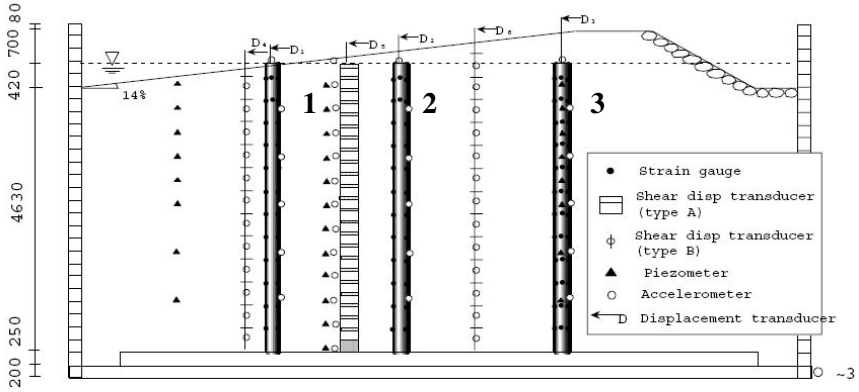

Figure 2.15 Full scale lateral spreading experiment on piles (Yasuda et al. 2000)

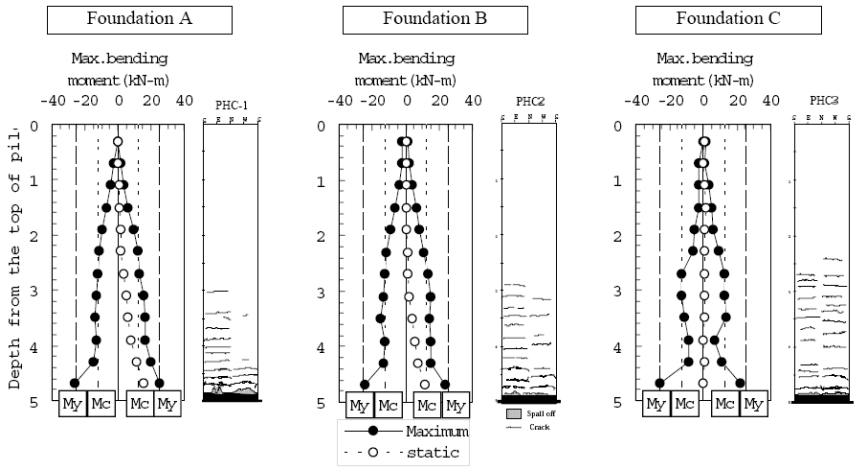

Figure 2.16 Measured maximum moments and observed crack patterns for piles during the lateral spreading experiment (Yasuda et al. 2000). Foundation A (Pile No. 1) experienced the most lateral ground displacement and Foundation C (Pile No. 3) experienced the least.

During the cyclic phase loads act on the pile from two sources: inertial loads from the superstructure and kinematic loads from cyclic ground displacements. Tokimatsu *et al*. (2005) investigated the interaction between the kinematic and inertial loads through large scale shake table tests on piles embedded in both dry and liquefied soil. The series of experiments are shown in Figure 2.17, with the D series indicating dry sand and S indicating saturated sand. For DBS and SBS, the natural period of the superstructure is less than the natural period of the ground, whereas the superstructures of DBL and SBL have a longer natural period than the unliquefied ground but shorter than that of the liquefied ground.

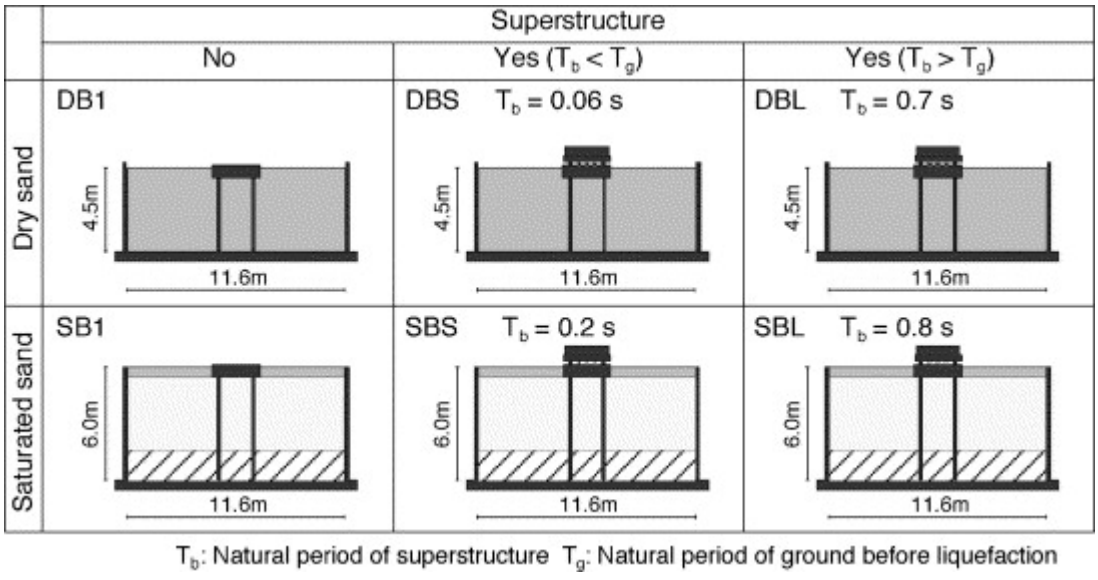

Figure 2.17 Soil-pile-structure models used in shaking table tests (Tokimatsu et al. 2005)

For the tests in dry soil, it was found that the inertial force and the earth pressure acted in opposite directions. Also, the earth pressure was out of phase with the inertial force in the DBS (short period superstructure) case, and in phase in the DBL (long period superstructure) case. As shown in Figure 2.18a, when the loads are out of phase the earth pressure in not completely in phase, thus its contribution towards reducing the shear force in the pile is small, whereas the completely in phase loads shown in Figure 2.18b reduce the shear force transmitted to the pile. The Fourier spectrum of the input motion and accelerations of the ground surface, foundation and superstructure are shown in Figure 2.19 for both experiments. It can be seen that in experiment DBL the Fourier spectrum of the superstructure has a peak at a longer period than the ground and foundation, whereas for the DBS experiment the peaks occur at the same period. Therefore the effects of soil displacement and inertial force tend to be in phase if the natural period of the superstructure is shorter than that of the ground, but out of phase if it is longer.

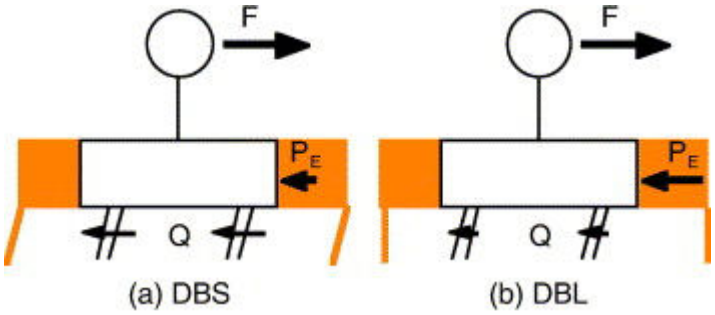

Figure 2.18 *Interaction of inertial loads and earth pressures for DBS and DBL experiments (Tokimatsu et al. 2005)*

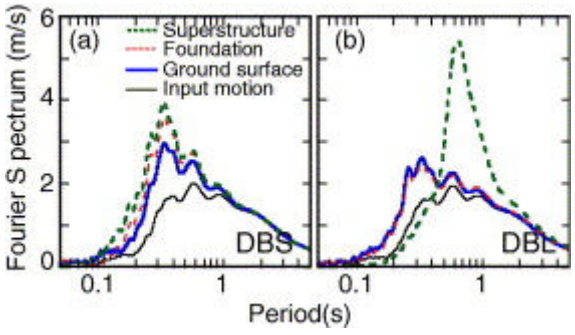

Figure 2.19 *Fourier spectra of accelerations for DBS and DBL experiments (Tokimatsu et al. 2005)*

For the tests in saturated sand, the effects of liquefaction on the interaction of kinematic and inertial loads were studied. It was found that before liquefaction the inertial and kinematic loads acted in opposite directions, but after liquefaction the inertial force and the earth pressure act in the same direction, increasing the shear force transmitted to the pile (Figure 2.20). For both the SBS (short period) and SBL (long period) experiments, after liquefaction the maximum bending moment occurred when both the ground displacement and inertial force were large. This indicates that the inertial and kinematic forces are in phase with each other as for both cases the natural period of the liquefied soil was greater than that of the superstructure. Therefore piles in liquefiable soils should be designed considering both the inertial and kinematic loads act at the same time.

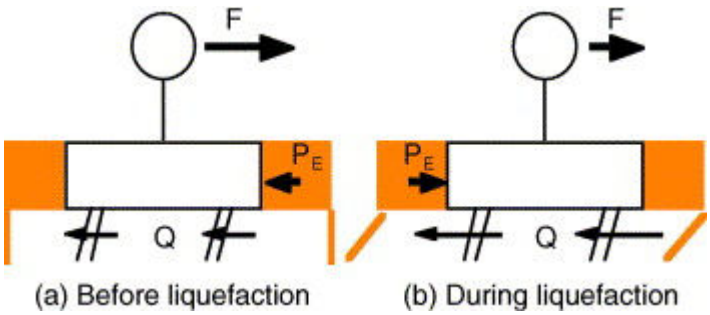

Figure 2.20 Change of action in earth pressure after liquefaction (Tokimatsu et al. 2005)

Tamura *et al*. (2000) describes the results of a large-scale shake table experiment on four piles fixed to a rigid body at the pile head in order to clarify the failure mechanism and dynamic response of piles during liquefaction. Figure 2.21 schematically shows the pile damage during four phases of the dynamic response. Also shown is the excess pore water pressure ratio, inertial force and ground displacement. The characteristics and damage features during the four stages can be summarised as follows:

1. The excess pore pressure ratio reaches 0.5, the inertial force is large and cracks start to appear at the pile head.

2. Soil liquefaction is progressing; now the pore pressure ratio reaches 0.8 near the ground surface. The inertial force remains large and the deformation of the soil is increasing. Reinforcement starts to yield at the pile head, this damage is caused not only by the inertial force but also the soil movement.

3. Now the upper part of the soil is liquefied, the lower part is not yet completely liquefied. Liquefaction has caused large relative displacement between the piles and the soil. The concrete is crushed in the middle part of the piles at the interface

between the liquefied and non-liquefied soil, this results in a large sudden movement of the rigid body at the pile head.

4. The soil has completely liquefied and the soil deformation is large whilst the inertia force is now small. The pile deformation is concentrated at the plastic hinges and the rigid body moves to one side and settles.

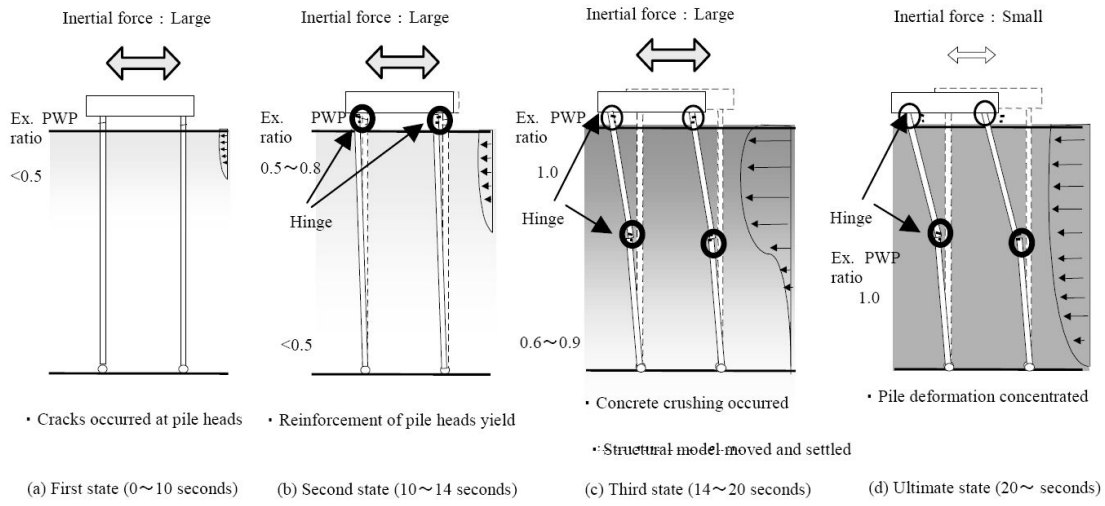

Figure 2.21 Schematic figures showing damage mechanism to piles during a large-scale shake table cyclic phase experiment (Tamura et al. 2000)

2.3.2 Lateral spreading

A large-scale shake table lateral spreading test on both stiff and flexible piles in liquefied soil is described in Cubrinovski *et al*. (2006b). The experiment shows the general behaviour of stiff and flexible piles during the lateral spreading phase, and in addition examines both the lateral loads from non-liquefied crust soil and the stiffness characteristics of laterally spreading soils. The experiment consisted of a relatively stiff steel pile and a relatively flexible prestressed concrete (PHC) pile embedded in a laminar box filled with saturated sand with a crust layer of sand above the water table. The experiment was conducted in two phases: a dynamic excitation phase to induce liquefaction and a lateral loading phase to simulate lateral spreading of soil. Once the soil had liquefied, the lateral loading was applied through pushing the side of the laminar box, applying a permanent horizontal displacement of 0.84m at the top of the liquefied soil. Figure 2.22 shows the pile response for both the stiff and flexible piles. The flexible PHC pile followed the ground displacement and the ultimate moment of the pile was exceeded at a ground displacement of 9cm. By contrast the steel pile

resisted the lateral soil movement; the pile displacement increased until a value of 6cm then remained constant throughout the rest of the ground movement. A similar pattern was observed in the bending moment, with the bending moment reaching 60% of the steel pile yield moment and remaining relatively constant. These results were caused by both the movement of the liquefied soil and lateral pressure from the crust soil, these effects were then evaluated separately to gain further insight into the soil-pile interaction.

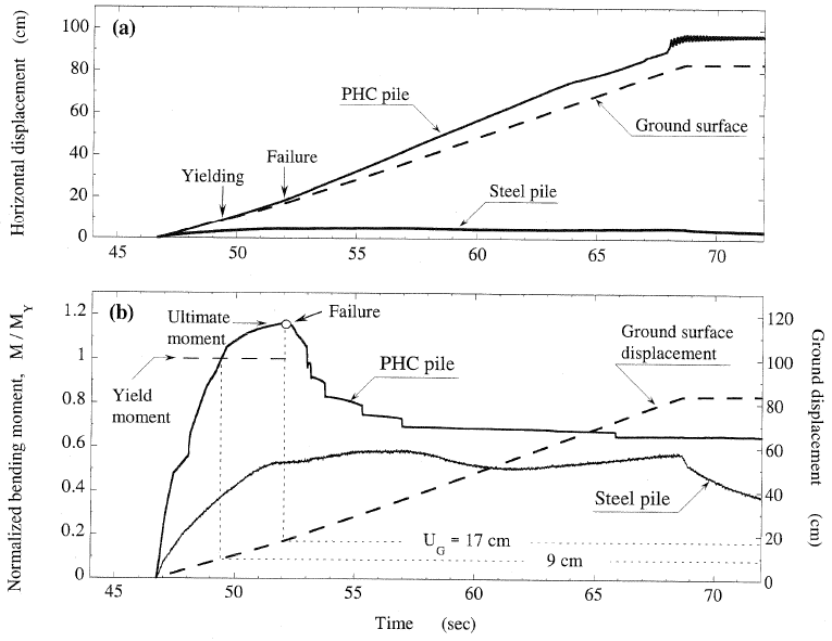

Figure 2.22 Measured displacements and bending moments of piles during lateral spreading: (a) Displacement at the pile head; (b) Maximum bending moment near the base of the pile (Cubrinovski et al. 2006b)

Figure 2.23a shows the measured ultimate pressure acting on the pile from the non-liquefied surface layer, expressed as a function of the Rankine passive pressure. The lateral pressure per unit width acting on a single pile is larger than that of an equivalent wall due to shearing resistance on the vertical sides of the failure wedge in the soil. In this experiment the ultimate lateral pressure was found to be 4.5 times greater than the Rankine passive pressure for an equivalent wall. Comparing the development of lateral displacement and bending moments in the piles (Figure 2.22) and the measured lateral pressure in the crust layer (Figure 2.23a), it can be concluded that the maximum bending moments occurred once the ultimate lateral pressure had been mobilised. This indicates that the lateral load from the surface layer was the key factor in the response of the piles.

The effect of liquefaction on the soil stiffness was quantified by multiplying the subgrade reaction coefficient by a degradation constant β. The value of β that best represented the pile response was back-calculated for different ground displacements, as shown in Figure 2.23b. The shaded area represents the range of β values for which the computed response was within ±10% deviation from the observed response, whereas the solid line is the best fit values. It can be seen that the best fit value of β is in the range between 1/30 and 1/80, and decreases gradually with increasing ground displacement (or relative displacement between the soil and the pile). The vertical size of the shaded area shows the sensitivity of the analytical response on the value of β; therefore for small relative displacements the stiffness of the liquefied soil does not have a dramatic effect on the response. Conversely, for large relative displacements the pile response is sensitive to the stiffness of the liquefied soil.

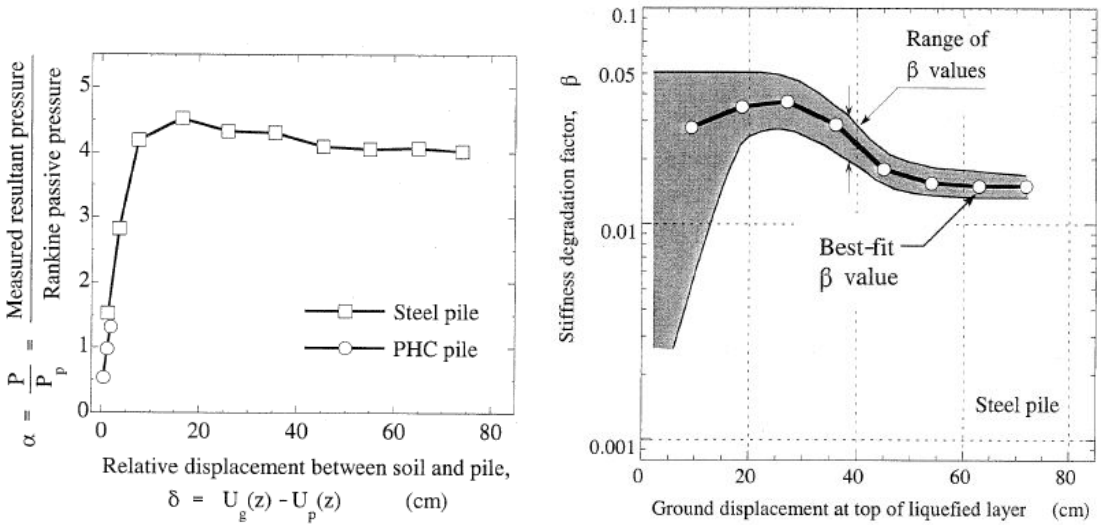

Figure 2.23 (a) Ultimate pressure applied to the pile from the crust layer as a function of relative displacement; (b) Back-calculated degradation of stiffness in liquefied layer as a function of ground displacement (Cubrinovski et al. 2006b)

Abdoun *et al*. (2005) investigated the behaviour of piles undergoing lateral spreading using a centrifuge; key considerations were the effects of inertial loads and superstructure stiffness. The models were inclined at an angle of 2° to induce lateral spreading, and consisted of a single pile embedded in a three layer soil profile as shown in Figure 2.24. Experiments were conducted with and without an added mass above the ground to model inertial loads; in addition the stiffness of the spring *k* shown in Figure 2.24 was varied to determine the effects of superstructure stiffness.

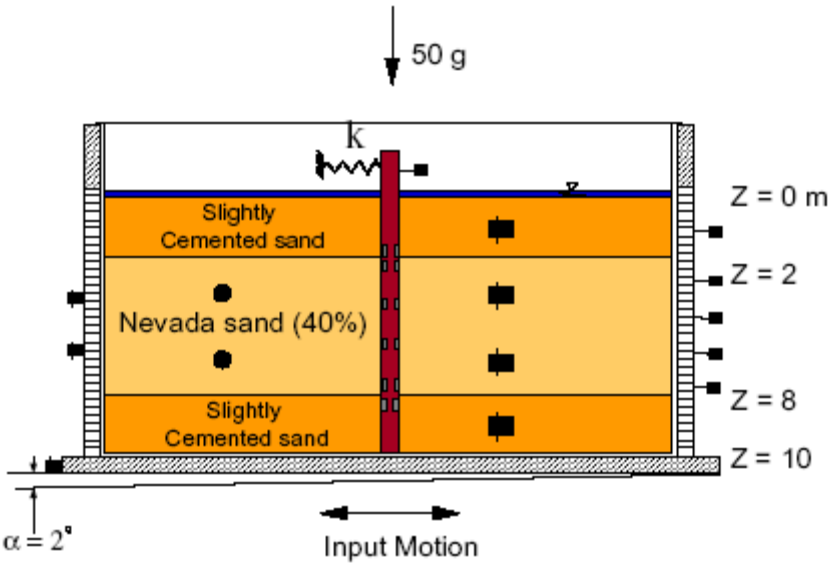

Figure 2.24 *Lateral spreading pile centrifuge model incorporating effects of superstructural stiffness and mass (Abdoun et al. 2005)*

In all cases the middle sand layer liquefied early in the shaking and the lateral spreading increased monotonically to a value of 0.7m in the prototype scale. Figure 2.25 shows the bending moment of the pile at different levels of ground displacement for both cases without (Model 2) and with (Model 2m) inertial loading. The pile with no added mass or stiffness experienced an increase in bending moment with time, and then a decrease in pile bending moment occurred after passive failure of the non-liquefied layer took place against the pile. After the soil in the top layer failed, the pile head and cap rebounded, i.e. the pile was pushing the soil rather than the other way around. With the added mass, superstructural inertial forces were introduced to the model; it was found that lateral spreading still dominates the response and the effects of inertial load are only significant in the top 2-3m of the model. However, even at shallow depths less than 2m, the non-liquefied crust failed in the same passive manner as the case without the added mass, and the maximum moments still occurred at the upper and lower boundaries of the liquefied layer. This shows that the pile behaviour and soil failure mechanism remain the same. Note that the first plot in Figure 2.25 has a smaller horizontal scale.

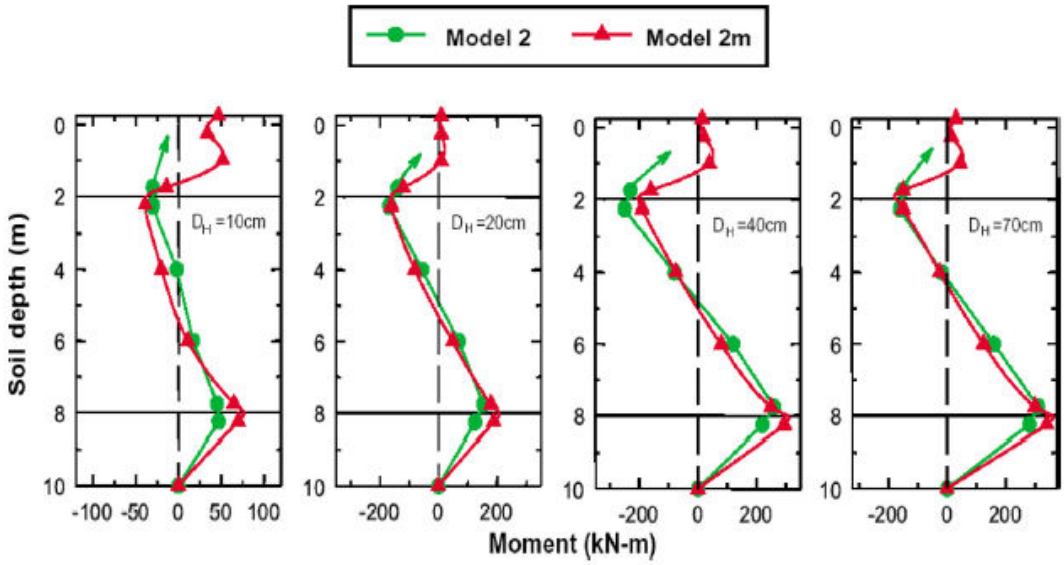

Figure 2.25 Measured bending moment response along pile in lateral spreading centrifuge models without (Model 2) and with (Model 2m) inertial loading (Abdoun et al. 2005)

The effects of superstructure stiffness on the pile response were also examined by applying a very stiff spring ($k = \infty$) to the top of the pile. Here the pile foundation has enough lateral stiffness and strength to resist the maximum passive pressure of the non-liquefied crust layer. This stiffness attracted more load, as seen in the comparison with k=0 in Figure 2.26a. No rebounding of the pile occurred at shallow depths, i.e. the soil was always pushing the pile, as shown in Figure 2.26b where the crust soil failed in a passive mode against the pile and all failed soil is upslope of the piles.

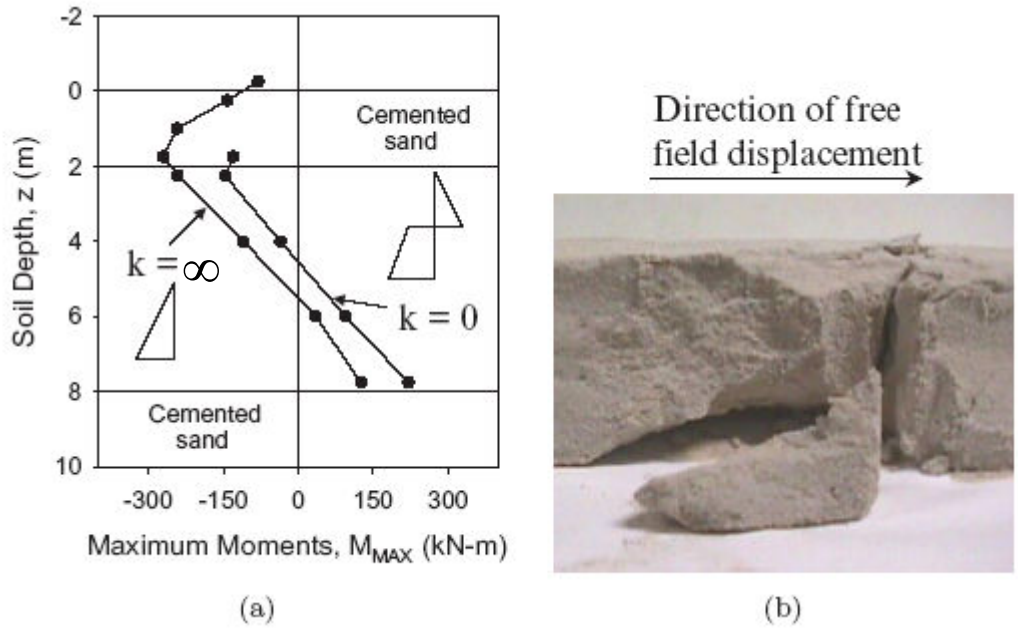

Figure 2.26 *Effect of superstructure stiffness on pile foundation response (Abdoun et al. 2005)*

Brandenberg *et al*. (2005) studied the behaviour of single piles and pile groups in laterally spreading ground using a seismic centrifuge. The piles were embedded in a soil profile consisting of a non-liquefiable crust overlying a loose sand layer which overlies dense sand. The layers sloped towards a river channel carved into the crust layer at one end of the model. Attention was given to the timing of the lateral loads from the crust layer and the liquefiable layer; it was found that in general the peak bending moment occurred at the peak downslope loading from the unliquefied crust layer. The direction of loads from the liquefied soil depended on the mode of pile deflection relative to the soil; three modes were identified, corresponding to the three dashed lines in Figure 2.27. For Case A, the pile is stiff enough to resist the loads imposed by the crust and it displaces less than the soil in the liquefied sand layer. Hence the pile attracts a downslope load from the liquefied layer in addition to the downslope load from the crust layer. For Case B, the foundation is stiff enough to resist the load from the crust layer, however the pile displaces more than the liquefied soil and thus the liquefied soil provides an upslope resisting load. Case C shows the behaviour of flexible piles, here the full downslope pressure from the crust layer is not mobilised. Note that in this case the large displacement discontinuity between the crust and liquefied soil is caused by trapping of pore water beneath the low-permeability clay crust layer. This enables the clay crust to slide on top of the very loose sand at the top of the liquefied layer.

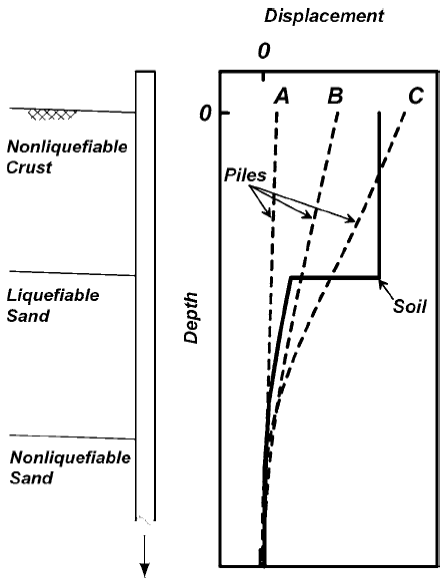

Figure 2.27 Soil and pile displacements for different cases of pile behaviour during lateral spreading (Brandenberg et al. 2005)

2.4 Analysis

There are many analysis methods that predict the seismic response of pile foundations in liquefied soil. In this study, two categories of analysis are studied: simplified approaches based on empirical and pseudo-static methods, and detailed dynamic analyses using the time history or step-by-step procedures. The former approach is appropriate for preliminary assessment and design of piles, while the latter is suitable for performance based assessment of important structures.

2.4.1 Simplifed methods

Simplified, design orientated methods generally apply inertial loads from the superstructure as a point load at the pile head. The effects of cyclic and permanent ground displacements on the pile response are modelled using one of the following three approaches:

(a) The loads on the pile are estimated and then applied as either a load at the pile head or lateral pressure acting along the pile.

(b) The ground displacement is first evaluated for a free field soil profile; this displacement is then applied to the pile through a series of springs. The stiffness of the soil springs can be reduced to account for the effects of liquefaction.

(c) The moving soil is treated as a viscous fluid; the load on the pile is calculated as the drag force on the pile.

The first two approaches are well established, whereas the third method has not been adopted widely in practice. It is noted in Berrill and Yasuda (2002) that for the viscous fluid method the liquefied soil must be treated as a non-Newtonian fluid, as it has been observed that the shearing resistance of a liquefied soil is the least when the strain rate is greatest.

The first method is often termed the *seismic coefficient* method, whereas the second is termed the *seismic displacement* method. Both methods are used in practice, for example the seismic coefficient method is used in the Japanese code for design of highway bridges; for cyclic phase cases only the inertial load is applied and the effects of ground displacements are ignored whereas for highway bridges subjected to lateral spreading an earth pressure is applied to the pile (Uchida and Tokimatsu 2006). The Japanese design codes for railway facilities and buildings both use a seismic deformation method for lateral spreading; in both cases the soil springs are degraded to account for liquefaction effects. For cyclic cases however railway facilities are designed using the seismic coefficient method, where an additional load is applied at the pile head to account for soil displacement.

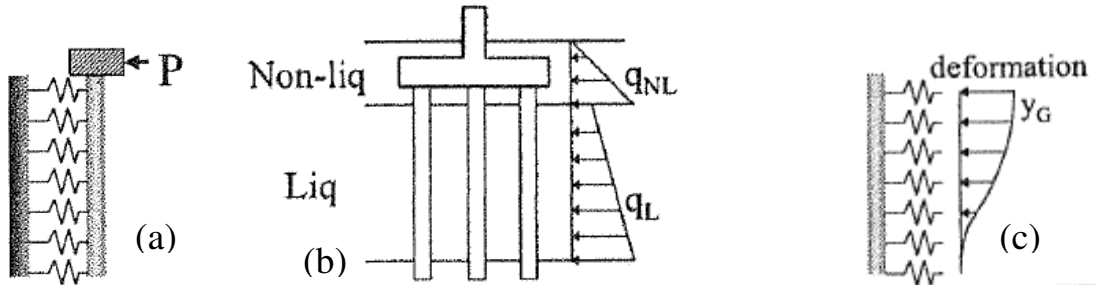

Figure 2.28 Different methods of modelling the effects of ground movements on a pile: (a) estimated load is applied at the pile head; (b) estimated earth pressure is applied throughout the length of the pile; (b) free field ground displacement is applied through a series of springs representing the soil stiffness (Uchida and Tokimatsu 2006)

As demonstrated by case studies and experimental tests in Sections 2.2 and 2.3 the pile behaviour and damage features are vastly different depending on the relative stiffness of the pile. Flexible piles move with the ground displacement, hence there are small relative displacements between the soil and the pile. Stiff piles on the other hand resist the ground movement. This causes large relative displacements which can cause the full passive pressure from the crust layer to be mobilised, as seen in the Landing Road Bridge case study and shake table and centrifuge tests on stiff piles. Clearly the loads acting on the pile are affected by the relative displacement between the soil and the pile. Therefore the seismic deformation method, where the loads on the pile are calculated based on the displacement of the ground, is more representative of the actual loading on the pile. The seismic coefficient methods, where the same loads are applied to the pile regardless of its relative stiffness, are less representative.

The simplified design-orientated methods used in this study use the seismic deformation method to model the effects of both cyclic and permanent ground displacements. Details of other seismic deformation type models will be explained briefly to determine the critical issues in simplified analysis.

2.4.2 Beam-spring methods

Seismic analyses of pile foundations using the seismic deformation model often use a beam representing the pile connected to a bed of springs representing the lateral soil stiffness and strength. The key considerations in the analysis are:

(a) The modelling of the stress-strain behaviour of the soil

(b) The degradation of soil stiffness due to liquefaction

(c) The ultimate pressure from both the crust and liquefied soil

(d) The magnitude of inertial load applied

(e) The magnitude of free field horizontal ground displacement applied

As there is a difference in both the pile loading and the soil characteristics during the cyclic and lateral spreading phases, it is necessary to consider these two phases separately. To illustrate the different approaches taken in pseudo static analysis by researchers, five analytical models are described with particular attention to the five considerations above.

Cubrinovski and Ishihara (2004) describe a three layer model with a liquefied layer sandwiched in between non-liquefied crust and base layers. The method uses a closed form solution to the beam on elastic foundation equation that is extended to account for non-linear behaviour using an equivalent linear approach. The method uses bi-linear p-δ curves for the crust and base soils, with the subgrade reaction coefficient calculated using an empirical formula based on SPT blow count and an ultimate pressure calculated as the Rankine passive pressure times a coefficient to account for the failure wedge of soil around a pile. The liquefied soil however is modelled using an equivalent linear p-δ curve, where the subgrade reaction is degraded by a factor β to account for the loss of soil stiffness due to liquefaction. The free field displacement in lateral spreading analyses is assumed to have a cosine distribution with a magnitude at the top of the liquefied layer of predicted using an empirical formula. The paper also gives guidance on the selection of the stiffness degradation coefficient for liquefied soil, suggesting β values between 1/50 and 1/10 for the cyclic phase and between 1/1000 and 1/50 for lateral spreading. Additionally it is recommended to adopt an ultimate pressure of 4-5 times the Rankine passive pressure for an equivalent wall in the crust and base layers. Key parameters are identified as the magnitude of ground displacement, the stiffness of the liquefied soil and the load form the crust layer. It is recommended that due to large uncertainties inherent in predicting these parameters a wide range of values should be considered in design. This method was extended to a more rigorous finite element model in Cubrinovski *et al*. (2006a).

In Tokimatsu *et al*. (2005) a simplified pseudo-static procedure is described for cyclic phase cases. Here the subgrade reaction is calculated using the SPT blow count and the earth pressure on an embedded footing is calculated as a combination of active and passive pressures on each side of the footing. The p-y curves are degraded for liquefaction by a factor β. Considering the interaction of inertial forces and kinematic forces, the paper recommends that for cases where the natural period of the superstructure is less than that of the ground, the pile response should be calculated by analysing the maximum inertial load and the maximum cyclic ground displacement acting at the same time. The maximum inertial load is calculated as the peak ground acceleration (PGA) times the axial load on the pile, and the maximum displacement is obtained through empirical methods such as that described in Tokimatsu and Asaka (1998) or from a free field site response analysis such as SHAKE. On the other hand, if the natural period of the structure is greater than that of the ground the response should be evaluated individually for the maximum inertial load and the maximum ground displacement, the response is then calculated as the square root of the sum of squares of the two values, as shown in Figure 2.29.

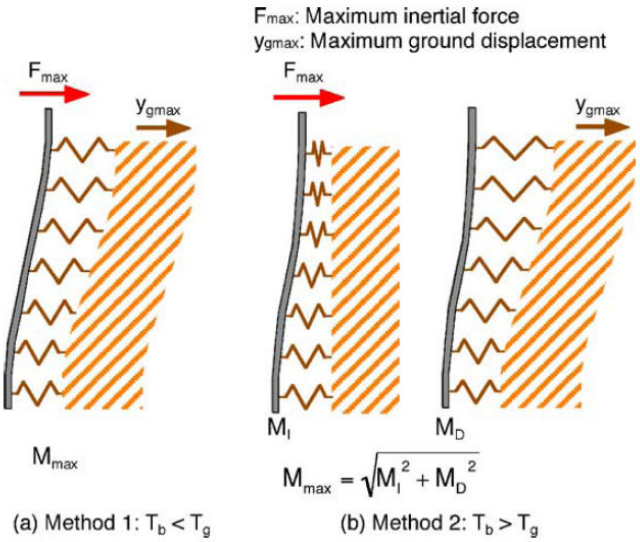

Figure 2.29 Combination of inertial and kinematic effects on piles (Tokimatsu et al. 2005)

The finite element (FE) beam spring method described by Liyanapathirana and Poulos (2005) for cyclic phase analysis recommends applying the maximum inertial force at the same time as the maximum cyclic ground displacement. The maximum inertial load is again calculated as the PGA times the axial load on the pile. A 1D free field site response analysis is conducted to determine (a) the maximum cyclic ground displacement, and (b) the minimum effective stresses throughout depth. These minimum effective stresses are used to calculate the soil spring stiffness using Mindlin's equation, and the ultimate pressure is limited based on the limit proposed by Broms (1964). The pseudo-static analytical model is shown schematically in Figure 2.30. This method was used in a parametric study, where it was found that inclusion of a pile cap mass significantly increases the bending moment in the pile. When analyses were repeated without considering pore pressure effects, it was found that the bending moments and relative displacements were less; however the maximum cap-mass acceleration was higher.

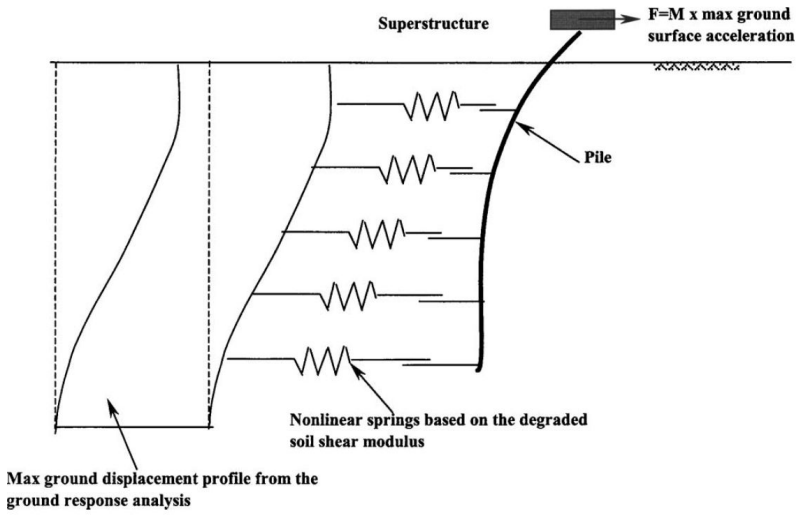

Figure 2.30 *Beam on spring foundation model for pseudo-static analysis (Liyanapathirana and Poulos 2005)*

O'Rourke *et al.* (1994) described a pseudo-static method for lateral spreading analysis by applying a ground displacement to a series of bi-linear springs representing soil stiffness. Here the subgrade reaction is calculated using the relationship of Terzaghi (1955), and the ultimate pressure is calculated using the ultimate lateral bearing capacity factors of Hancock (1961). To account for the effects of liquefaction both the subgrade reaction and the ultimate pressure are divided by R_f, a reduction factor which is greater than one. It is noted that because the mechanical behaviour of liquefied soil is complex, a relatively simple procedure was developed to account for soil strength and stiffness. This permits evaluation of important trends and influential parameters without introducing undue complexity.

The pseudo-static method presented by Wang and Reese (1998) consists of a beams spring model using non-linear *p-y* curves. It is noted that the key point is dealing with soil movement in the analysis of piles is the relative displacement between the soil and the pile. If the pile deflection is less than the soil movement at a point along the pile the soil gives the pile a driving force. If the pile deflection is more than the soil movement the soil is now resisting the pile movement. The pseudo-static method accounts for the relative displacement in the *p-y* curves used, also for the liquefied layers the residual strength of the liquefied soil was used as ultimate pressure acting on the pile. The residual strength of a soil is the steady state strength at which the soil will continue to deform without change in the resistance to deformation, and it is calculated using a correlation with SPT blow count found in Seed and Harder (1991). Wang and Reese note that the weakness in simplified methods is not in the modelling or the

ability to make the computations but in predicting (1) when the soil will liquefy, (2) the residual strength of liquefied soil, and (3) the magnitude of ground movement.

2.4.3 Advanced methods

Advanced dynamic time history analysis has many advantages over simplified analysis. The effects of seismic soil-pile interaction, excess pore water pressure and soil liquefaction can be evaluated directly, rather estimated using empirical correlations. The accuracy of such analysis methods has been demonstrated by many studies, and provided there is sufficient data on the *in-situ* condition of the soil and sufficient user expertise regarding the nature of the phenomena and the numerical procedure, advanced methods are suitable for performance based assessments of important structures. To illustrate salient features of advanced modelling of pile foundations in liquefiable soil four techniques described in literature are discussed.

The effects of excess pore water pressure can be dealt with by using either a fully coupled analysis, where the soil materials are treated as two-phase soil-water materials and the effects of pore water are evaluated directly, or by coupling the pore water pressure to an external model.

Uzuoka *et al*. (2007) and Uzuoka *et al*. (2006) describe the simulation of a case study during the Kobe earthquake and large scale shake table test respectively using a fully coupled 3D finite element analysis using the computer code LIQCA. The governing equations for the model are based on Biot's porous media theory (1962). The authors note that while many formulations exist for solving Biot's equations the differences between the methods are not significant for liquefaction problems. Rather, the key consideration is the constitutive model of the soil, which affects the results significantly. The constitutive model is based on elastoplastic kinematic hardening law, and the stress-strain characteristics of the soil are based on the current level of strain in the soil.

Cubrinovski *et al*. (2005) use a 3D fully coupled analysis of a large scale shake table experiment using the computer code DIANA-J. An advanced constitutive soil model (Cubrinovski and Ishihara 1998b), that uses an elastoplastic deformation law is employed in the analysis. The stress-strain behaviour of the soil is calculated depending on the current

density and confining pressure. The plasticity formulation of the model is characterised by many modifications of and departures from the classical plasticity framework. The most important features of this formulation are:

- A vanishing elastic region with the stress point being always coincident with a point-yield surface, providing a purely kinematic hardening rule;
- Discrete memory for the loading, unloading and reloading surfaces with mixed hardening rule for their evolution; and
- Plastic flow dependent on the stress-rate direction, with the failure surface used as a plastic potential.

This is an advanced analysis that permits consideration of excess pore water pressure, flow of pore water through the soil and detailed modelling of the stress-strain behaviour of soils. The accuracy of the analysis has been extensively verified through case studies (Cubrinovski et al. 2001) and large-scale shake table tests (Cubrinovski et al. 2005).

Finn and Fujita (2002) describe a 3D finite element analysis procedure using an effective stress version of the program PILE-3D. The boundary conditions of the wave equation are relaxed, thus reducing the computational effort. It is assumed that the response is governed by shear waves in the x-y and y-z planes (see Figure 2.31) and compressional waves in the direction of the shaking. Deformations in the vertical direction and normal to the direction of shaking are neglected. The constitutive soil model uses an equivalent linear method to model the non-linear hysteretic behaviour of the soil. It assumes the hysteretic behaviour can be modelled by secant shear moduli and viscous damping ratios that are compatible with current levels of shear strain. The compatibility among the secant shear modulus, damping ratio and shear strain is enforced at each time step.

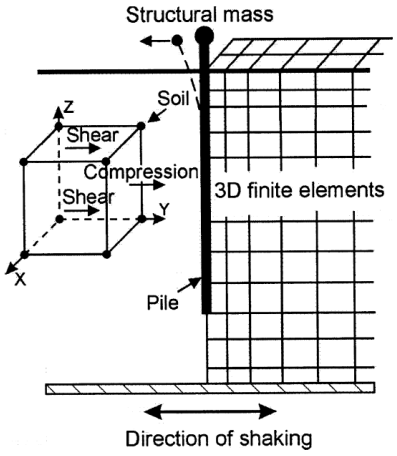

Figure 2.31 Quasi-3D model used in PILE-3D analysis (Finn and Fujita 2002)

Boulanger *et al*. (2004) described the simulation of centrifuge tests with a 2D dynamic finite element analysis. In the analysis sand was modelled using a mixed stress-strain space, pressure dependent, multiple yield surface constitutive model, whereas clay was modelled using a pressure independent constitutive model. The model parameters were found as follows; the maximum shear modulus was estimated from the shear wave velocity, the parameters for the yield surfaces were found based on G/G_{max} relationships and ultimate strength parameters and the liquefaction resistance parameters were specified to produce a desired cyclic resistance ratio. The soil elements were coupled with an excess pore water pressure model and connected with zero-length soil springs at each node. *p-y* springs were used for the subgrade reaction, with *t-z* and *q-z* springs for the skin friction and tip resistance respectively.

2.5 Conclusions

Damage to piles due to liquefaction has occurred in previous earthquakes resulting in damage to many bridges and buildings. Previous research has examined the characteristics and failure mechanisms of piles in liquefiable soils by documenting case histories, conducting experimental tests and developing analytical models. Key conclusions include:

- The cyclic phase and lateral spreading are two distinct phases in the seismic response of piles in liquefiable soil.
- For both cases the pile behaviour depends on the stiffness of the pile relative to the liquefied soil. Relatively flexible piles move with the ground; whereas relatively stiff piles resist the ground movement.

- In the cyclic phase, large cyclic ground displacements and inertial loads occur. Piles suffered damage at the pile head and at the interface between liquefied and non-liquefied soil layers.
- Pile damage has been observed at large depths and in piles without superstructures, therefore cyclic ground displacements cause significant loads. Experimental tests show that the damage observed is strongly affected by the magnitude of the cyclic ground displacements.
- Tests examining the interaction of kinematic and inertial loads suggest that the effects of soil displacement and inertial load tend to be in phase if the natural period of the superstructure is shorter than that of the ground, but out of phase if it is longer. For liquefied soils, where the natural period of the ground often elongates, the kinematic and inertial loads tend to act at the same time.
- In the lateral spreading phase the soil has lost stiffness and large unilateral ground displacements occur. Inertial loads are small during this phase, and damage is again concentrated at the interface between liquefied and non-liquefied soil layers.
- During lateral spreading stiff piles can attract large loads from overlying non-liquefied layers, these forces are much larger than drag forces from the liquefied soil.
- The nature of lateral spreading causes different lateral ground displacements to be applied to different piles connected at the same pile cap. This causes different lateral loads on the piles, resulting in distinct damage features depending on the location of the pile in the group.
- Pile head fixity has an important role; fixed head piles suffered damage at the pile head, pinned head piles did not. The stiffness of the pile cap also affects the pile behaviour.
- Many simplified methods exist to model the pile foundations in liquefiable soil; seismic deformation methods are the most appropriate as they take into account the magnitude of ground displacement and the relative stiffness of the pile.
- Pseudo static beam-spring models based on the seismic deformation method can capture the behaviour of piles in liquefied soil. The key consideration is accounting for the large uncertainties present in a simplified analysis, not the modelling details.
- Advanced time-history methods are available that can accurately model the development of liquefaction and the subsequent soil-structure interaction between the soil-pile-structure systems.

3. Simplified pseudo-static analysis

3.1 Introduction

The phenomenon of soil liquefaction and lateral spreading is complex and predictions of the seismic response of piles in liquefied soil are subject to a high level of aleatoric uncertainty. This suggests that when simplified analysis is performed, the key consideration is not the modelling technique itself; rather it is dealing with the uncertainties in a sensible manner. Many simplified design orientated approaches are available to analyse the seismic response of pile foundations, some of these are described in Chapter 2.

In this chapter a pseudo-static analysis procedure proposed in Cubrinovski *et al*. (2006a) is examined somewhat in detail. This analysis uses a beam spring model and can be performed using common site investigation data such as the SPT blow count, yet it captures the basic mechanism of pile behaviour. Presented here are details of the adopted modelling technique and its application to a case study of a bridge foundation in liquefiable soil. The key input parameters of the model, namely the magnitude of applied free field ground displacement, the degradation of soil stiffness and strength due to liquefaction and the magnitude of inertial load from the superstructure are varied parametrically to identify important features of the response. The objective of this chapter is to determine how variations in these key parameters affect the soil-pile interaction and to emphasise the need to consider a wide range of values of input parameters when simplified analysis is performed.

3.2 Beam – spring model

3.2.1 Analytical model

The analytical model used in this chapter is based on a simplified three layer model described in Cubrinovski and Ishihara (2004) that consists of a non liquefiable crust layer, liquefied layers and a non-liquefied base layer. The original model used a closed form solution to solve a three layer problem; here a more rigorous model was adopted where a finite element (FE) beam-spring model is used to incorporate more complex soil layering. Figure 3.1 shows the analytical model: the pile is modelled as a beam connected to a series of springs representing the lateral stiffness of the soil. The effects of liquefaction on the soil are accounted for by degrading the stiffness of the soil springs and limiting the lateral force in the liquefied layers.

The complex dynamic forces applied to piles in liquefied soil are approximated by the sum of two static loads applied to the pile:

(1) Kinematic loads from the soil movement are applied through free field ground displacements acting on a series of soil springs, as shown in Figure 3.1. These displacements can represent either cyclic ground displacements or lateral spreading displacements of liquefied soils. Note that these are free field ground displacements unaffected by the presence or response of the pile foundation.

(2) Inertial loads from the superstructure are modelled as a lateral point load applied at the pile head. It was adopted in the analysis that this load acts in the same direction as the applied ground displacement.

In the pseudo-static analyses, the cyclic phase of the loading and subsequent lateral spreading phase were considered separately since the loads and soil conditions (stiffness and strength) are greatly different between these two phases.

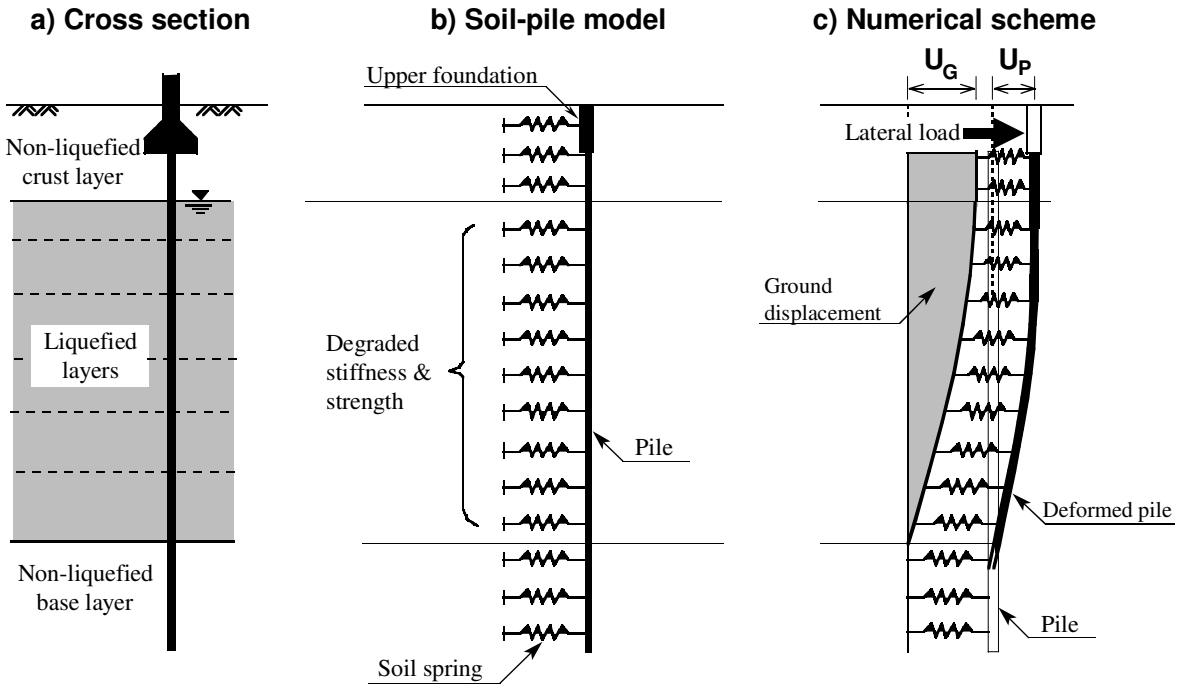

Figure 3.1 Simplified pseudo static analytical model (after Cubrinovski and Ishihara 2004)

3.2.2 Input parameters

The input parameters of the model are summarized in Figure 3.2 for a three layer model configuration. Soil springs are represented using bi-linear p-δ relationships, with an initial stiffness k and ultimate pressure p_{max}. Here δ represents the relative displacement between the pile and the soil. In liquefied soil layers the loss of stiffness is represented by a degradation factor, β. The pile is modelled with a series of beam elements and a tri-linear moment-curvature (M-ϕ) relationship. The three points on the M-ϕ curve correspond to the cracking, yielding and ultimate moments of the pile. The FE model allows complex soil layering to be taken into account; changes in soil stiffness between layers and different pile diameters throughout the depth can be incorporated easily into the model.

The external loads on the pile are modelled using a lateral ground displacement U_G and an inertial load F. The ground displacement applied to the pile can take any form throughout the soil profile; U_G represents the maximum lateral ground displacement at the top of the liquefied soil layer and also represents the movement of the crust layer in the free field.

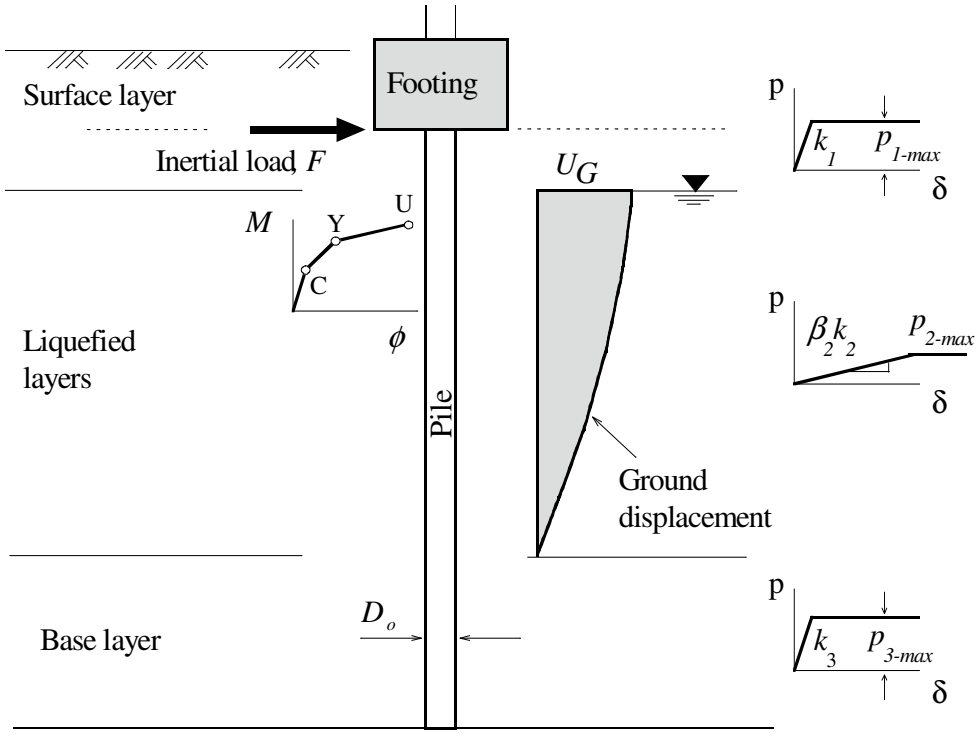

Figure 3.2 Input parameters and characterisation of non-linear behaviour for pseudo-static analysis (after Cubrinovski and Ishihara 2004)

3.2.3 Key parameters and uncertainties

Cubrinovski and Ishihara (2004) identified the following key parameters affecting the pile response:

- The stiffness and strength of the liquefied soils, β and $p_{2\text{-}max}$
- The ultimate pressure exerted by the crust layer, $p_{1\text{-}max}$
- The magnitude of the lateral ground displacement, U_{G2}
- The inertial load applied, F

The intrinsic uncertainties associated with piles in liquefiable ground are directly reflected on these key parameters. Therefore for the analysis of piles in liquefiable soil these parameters should not be uniquely determined; rather a range of values should be considered. For this reason a parametric study was performed on a case study to examine how variations in these four key parameters affect the pile response.

3.3 Case study – Fitzgerald Bridge

3.3.1 Overview

To illustrate the effects of variation in key parameters on the pile performance, parametric studies were conducted on a case study of twin bridges crossing the Avon River in Christchurch, New Zealand. The Fitzgerald Avenue Twin Bridges, shown in Figure 3.3, cross the Avon River and carry three lanes of southbound traffic on the east bridge and two lanes of northbound traffic on the west bridge. Both bridges are supported by piled abutments on the banks with a central piled pier at the mid-span. According to the initial investigations, the existing piles were founded on potentially liquefiable soils.

Figure 3.3 Fitzgerald Avenue Twin Bridges over the Avon River

The bridges have been identified as an important lifeline for post-disaster emergency services and recovery operations. To avoid structural failure of the foundations or significant damage causing loss of function of the bridge in an anticipated earthquake event, a structural retrofit has been proposed by the Christchurch City Council. In conjunction with bridge widening, this retrofit involves strengthening of the foundation with new large diameter bored piles to be installed; the location of the new piles are shown schematically by the solid circles on the plan of the site shown in Figure 3.4. The new piles will be connected rigidly to the existing foundation and superstructure, and founded into deeper strata consisting of non-liquefiable soils.

3.3.2 Soil conditions

Detailed investigations were conducted at several locations at the site using SPT and CPT, as indicated in Figure 3.4. The results of these field tests reveal the highly variable stratigraphy and penetration resistance of the investigated locations. Testing was conducted on the north and south banks of the river, at locations on both the east and west sides of the bridge and in between the two bridges. The site investigation data is summarised in Figure 3.4, showing the inferred range of SPT blow counts at the four corners of the bridge. Figure 3.5 shows the assumed soil layering at each corner of the bridge identified using the site investigation data.

The occurrence of liquefaction at the site was assessed based on the results of the *in situ* testing and by considering the ground shaking hazard. In general the soil on the north bank is

looser and more susceptible to liquefaction than the soil on the south bank. This is consistent with the assumed nature of soil deposition at the site; the north bank is on the inside of a bend in the river while the south bank is on the outside. As the river has progressed soil has been eroded from the outside of bends and deposited on the insides, thus the soil on the inside of a bend is likely to have been laterally accreted in a low energy environment.

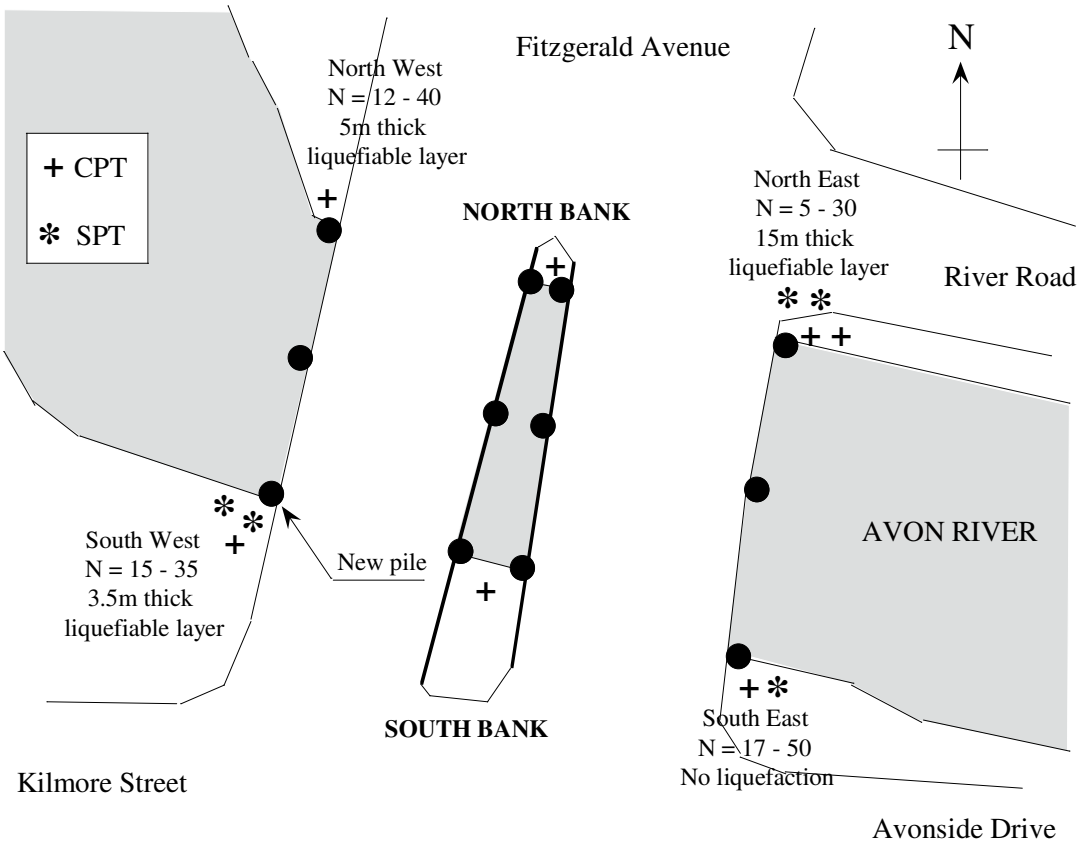

Figure 3.4 Plan view of the bridge site, showing site investigation locations

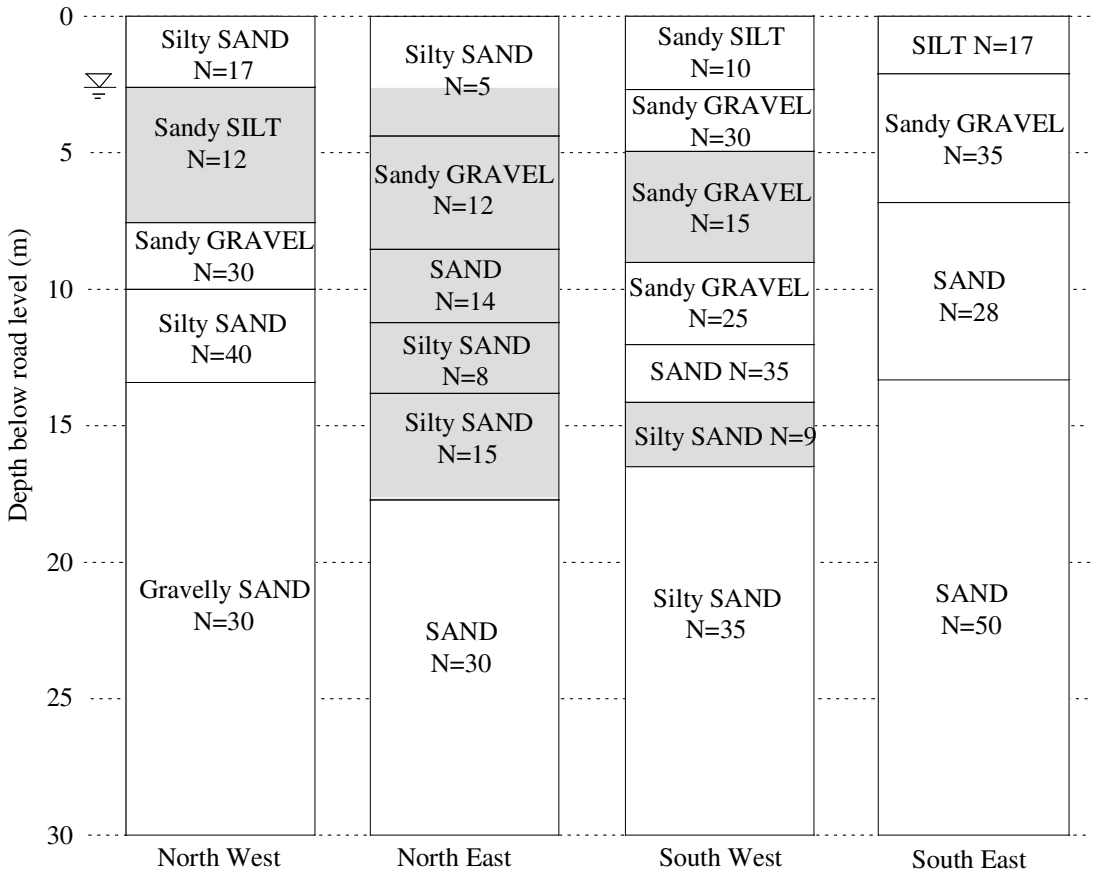

Figure 3.5 Summarised soil profiles and assumed SPT blow counts for locations at the four corners of the bridge. The shaded areas indicate soil layers deemed to be liquefiable.

The worst soil conditions were encountered at the North-East corner; the analysis in this chapter is based on the soil properties at this corner and hence represents a conservative assessment. Here the soil between 2.5m and 17.5m is considered to be liquefiable, with layers of silty sand, sandy gravel, sandy silt and sand, with a dense sand base layer below 17.5m depth. Figure 3.6 shows the results of SPT and CPT testing; the assumed soil profile and SPT blow counts used in the analysis are also shown. From the CPT results at the north east corner, a fines content of approximately 10% was inferred for the liquefiable soil.

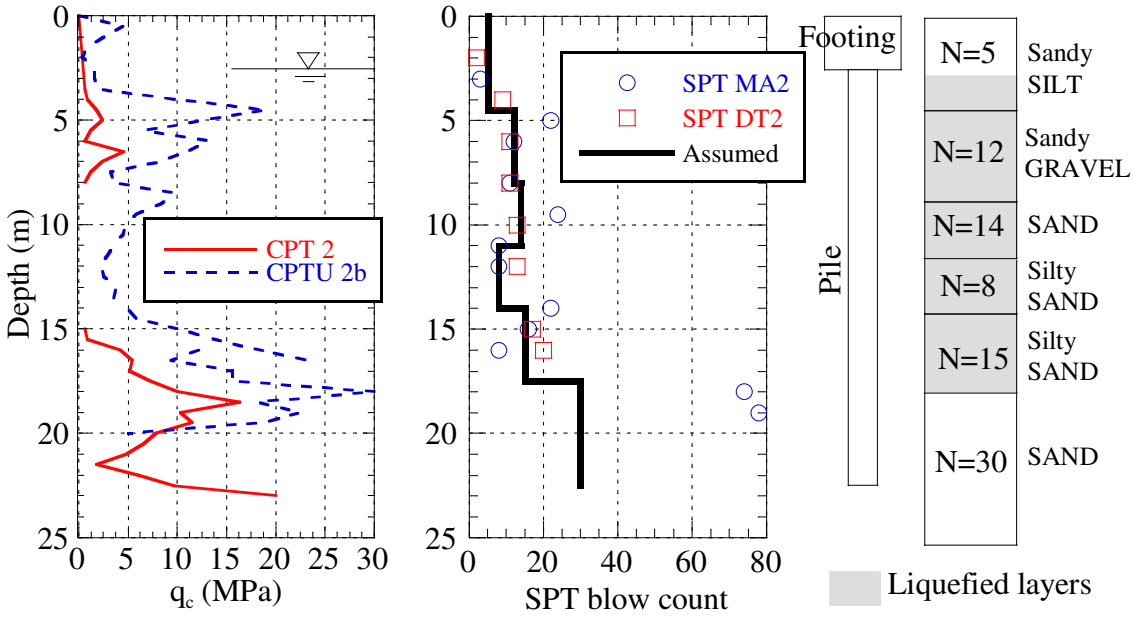

Figure 3.6 *CPT and SPT results for the north – east corner*

3.3.3 Bridge foundation

Figure 3.7 shows a cross section of the east bridge; the abutments and piers are supported by driven reinforced concrete piles connected to a reinforced concrete pile-cap at the river level. The existing piles are approximately 10-11m in length and 0.3m in diameter. The central pier is supported by 8 existing piles at 5*D* spacing; the abutments are supported by four vertical piles and five raked piles at 4*D* spacing. The two bridges have identical foundations and the river level is approximately 2.5m below the road level.

The proposed new piles will be founded at a depth below the expected depth of liquefaction and installed outside the existing pile cap. In conjunction with proposed widening of the bridge the pile cap will be extended and the new piles will be rigidly connected to the superstructure. The new piles will be steel-encased reinforced concrete piles designed to carry the entire load from the existing bridge and any additional loads from the bridge widening. Shown in Figure 3.7 are the proposed piles; they are 1.2m in diameter under the abutments and 1.5m in diameter under the central pier.

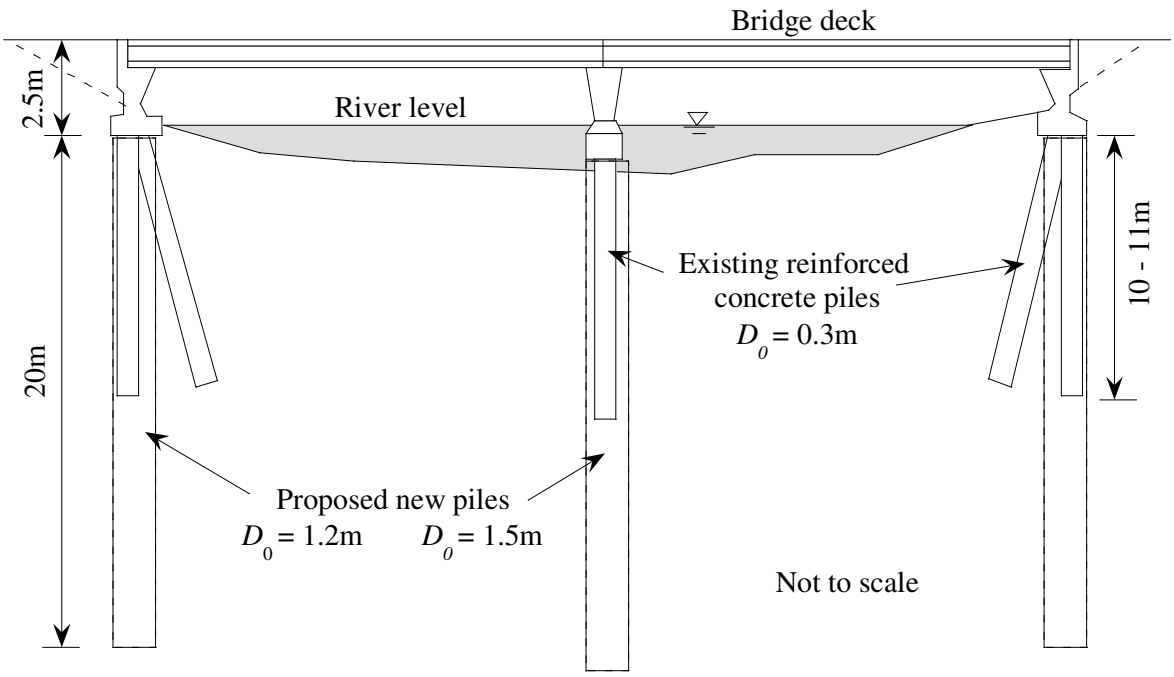

Figure 3.7 Bridge cross section showing existing piles and proposed new piles

3.3.4 Seismic hazard

Previous seismic hazard studies for Christchurch (Dowrick et al. 1998; Stirling et al. 2001) indicate that the most significant contribution to the ground shaking hazard arises from a magnitude 7.2-7.4 event on the strike-slip Porters Pass fault, which is located at a distance of about 40-60km from the site. Stirling *et al*. (2001) give the following peak ground acceleration values for Christchurch:

- 0.25g in a 150 year event
- 0.37g in a 475yr event and
- 0.47g in a 1000yr event.

With regard to the importance level of the bridge as a lifeline, the loadings standard NZS1170.5 requires an ultimate limit state (ULS) design seismic event with an annual probability of exceedance of 1/2500, i.e. a 2500 year event. This corresponds to a peak ground acceleration of 0.44g, as calculated in NZS1170.5 based on the soil conditions and period of the structure. This is roughly in agreement with the above mentioned peak ground acceleration from Stirling *et al*. (2001).

3.3.5 Determination of material parameters

As the procedure is a simplified, design orientated approach, all input parameters can be determined using empirical correlations with common site investigation data. The input parameters can be divided into the four categories; soil properties (k, p_{max}), effects of liquefaction on the soil stiffness and strength (β, S_u), pile properties (D_0, M-ϕ curve) and external loads (U_G and F).

Soil properties

The stiffness and ultimate pressure of the soil springs were evaluated using correlations with the SPT blow count, N. The stiffness was calculated by first evaluating the subgrade reaction coefficient, κ, using an empirical formula (Architectural Institute of Japan 2001):

$$\kappa = 56\, N\, D_o^{-3/4} \quad [\mathrm{MN/m^3}] \tag{3.1}$$

where N is the SPT blow count and D_o is the pile diameter in cm. The stiffness, k, is then evaluated by the formula

$$k = \kappa\, D_0\, l \tag{3.2}$$

where l is the spacing between nodes or the length of the beam element used in the FE analytical model. The ultimate pressure, p_{max}, exerted by the soil on the pile in non-liquefied soil is given by the expression

$$p_{max} = \alpha_u\, p_p(z) \tag{3.3}$$

where $p_p(z)$ is the Rankine passive pressure as a function of depth and α_u is a factor introduced to account for the difference in lateral pressure between a single pile and an equivalent wall. Note that α_u may take a value as high as 4.5. The Rankine passive pressure is calculated as

$$p_p(z) = K_p \sigma'_v \tag{3.4}$$

where σ'_v is the vertical effective stress and K_p is Rankine passive earth pressure coefficient calculated as

$$K_p = \tan^2(45 + \phi/2) \tag{3.5}$$

where ϕ can be estimated, for example as

$$\phi = 20 + (20N_{1(60)})^{0.5} \tag{3.6}$$

and $N_{1(60)}$ can be calculated using the method of Liao and Whitman (1986)

$$N_{1(60)} = N\left(\frac{98}{\sigma_v'}\right)^{0.5} \tag{3.7}$$

Here $N_{1(60)}$ is an SPT blow count normalised for the effective overburden stress corresponding to 60% energy of the theoretical free fall energy. In Table 3.1 the corrected blow count and calculated friction angle is shown for each layer at the North East corner.

Table 3.1 Soil profile used in analysis for north east corner

Layer #	**Description**	**Depth (m)**	**SPT N value**	**σ'_v (kPa)**	**N_1**	**ϕ**
1	Crust layer	0 - 2.5	5	22.4	10	34
2	Sandy SILT	2.5 – 4.5	5	53.0	7	32
3	Sandy GRAVEL	4.5 – 8	12	75.4	14	37
4	SAND	8 – 11	14	101.9	14	37
5	Silty SAND	11 -14	8	126.3	7	32
6	Silty SAND	14 – 17.5	15	152.8	12	36
7	SAND	17.5 – 22.5	30	187.4	22	41

Effects of liquefaction on soil stiffness and strength

In liquefied soil the stiffness k is degraded by a factor β which is less than one. With reference to case studies and experimental tests (Cubrinovski et al. 2006b; Ishihara and Cubrinovski 1998; O'Rourke et al. 1994; Orense et al. 2000; Tokimatsu et al. 2005; Yasuda and Berrill 2000), the stiffness degradation of liquefied soils can be assumed to vary between β = 1/10 and 1/50 for the cyclic phase cases, and between β = 1/50 and 1/1000 for lateral spreading cases. The prediction of the liquefied soil stiffness is very difficult and depends on many factors, including the density of the soil, development of excess pore pressures, the magnitude and rate of ground displacement and the drainage conditions. Furthermore, full scale shake table tests (Cubrinovski et al. 2006b) show that the stiffness of liquefied soils varies considerably during the course of both the cyclic and lateral spreading phases.

The ultimate pressure exerted on the piles from the liquefied soil is also subject to uncertainty. The interaction in the liquefied layer can be treated in a simplified manner by an equivalent linear p-δ relationship with a degraded stiffness and no limiting ultimate pressure. Alternatively and more rigorously, a limit can be placed on the pressure exerted by the liquefied soil. The approach used herein is to define the ultimate pressure from the liquefied layers, $p_{2\text{-}max}$, using the undrained or residual strength of the sandy soils, S_u. Here S_u is evaluated from empirical correlation with SPT value originally proposed by Seed and Harder (1990) as shown in Figure 3.8. The data in this figure were back calculated from case history observations during previous earthquakes in which flow slides occurred. Post-earthquake static stability analyses were conducted by many researchers (Idriss and Boulanger 2007; Olson and Stark 2002; Seed 1987; Seed and Harder 1990) investigating liquefaction flow slides; the undrained shear strength was estimated by back calculating a value of S_u based on the deformed geometry after the event. Hence in this plot, each point represents the estimate of S_u for one case history. Since the scatter of the data is quite significant, an upper ($S_{u\text{-}ub}$) and lower bound ($S_{u\text{-}lb}$) values as indicted in Figure 3.8 were used to cover the range of values. Table 3.2 summarises the soil properties used in the analysis of cyclic and lateral spreading cases, as calculated according to the expressions and procedures outlined above.

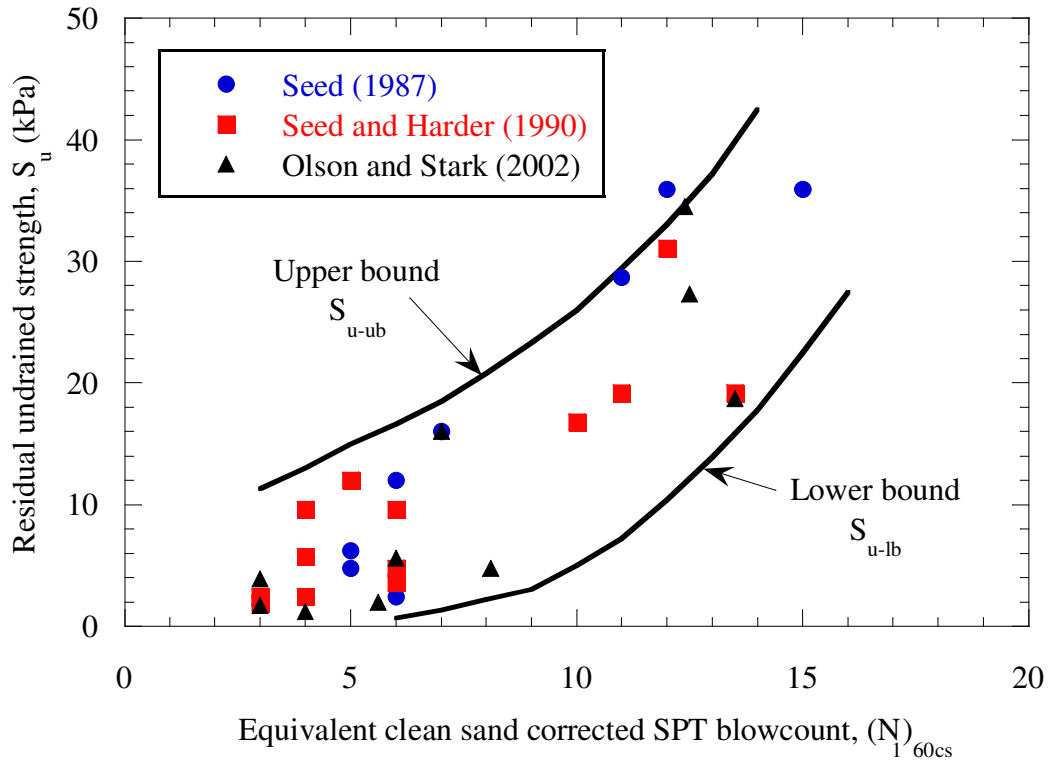

Figure 3.8 *Empirical chart used to evaluate ultimate pressure exerted by liquefied soil through undrained shear strength (after Idriss and Boulanger 2007)*

Table 3.2 *Soil properties used in parametric study*

	Description	**Stiffness, *k* (kN/m)**				**Ultimate pressure, $p_{2\text{-}max}$ (kPa)**	
		Cyclic phase		**Lateral spreading**		$S_{u\text{-}lb}$	$S_{u\text{-}ub}$
		β_{lb}=1/10	β_{ub} =1/50	β_{lb} =1/50	β_{ub} =1/1000		
1	Crust layer	1853				K_p = 3.6	
2	Sandy SILT	185	37.1	37.1	1.85	2	28
3	Sandy GRAVEL	445	89.0	89.0	4.45	17	43
4	SAND	519	104.8	104.8	5.19	17	43
5	Silty SAND	297	59.3	59.3	2.97	2	28
6	Silty SAND	556	111.2	111.2	5.56	10	33
7	SAND	11121				410	

Pile properties

The yielding, cracking and ultimate points of the pile were calculated by assuming that the concrete and reinforcing steel are elastic-perfectly plastic materials with bi-linear stress strain relationships. By specifying the pile cross section and characteristics (dimensions, area and position of reinforcement, Young's modulus and strengths of materials, prestress level, axial force) the tri-linear moment curvature relationship of the pile was calculated. The three points are defined as follows:

(1) Cracking is the point where the tensile stress in the concrete exceeds the concrete tensile strength.

(2) Yielding is the point where the yield stress of the reinforcement exceeds the reinforcement yield strength.

(3) Ultimate is the point where compressive strain in the concrete is exceeds the ultimate concrete compressive strain level, usually in the range between 0.0025 and 0.0035.

The moment curvature relationship for the new 1.2m diameter pile was calculated assuming 30MPa concrete, 500MPa steel reinforcement at a 0.8% longitudinal reinforcement ratio and a 10mm thick steel casing with a strength of 250MPa. The axial loads on the piles are preliminary estimates; Figure 3.9 shows the calculated M-ϕ relationships for both the serviceability limit state (SLS) and the ultimate limit state (ULS) axial loads to give an indication of the effect of increasing axial load on the pile bending capacity. For consideration of the seismic response an axial load of 1600kN was used.

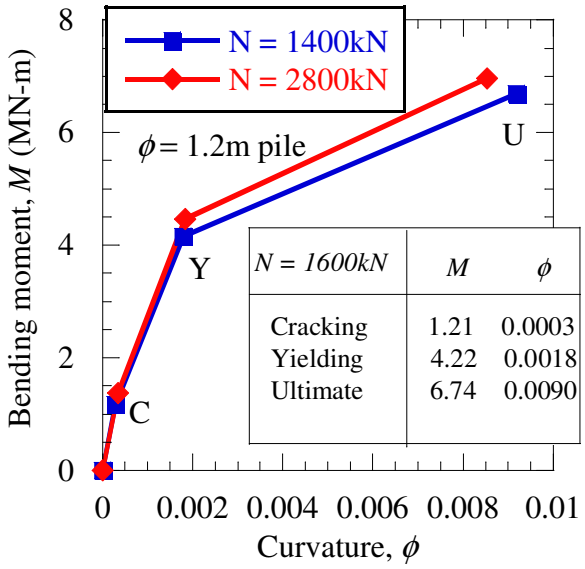

Figure 3.9 *Moment curvature relationship for the new 1.2m pile*

External loads

Two external loads are applied to the pile: an inertial force at the pile head and a ground displacement. The level of inertial load applied at the pile head can be calculated as the ground acceleration times the tributary mass of the superstructure taken by the pile. The level of acceleration can either be the peak ground acceleration or a lesser value. For the pile at the north east corner, the maximum inertial load considered was calculated as the tributary superstructure mass of 1600kN multiplied by the peak ground acceleration of 0.44g giving a maximum inertial load of 704kN.

In the analysis the lateral ground displacement can represent either cyclic displacements during the shaking phase or a permanent displacement at the end of the spreading phase. Lateral spreading displacements were modelled as having a cosine distribution throughout the liquefied layers, with a displacement at the ground surface, U_G, describing the magnitude of the ground movement. Many empirical methods exist for predicting this displacement (e.g. Ishihara et al. 1997; Tokimatsu and Asaka 1998; Youd et al. 2002) however it is very difficult to make an accurate prediction. The lateral spreading distance at the north east corner was predicted using the method of Youd *et al.* (2002). A free face height of 2.5m was assumed, and a displacement of 2.2m was calculated at the riverbank. Due to the considerable uncertainty in predicting the ground displacement Youd *et al*. suggest a factor of 2 be used for displacements predicted using their model to cover the range of expected values. With this in

mind, and considering the large differences between different empirical methods, a wide range of values were considered in the parametric study.

Maximum cyclic ground displacements in liquefied soils during the cyclic phase were estimated using a simplified procedure described in Tokimatsu and Asaka (1998). The procedure is based on observations from previous earthquakes, where cyclic shear strains in liquefied soil layers were evaluated from analysis of strong motion records and detailed surveys of piles in level ground and then plotted against SPT value, as shown in Figure 3.10. The chart is essentially equivalent to the conventional SPT-based charts for evaluation of liquefaction; the cyclic stress ratio τ_{av}/σ'_{vo} on the y-axis is calculated using the standard method of Seed and Idriss (Youd et al. 2001).

To estimate the cyclic ground displacement, for each liquefied soil layer the cyclic shear strain is first evaluated using the chart. Then, these strains are integrated throughout the soil profile to obtain a cyclic ground displacement profile. Shown in Figure 3.10 is the calculation of the induced cyclic shear strain for a soil layer with a corrected SPT blow count of N_1 =14 and a cyclic stress ratio of τ_{av}/σ'_{vo} = 0.46. For the North-East corner soil profile, Table 3.3 and Figure 3.11 show the maximum shear strains and corresponding maximum cyclic horizontal ground displacements calculated using the procedure described above.

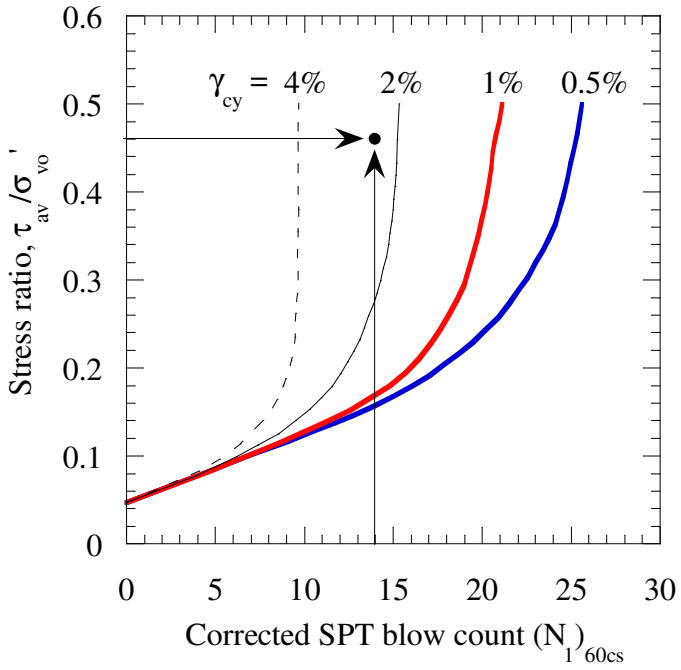

Figure 3.10 Empirical chart used to evaluate cyclic ground displacements through induced shear strains (after Tokimatsu and Asaka 1998). Shown is the shear strain evaluated for a soil layer with N_1 =14 and τ_{av}/σ_{vo}' = 0.46

Table 3.3 Liquefaction induced cyclic ground displacement calculations

Layer #	Description	Liq.	Cyclic stress ratio τ/σ'_v	Max. cyclic shear strain γ_{cyc} (%)	Disp. in each layer (m)	Cumulative disp. at top of layer (m)
1	Crust layer	No	-	-	-	0.395
2	Sandy SILT	Yes	0.342	2*	0.04	0.395
3	Sandy GRAVEL	Yes	0.411	2	0.07	0.355
4	SAND	Yes	0.437	2	0.06	0.285
5	Silty SAND	Yes	0.440	4	0.12	0.225
6	Silty SAND	Yes	0.430	3	0.105	0.105
7	SAND	No	-	-	-	0

* The Tokimatsu and Asaka (1998) procedure predicted a maximum cyclic shear strain of 4% for this layer. A value of γ_{cyc} = 2% was used in the calculation however as it is not envisioned that such a large strain would develop immediately below the crust layer.

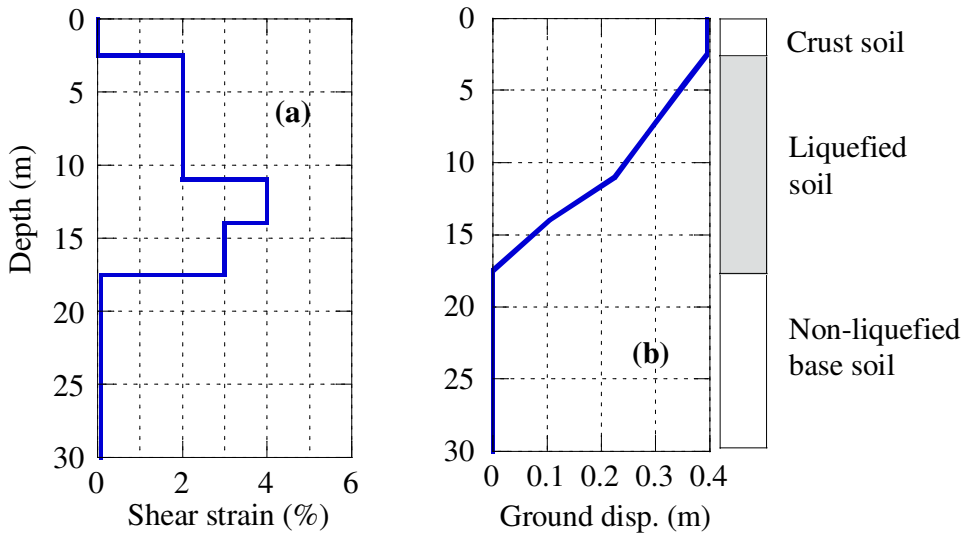

Figure 3.11 Liquefaction induced cyclic ground deformation: (a) maximum cyclic shear strains, (b) maximum cyclic ground profile

3.4 Parametric study

3.4.1 Overview

The seismic response of the proposed 1.2m diameter pile at the north-east corner is evaluated using the pseudo static approach described in Section 2. The key parameters in the procedure identified in Section 2.3 are varied to account for uncertainties in the analysis; this is to gain insight into how variations in these parameters affect the analysis results. In all analyses the properties of the pile, the crust and base soil layers were kept constant.

The two phases in the response, the cyclic phase and lateral spreading, were treated separately. In cyclic phase analyses, an inertial load was applied at the pile head in addition to the ground displacement shown in Figure 3.11b. In contrast, the lateral spreading cases have no inertial load and the ground displacement has a cosine profile throughout the liquefied layers with a magnitude U_G at the top of the liquefied layer. Lateral spreading cases with reduced inertial loads were also considered but are not discussed herein.

3.4.2 Typical results

In order to demonstrate key features of the pile response, one analysis case is described in detail. Figure 3.12 shows the results of a lateral spreading analysis, where the magnitude of free field ground displacement was one metre, and relatively high degradation of stiffness and strength was used with β = 1/1000 and $p_{2\text{-}max} = S_{u\text{-}lb}$ (which corresponds to a range of 2-17kPa throughout the liquefied layers). Figure 3.12a shows the computed bending moment distribution with reference to the cracking, yielding and ultimate moments of the pile. It can be seen that the maximum moments occur at the pile head and at the interface between the liquefied and base layers, and that the bending moment exceeds the yield level at the pile head. Figure 3.12b shows the pile displacement compared to the free field ground displacement. The pile exhibits behaviour typical of stiff piles, and resists the large lateral movement of the surrounding soils. The resulting relative displacement between the soil and the pile is therefore quite large as shown in Figure 3.12c. The dashed line in this figure indicates the relative displacement δ_y at which yielding occurs in the soil or the displacement at which $p_{2\text{-}max}$ has been reached in the bi-linear relationship. Hence the shaded areas indicate parts of the soil profile where the relative displacement exceeds the yield level of the soil; here the pressure acting on the pile has reached the maximum level as defined by the p-δ relationship.

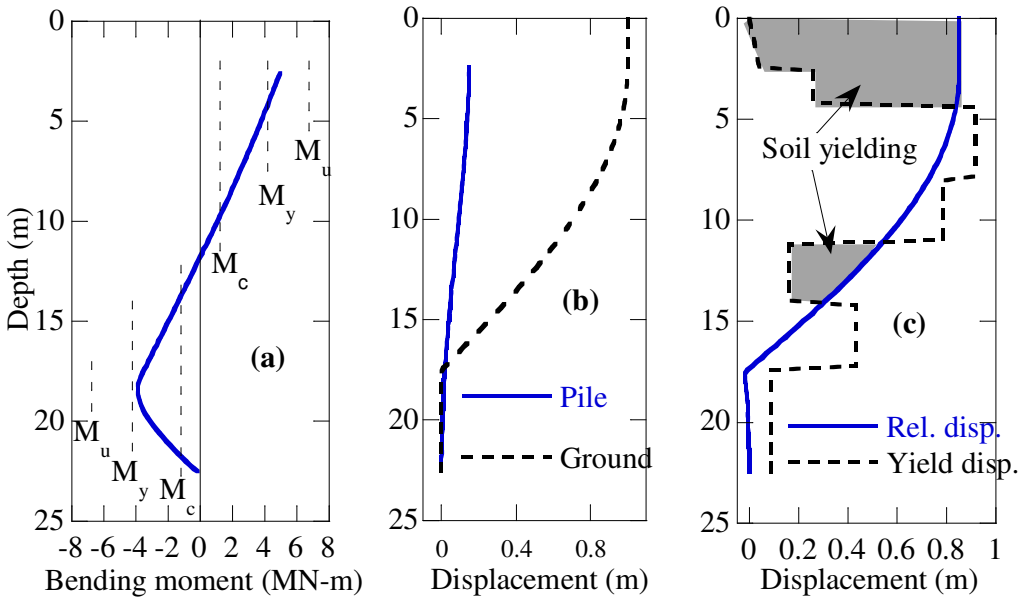

Figure 3.12 Typical analysis result showing the pile response to a lateral spreading displacement of one metre: (a) bending moment versus depth plot; (b) pile and ground displacements; and (c) relative displacement between the soil and pile compared to the soil yield displacement

3.4.3 Degradation of liquefied soil stiffness and strength

Due to the uncertainty of the effect of liquefaction on the soil stiffness and strength, analyses were conducted using two p-δ relationships, an upper bound and lower bound p-δ curve. In this way two extremes of liquefied soil stiffness and strength were considered, with the upper bound p-δ curve combining, for lateral spreading cases, a stiffness degradation of β = 1/50 and $p_{2\text{-}max} = S_{u\text{-}ub}$. Conversely, the lower bound p-δ curve was defined by β = 1/1000 and $p_{2\text{-}max} = S_{u\text{-}lb}$. For the cyclic cases the upper bound p-δ curve was defined using β = 1/10 and $p_{2\text{-}max} = S_{u\text{-}ub}$; the cyclic lower bound p-δ curve used β = 1/50 and $p_{2\text{-}max} = S_{u\text{-}lb}$.

Effects on stiff and flexible piles

For both cyclic and lateral spreading phases the pile behaviour depends on the stiffness of the pile relative to the liquefied or displacing soil. Relatively flexible piles move together with the lateral ground displacement; whereas relatively stiff piles resist the movement of the surrounding ground. Therefore to evaluate the effects of different liquefied soil properties on the pile response two cases need to be analysed corresponding to the stiff and flexible behaviour respectively. Needless to say, the stiff pile behaviour is more relevant to design,

because the flexible pile behaviour by default provides unacceptable performance due to the excessive lateral displacements of the pile.

Figure 3.13 shows the pile response for a cyclic phase analysis where a large inertial load corresponding to 0.44g was applied at the pile head in addition to the maximum cyclic ground displacement shown in Figure 3.11b. Two cases are shown corresponding to the upper bound and lower bound bi-linear p-δ curves, shown in Figure 3.13d. Figure 3.13a shows that for both cases of degradation the pile acts in a flexible manner with little relative displacement between the pile and the soil. It can be seen that despite differences in the forces acting on the pile from the liquefied layers the bending moments and pile displacements are very similar. This suggests that for this flexible pile behaviour the liquefied layer does not have a large bearing on the pile response as the pile behaviour is governed by the large inertial load. Note that due to the small relative displacement between the soil and the pile, the full passive pressure of the crust layer has not been mobilised in this case.

In contrast, Figure 3.14 shows the results of a lateral spreading analysis with different liquefied soil properties and no inertial load. Here, both cases of upper bound and lower bound p-δ curves show stiff pile behaviour, as such the large relative displacements between the pile and the soil result in the liquefied soil properties having a significant effect on the pile response. For the upper bound liquefied p-δ relationship the forces from the liquefied soil are larger, resulting in larger pile displacements and bending moments than those observed for the lower bound p-δ curve. Because of the large relative displacements, in both cases stiff pile behaviour was observed, resulting in full mobilisation of the passive load from the non-liquefied crust soil. In the absence of a large inertial load, the pile exhibited stiffer behaviour and the loads from the crust and liquefied layers had a larger effect on the pile response.

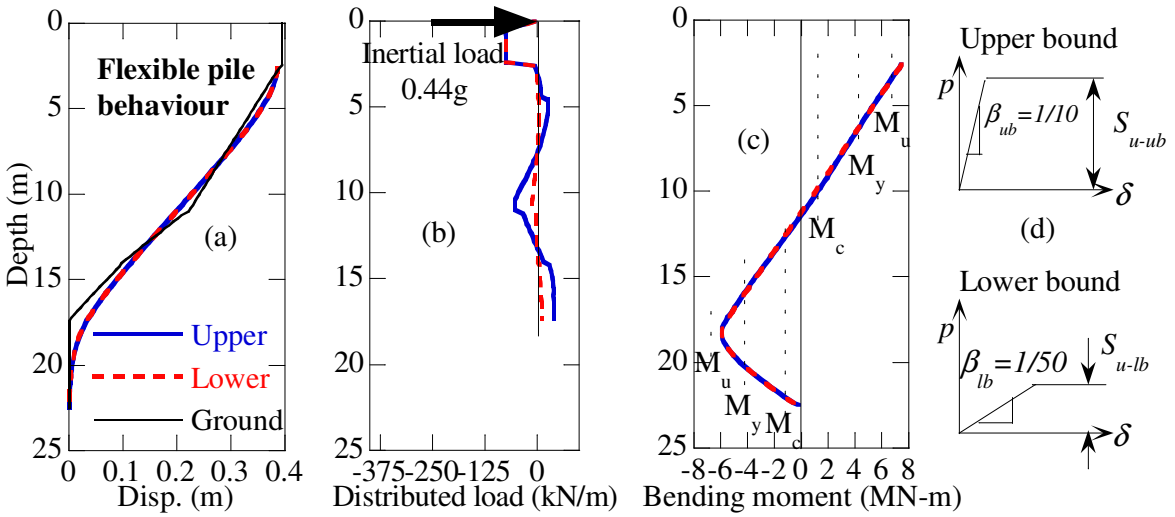

Figure 3.13 Variation of pile response due to liquefied layer properties for a cyclic phase case with a large inertial load, showing pile displacement, distributed load on the pile and pile bending moment

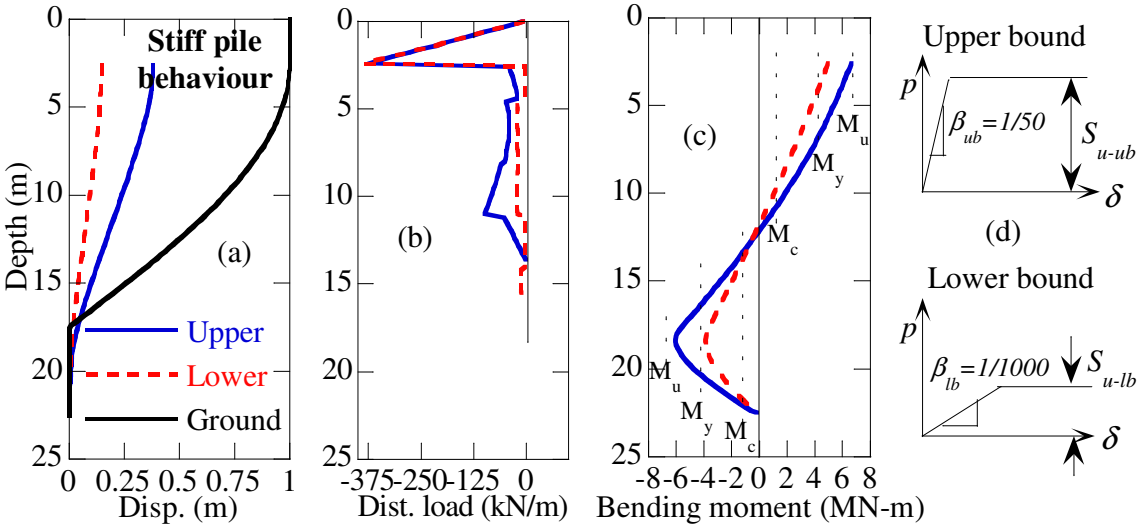

Figure 3.14 Variation of pile response due to liquefied layer properties for a lateral spreading case with U_{G2} = 1m, showing pile displacement, distributed load on the pile and pile bending moment

Effect of ultimate pressure, $p_{2\text{-}max}$

To examine how the ultimate pressure exerted by the liquefied soil on the pile affects the pile response, two analyses were conducted on a lateral spreading case with U_{G2} = 0.5m and β at 1/50. Figure 3.15 shows the computed pile response for cases where (a) the ultimate pressure was limited to $p_{2\text{-}max} = S_{u\text{-}lb}$ (in the range of 2 - 17kPa), and (b) $p_{2\text{-}max} = S_{u\text{-}ub}$ (28 – 43kPa). It can be seen that adopting $p_{2\text{-}max} = S_{u\text{-}ub}$ for the ultimate pressure in the liquefied soil results in more flexible behaviour and higher bending moments than the $p_{2\text{-}max} = S_{u\text{-}lb}$ case. These observations can be explained by considering the relative displacements between the soil and the pile for both cases. Figure 3.16 shows the relative displacement between the soil and the pile plotted with the soil yield displacement for the two cases. It can be seen that the lower bound S_u case has low yield displacements and high relative displacements, whereas the upper bound S_u case has higher yield displacements and lower relative displacements. A large part of the soil profile has yielded with the lower bound case of $p_{2\text{-}max} = S_{u\text{-}lb}$, thus the pressure is limited to $S_{u\text{-}lb}$ for a large length of the pile in this case.

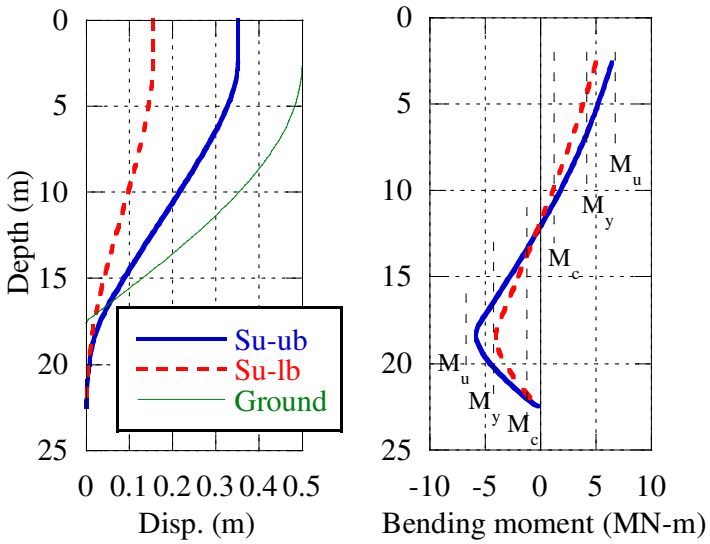

Figure 3.15 *Pile response for a lateral spreading case with U_{G2} = 0.5m and β = 1/50, showing the effects of changing the ultimate pressure in the liquefied soil*

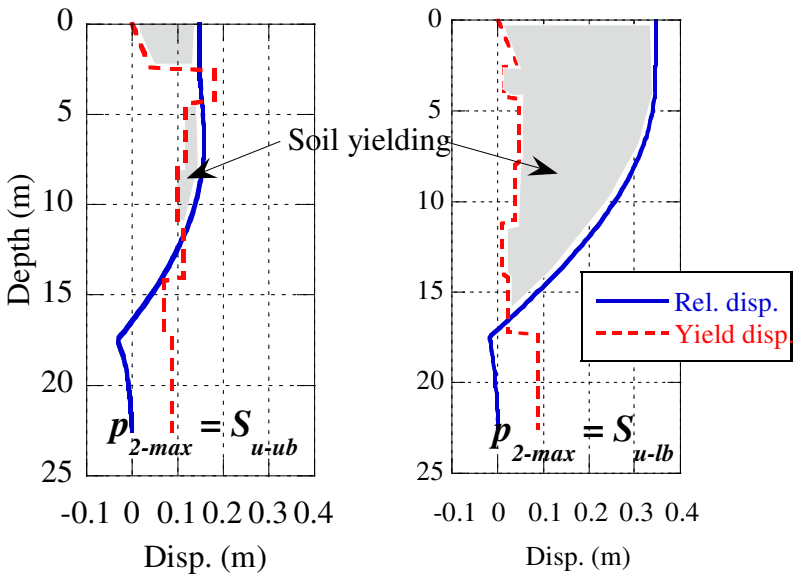

Figure 3.16 *Comparison of relative and yield displacements for $p_{2\text{-}max} = S_{u\text{-}lb}$ and $p_{2\text{-}max} = S_{u\text{-}ub}$*

Forces from crust and liquefied soil

In the case of stiff pile behaviour, the soil pressure from the crust and liquefied layers provide a driving force, while the non-liquefied base layer provides a resisting force. With changes in the liquefied soil stiffness and strength the forces applied to the pile from both the crust and liquefied layers change. To quantify these changes lateral spreading analyses were conducted using U_G = 0.5m with the ultimate pressure in the liquefied layer given by $p_{2\text{-}max} = S_{u\text{-}ub}$ or $p_{2\text{-}max} = S_{u\text{-}lb}$. In both cases the stiffness degradation β varied from 1/50 to 1/1000 and the total force on the pile, including contributions from the crust and liquefied layers, was calculated and plotted against β as shown in Figure 3.17.

It was observed that all cases exhibited stiff pile behaviour; the piles in general resisted the ground movement and the bending moments exceeded the yield level at the pile head. It was observed that the total load from the crust layer remained the same regardless of β or S_u. This is because the large relative displacements between the stiff pile and the soil caused the entire crust layer to yield. For the $p_{2\text{-}max} = S_{u\text{-}ub}$ case shown in Figure 3.17a the load from the liquefied layer increases with increasing β, when β = 1/50 (0.02) the load from the liquefied layer is as large as the load from the crust layer. Figure 3.17b shows the case where $p_{2\text{-}max} = S_{u\text{-}lb}$ was used; here the load from the liquefied layer is limited by the lower bound ultimate pressure from the liquefied soil.

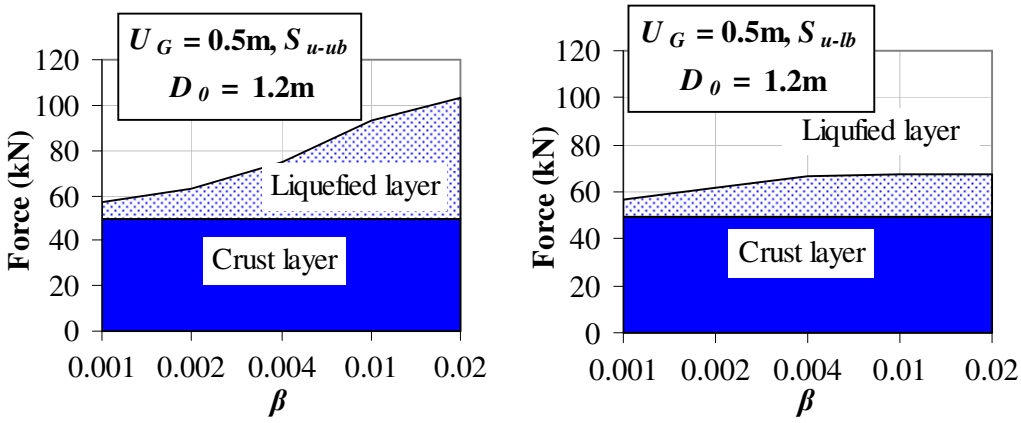

Figure 3.17 *Force applied to stiff piles from the crust and liquefied layers as a function of the stiffness degradation due to liquefaction, β*

The same analysis was repeated for a pile with a diameter of 0.6m to examine the interaction between the crust and liquefied layer loads for more flexible piles. For all these cases flexible behaviour was observed and the pile moved together with the ground; the bending moment reached the ultimate level at the pile head. Figure 3.18 shows the contribution of loads for the flexible pile cases. Here the load from the crust layer is much smaller than that for the stiff pile cases, and decreases with increasing β. This is because a large β value results in smaller relative displacement between the pile and the soil and hence a lower load from the crust layer. The load from the liquefied layer increases with increasing β, and the combination of loads from the crust and liquefied soil result in an increase in the total load as β increases.

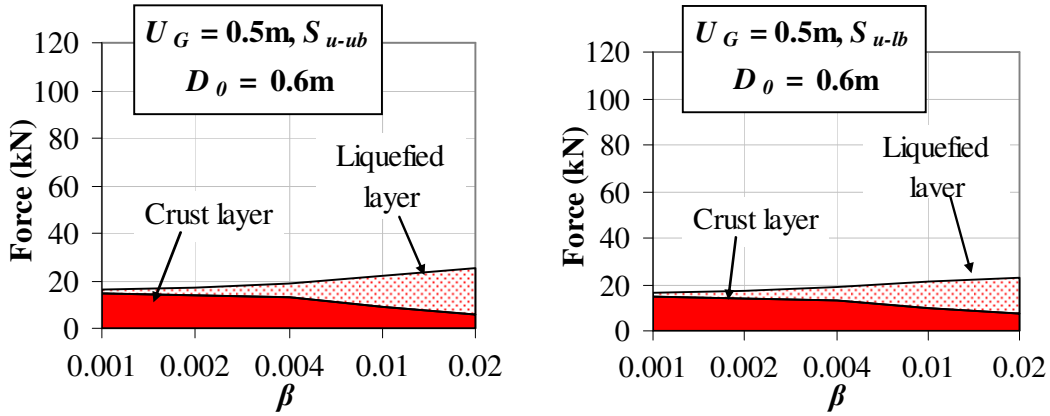

Figure 3.18 *Force applied to flexible piles from the crust and liquefied layers as a function of the stiffness degradation due to liquefaction, β*

3.4.4 *Effect of horizontal ground displacement*

For stiff piles undergoing lateral spreading, it is interesting to determine how the magnitude of horizontal ground displacement applied, U_G, affects the pile response. As the prediction of lateral spreading displacement is very difficult, and regarding the variation in empirical prediction methods, the approach taken here is to consider a wide range of lateral spreading displacements. Figure 3.19 shows the computed maximum pile displacements for cases with β = *1/50* and U_G = 0.5, 1, 2 and 3m. Results are calculated using three different p-δ curves for the liquefied soil; one without ultimate pressure in the liquefied soil (equivalent linear case), while the other two cases use $p_{2\text{-}max} = S_{u\text{-}ub}$ and $p_{2\text{-}max} = S_{u\text{-}lb}$ to limit the ultimate pressure. For the equivalent linear case the pile displacement increases with increasing ground displacement and the pile exhibits flexible behaviour. The equivalent linear cases predicted flexible behaviour and very large values of pile bending moment; at U_G = 3m the bending moment is well in excess of the ultimate moment of the pile. This result is unrealistic because the ultimate load from the liquefied soil exceeded any reasonable limit. Therefore the more rigorous p-δ curves with a limit on the ultimate pressure are necessary for cases with large relative displacements between the soil and the pile. In contrast, when limits are placed on the ultimate pressure in the liquefied soil, stiff pile behaviour is observed, and the magnitude of ground displacement has virtually no effect on the pile response. This observation is hardly surprising given that in these cases the applied ground displacement is sufficient to cause the vast majority of the soil profile to yield, thus for these cases the same lateral load corresponding to the limiting pressure is being exerted on the pile.

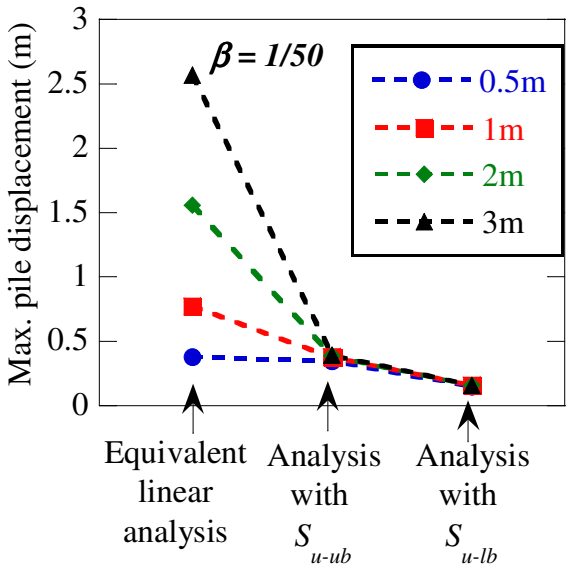

Figure 3.19 Variation of maximum pile bending moments with applied lateral ground displacement for different values of ultimate pressure from the liquefied soil

The above behaviour suggests that for a given pile a critical magnitude of U_G exists above which any increase in lateral ground displacement will have no effect on the pile response. In order to scrutinise this, a series of analyses were conducted with different values of applied ground displacement U_G using different values of β and $p_{2\text{-}max}$.The results of these analyses are shown in Figure 3.20, which plots the calculated pile displacement against the value of U_G applied in the analysis. Figure 3.20 shows that this threshold ground displacement exists; as the applied lateral ground displacement is increased a certain level is reached above which any further increase in the displacement has no effect on the pile response. It is also apparent that this critical value depends on the stiffness degradation constant β and the ultimate pressure $p_{2\text{-}max}$. Figure 3.21 plots this threshold value against β, where $U_{G\text{-}threshold}$ is defined as the applied ground displacement that results in a pile displacement which is 95% of the pile displacement calculated using a very large ground displacement. Quantitatively, for the $p_{2\text{-}max} = S_{u\text{-}ub}$ case, this is defined as 037m, which corresponds to 95% of 0.39m, the pile displacement calculated using a U_G value of 5m. The critical value decreases as β is increased and is $U_{G\text{-}threshold}$ = 0.6m and 2.3m for β = 1/50 and 1/500 respectively. It is apparent from Figure 3.20 that $U_{G\text{-}threshold}$ is much smaller in the $p_{2\text{-}max} = S_{u\text{-}lb}$ cases.

To illustrate the implications of Figure 3.21, suppose a β value of 1/100 was assumed. Figure 3.21 indicates that for any value of ground displacement greater than 0.8m practically the same pile response will be obtained. In other words, the accuracy in evaluating U_G is not relevant if the value of 0.8m could be exceeded.

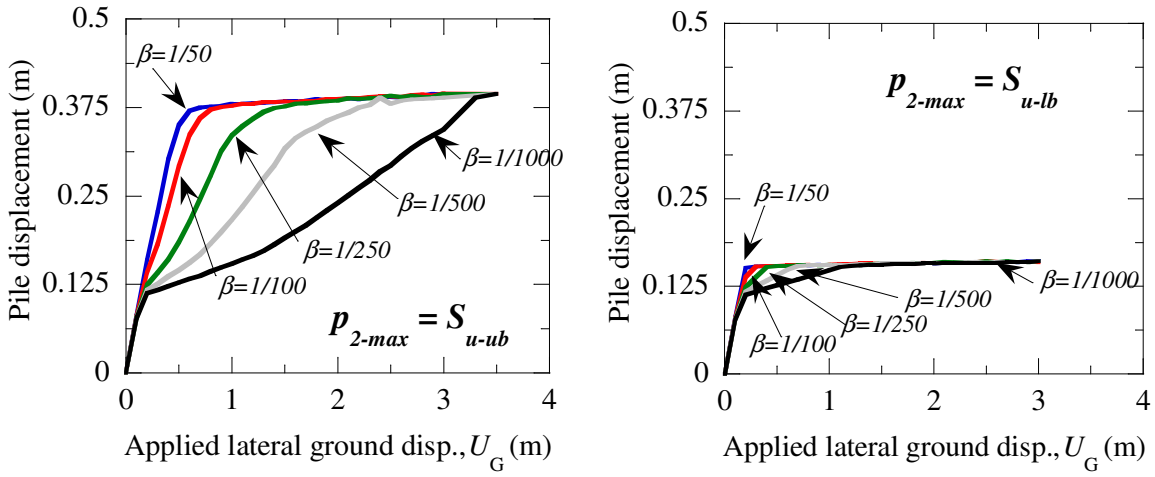

Figure 3.20 Plot of maximum bending moment versus applied ground displacement for different values of β

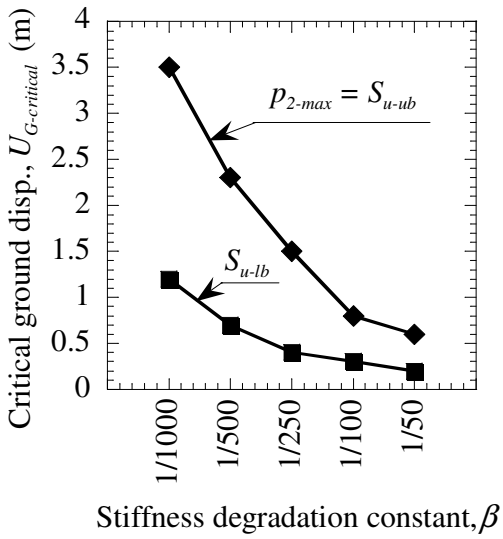

Figure 3.21 Critical ground displacement above which any further increases in U_G have no effect on the pile response plotted against stiffness degradation due to liquefaction.

3.4.5 Effect of loads at the pile head

In the pseudo static analysis procedure two loads are applied at the top of the pile; a point load representing the inertial loads from the superstructure, and a distributed load from the passive pressure exerted by the crust layer on the footing. Both these loads can vary in magnitude. The passive pressure exerted on the pile by the non-liquefied crust is generally only fully mobilised once a certain yield displacement in the soil is reached. Consequently flexible piles with small relative displacements will experience a smaller load when compared with a stiff pile where the full passive pressure has been mobilised in the crust layer.

The level of inertial load applied at the pile head is generally calculated using the peak ground acceleration and tributary mass for the pile. Analysis during the cyclic phase considers the pile response when the ground displacement is at a maximum; however the maximum inertial load is not necessarily being applied at the same time. Large-scale shaking table tests (Tokimatsu et al. 2005) and dynamic finite element analyses (Chang et al. 2005) have indicated that inertial loads and cyclic ground displacements act in phase when the natural period of the superstructure is less than that of the ground. Nevertheless there is a need to examine how variations in the combination of the inertial and crust loads affect the pile response. The effects of loads at the pile head have a large effect on the pile response; large loads can cause the pile to act in a flexible manner, while stiffer behaviour can be observed with no inertial load applied. Thus, it is interesting to examine the effect that loads applied at the pile head have on the response of piles.

The combination of inertial and crust layer loads can be discussed with reference to the total load applied at the pile head, as both loads act at practically the same location they produce similar effects on the pile response. Cyclic phase analyses with different loads at the pile head were conducted to determine how the addition of these two loads affects the pile behaviour. Six combinations of loads were analysed, corresponding to

- Three cases with inertial loads equivalent to peak ground accelerations of 0.44g, 0.22g and 0g using the original soil profile, and

- Three cases with the same inertial loads as above but using a soil profile without a crust layer.

As before, analyses with upper and lower bounds of p-δ relationships for the liquefied soil were conducted, the loads from the crust layer and the inertial loads for all twelve analysis cases are summarised in Table 3.4. A pile diameter of D_0 = 1.2m was used in all analyses. The maximum load from the crust layer is 490kN; this is observed in cases where the relative displacement between the soil and the pile is large enough to cause the entire crust layer to yield. Figure 3.22 shows the results of these analyses, where the peak pile displacements and bending moments were plotted against the total load at the pile head for both upper and lower bounds of liquefied soil stiffness and strength.

Table 3.4 Combinations of loads applied at the pile head

	Acc. (g)	Inertial load (kN)	Crust load (kN)		Total load (kN)	
			Upper bound	Lower bound	Upper bound	Lower bound
Crust layer	0.44	704	170	170	874	874
	0.22	352	383	454	735	806
	0	0	490*	490*	490	490
No crust layer	0.44	704	-	-	704	704
	0.22	352	-	-	352	352
	0	0	-	-	0	0

*corresponds to the maximum load from the crust layer

Figure 3.22a shows the ratio of maximum pile displacement to the maximum free field ground displacement plotted against the total load at the pile head for both the upper and

lower bound cases. It can be seen that both cases show flexible pile behaviour (ratio approaches one) when large loads are applied and stiff pile behaviour (ratio approaches zero) when relatively small load is applied. However the transition between stiff and flexible differs between the upper and lower bound cases adopted in the analysis. For cases with the upper bound liquefied stiffness and strength, flexible behaviour occurs at loads that are approximately 30% less than the lower bound cases; in other words, stiffer liquefied soil results in more flexible behaviour of the pile. For the case where no inertial load is applied (the total pile load is the 490kN from the crust layer), the upper bound case has a pile displacement twice as large as the lower bound case. These features are also observed in the maximum pile bending moments shown in Figure 3.22b.

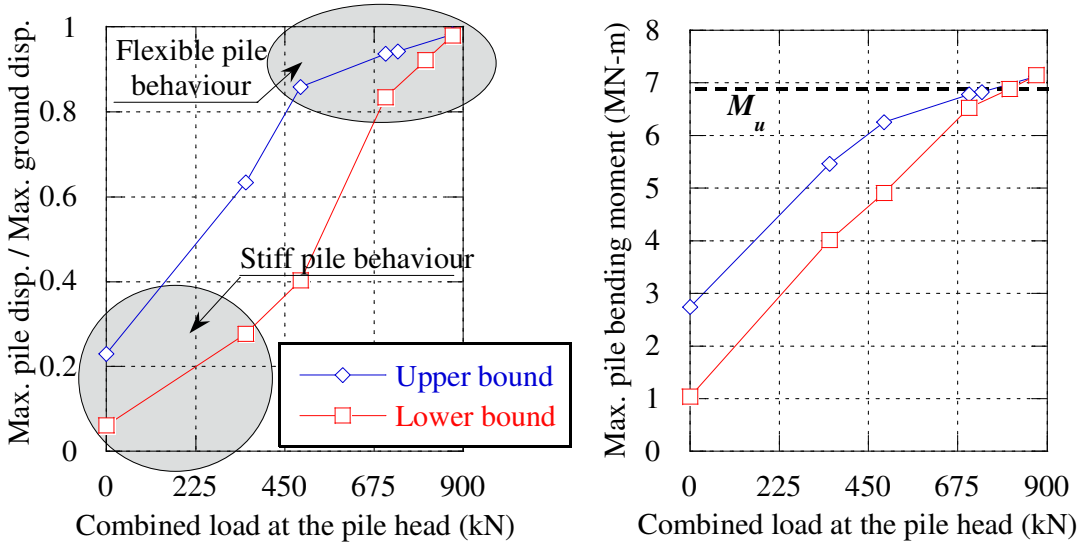

Figure 3.22 Effect of total load applied at the pile head on the peak pile displacements and bending moments for different combinations of inertial and crust layer loads, considering both relatively stiff and relatively soft liquefied soils

When considering lateral spreading cases stiff pile behaviour is predominately observed. This is reasonable as the liquefied soil must have relatively low stiffness and strength in order for lateral spreading to occur. Due to this stiff behaviour, the relative displacement in the crust layer is likely to be large; thus the crust soil will be yielding and the maximum pressure from the crust layer will always be applied. As inertial loads during this phase are likely to be small, consideration of variations in the total pile head load should be focussed to considerations of variations in the passive load from the crust layer.

3.5 Conclusions

Simplified analysis of pile foundations in liquefied soil is burdened by many uncertainties. In this chapter a case study is presented where a parametric study was conducted to determine the effects of these uncertainties on the pile response. Key findings include:

- The effect that the stiffness and ultimate strength of liquefied soil have on pile response depends on the behaviour of the pile under loading; flexible piles have small relative displacements hence the liquefied soil properties and ultimate pressure from the crust layer have little effect, in contrast to stiff piles with large relative displacements.
- For stiff piles, the level of stiffness and strength degradation due to liquefaction adopted in the analysis had a large effect on the pile response. When lower bound values of stiffness and strength were adopted the pile showed smaller lateral displacements and bending moments as compared to those obtained in the analysis with upper bound values.
- Using equivalent linear p-δ relationships in the liquefied layers have been shown to predict overly conservative bending moments in cases where the liquefied soil is relatively stiff and the relative displacements are large. A more appropriate approach is to use a bi-linear p-δ relationship for the liquefied soil where the ultimate pressure is limited to the undrained residual strength of the soil.
- For stiff piles undergoing lateral spreading, there exists a threshold magnitude of lateral ground displacement above which any further increase in the ground displacement has no effect on the pile response. This threshold value depends on the stiffness and strength of the liquefied soil.
- Increasing the load at the pile head may lead into a transition from stiff to flexible pile behaviour. This transition occurs earlier in relatively stiff liquefied soils.

In the design of pile foundations in liquefiable soil, stiff pile behaviour is desired. Flexible piles suffer large pile displacements and often fail in bending, thus the parameters that are

most important for design are those that affect stiff piles. The parametric study described in this chapter suggests that the choice of liquefied soil properties adopted in design have a large bearing on the computed response for stiff piles. In contrast it was shown that once a certain magnitude of ground displacement has been reached further increases in ground displacement have no effect. Therefore in design threshold ground displacement needs to be evaluated first and then accordingly attention should be paid to the effects of the crust layer and the liquefied soil properties. The study also showed the importance of inertial loads, as the magnitude of inertial load applied has a large effect on the relative pile stiffness.

4. Seismic effective stress analysis

4.1 Introduction

Effective stress analysis is a dynamic non-linear finite element analysis that considers the soil as a two-phase medium consisting of solid and fluid phases. The analysis incorporates the effective stress principle, meaning effects of pore water pressure generation and the flow of pore fluid throughout the soil are considered. The highly non-linear stress-strain-dilatancy behaviour of soil under seismic loading is modelled using an advanced constitutive model. In contrast to the pseudo static analysis described in Chapter 3, effective stress analysis is an advanced approach suitable for performance based assessment of important structures.

In this chapter effective stress analysis is applied to the Fitzgerald Avenue Bridges described in Chapter 3. This is to

- demonstrate the applicability of the analysis to a practical case study
- examine the seismic response of the bridge in detail, in particular by considering the effects that soil structure interaction, excess pore water pressure and eventual liquefaction have on the response of the free field soil, the foundation soil and the piles
- analyse the advantages and disadvantages of performing an advanced analysis over using a conventional design orientated approach

The effective stress procedure is described briefly, including details of the soil constitutive model and the numerical technique used. The application of the analysis to the Fitzgerald Avenue Bridges case study is then described, particularly with regard to the determination of material parameters. The computed response of the soil and foundations is then described in detail, and a brief comparison with the results of pseudo static analysis is also given.

4.2 Two phase finite element analysis

Effective stress analysis considers the soil as a two phase material with the governing equations based on Biot's porous media theory (1962). The numerical solution of Biot's equations can be obtained from many formulations, however the choice of numerical method does not affect the results significantly (Zienkiewicz and Shiomi 1984). Here a U-u

formulation is used in the finite element code DIANA. In contrast the constitutive model used in analysis of liquefaction problems has a large effect on the results (Arulanandan and Scott 1994).

In this chapter the stress-density constitutive model is used; DIANA based analysis using the stress-density constitutive model has been used to simulate the response of large scale shake table tests (Cubrinovski et al. 1999; Cubrinovski et al. 2005) and case histories (Cubrinovski et al. 2001; Cubrinovski et al. 1996). These simulations show very good agreement with experimental results and observed case history damage.

4.3 Stress – Density model

The effective stress analysis uses the Stress-Density Model (Cubrinovski and Ishihara 1998a; Cubrinovski and Ishihara 1998b) as a constitutive model. The model combines two fundamental sand modelling concepts. The first is the state concept, where the sand behaviour is characterised based on its density and confining stress. The second is a modified elastoplasticity theory that involves important modifications to the conventional plasticity framework. Some details of the model are described in the following.

4.3.1 State concept

The state concept is based around the observation that sand behaviour depends on the initial density and normal stress. The state index, I_s, is a parameter used as a measure of the combined influence of the density and normal stress and is defined as follows:

$$I_s = \frac{e_U - e}{e_U - e_Q} \tag{4.1}$$

where at a certain void ratio e the state index is calculated by considering both e_U and e_Q, the void ratios of the quasi steady state line and the upper reference line respectively at the current normal stress p. The quasi steady state (QSS) line is constructed from the void ratios obtained at quasi steady state at a given confining stress. Here the quasi steady state is defined as the state of phase transformation in the sand where a temporary drop in the shear stress occurs upon undrained shearing. The upper reference (UR) line is the lesser of the void ratio of the isotropically consolidated loosest state or the threshold void ratio, e_0, above which the initial states are associated with zero residual strength. The calculation of I_s is shown schematically in Figure 4.1.

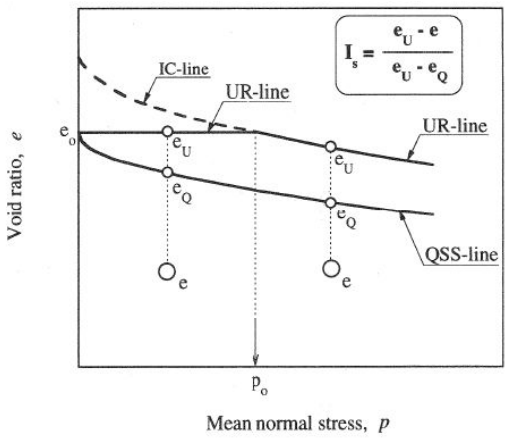

Figure 4.1 Definition of state index on the e-p *diagram (Cubrinovski and Ishihara 1998a)*

The stress-density model is formulated based on the following three observations from experimental tests on triaxial and torsional samples:

1. It is essential to consider the combined influence of density and normal stress on sand behaviour.

2. There is a clear link between the relative initial state (density and normal stress) and sand behaviour; two samples with identical relative initial states will show identical stress-strain behaviour.

3. The state index is a direct measure of the initial state, thus the state index can be used as a measure of the stress-strain behaviour.

The link between the state index and sand behaviour is clearly shown in Figure 4.2, where the results of torsional tests on Toyoura sand are presented. Three groups of soil samples with relative initial states corresponding to I_s values of 0, 4 and 10 are shown in the *e-p*' space in Figure 4.2a. I_s = 0 corresponds to soil at its loosest state, whereas when I_s = 1 the soil is at an initial state corresponding to the projection of the quasi steady state line in the *e-p*' plane. I_s values greater than 1 are denser than the quasi steady state; I_s = 10 corresponds to soil in a very dense state. Figure 4.2b shows the normalised stress-strain curves for the three groups, clearly initial states that have similar I_s values have similar stress-strain curves. As the state index decreases, both the initial shear modulus and the peak stress ratio decrease as well.

Conventional sand models consider each density of a given material as a separate material. In contrast the state concept approach allows modelling of the monotonic and cyclic behaviour of sand over a wide range of densities using only a single set of parameters.

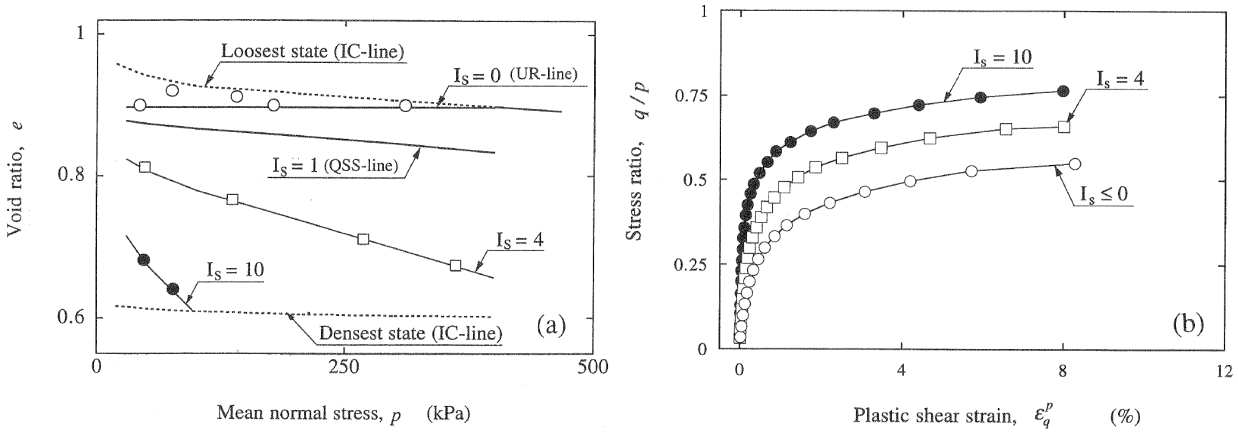

Figure 4.2 Illustration of the link between the state index and the normalised stress-strain curve: (a) initial states, (b) stress-strain curves (Cubrinovski and Ishihara 1998b)

4.3.2 Stress – strain – dilatancy model

A modified hyperbolic relationship is used to link the shear stress ratio τ/p and the plastic shear strain γ_p :

$$\frac{\tau}{p} = \frac{G_N \gamma_p \left(\frac{\tau}{p}\right)_{\max}}{\left(\frac{\tau}{p}\right)_{\max} + G_N \gamma_p} \tag{4.2}$$

Here G_N is the normalised initial plastic shear modulus equal to G/p, and $(\tau/p)_{max}$ is the peak stress ratio. If both these parameters are constant Equation (2) cannot fit a given stress-strain curve well over a wide range of strains. Therefore it is assumed that for a given initial *e-p* state $(\tau/p)_{max}$ is constant, while G_N varies as a function of the plastic shear strain γ_p as follows:

$$G_N = (G_{N,\max} - G_{N,\min}) \cdot \exp\left(-f \frac{\gamma_p}{0.01}\right) + G_{N,\min} \tag{4.3}$$

where $G_{N,\max}$ and $G_{N,\min}$ are the initial plastic moduli at small and large strains respectively, and f is a degradation constant.

Given the relationship between sand behaviour and state index, Cubrinovski and Ishihara (1998a) showed that a linear correlation exists between the state index I_s and the parameters of the modified hyperbolic stress strain model. The parameters $(\tau/p)_{max}$, $G_{N,\max}$ and $G_{N,\min}$ can be expressed as linear functions of the state index as given below:

$$\left(\frac{\tau}{p}\right)_{\max} = a_1 + b_1 \cdot I_s \tag{4.4}$$

$$G_{N,\max} = a_2 + b_2 \cdot I_s \tag{4.5}$$

$$G_{N,\min} = a_3 + b_3 \cdot I_s \tag{4.6}$$

The coefficients *a* and *b* are determined from drained monotonic *p*-constant tests; they describe the linear relationship between the stress-strain parameters and I_s. The state index not only works as an initial state parameter; in the stress-density model (SDM) the state index is calculated based on the current *e-p* state, i.e. I_s is used as a current variable. This enables changes in the stress-strain characteristics to be modelled along the *e-p* response path of the soil.

The link between the stress and dilatancy of the soil is described by the relationship between the plastic volumetric strain increment $d\varepsilon_v^p$ and the shear strain increment $d\varepsilon_q^p$. Here the ratio of these two strain increments is related to the shear stress ratio:

$$\frac{d\varepsilon_v^p}{d\varepsilon_q^p} = \mu - \frac{\tau}{p}c \tag{4.7}$$

where $\tau = (\sigma_1 - \sigma_3)/2$ is the shear stress, *c* is a non-coaxiality term and μ is a dilatancy parameter dependent on the shear strain, given by the relationship;

$$\mu = \mu_0 + \frac{2}{\pi}(M - \mu_0)\tan^{-1}\left(\frac{\varepsilon_q^p}{S_c}\right) \tag{4.8}$$

where μ_0 and *M* are the slopes of the normalised shear work versus plastic shear strain relationship $(\Omega - \varepsilon_q^p)$ at small and large strains respectively, and S_c specifies the shear strain at which $\mu = (\mu_0 + M)/2$ is attained. It is assumed that μ_0, *M* and S_c are independent of both initial density and normal stress of the sand.

4.3.3 Incremental formulation

The stress-strain-dilatancy relations described in the previous section are included in an incremental formulation that adopts a modified elastoplastic deformation law. The plasticity formulation of the model is characterised by many modifications to the classical plasticity framework. The most important features of the plasticity formulation are

- Continuous yielding, i.e. a purely elastic region does not exist.
- Dependence of the plastic strain increment on the stress increment direction (hypoplasticity). This allows the model to account for the effects of rotation of the principal stress directions.
- Discrete memory for the loading, unloading and reloading surfaces with a mixed hardening rule for their evolution.

The constitutive model is applied to time history finite element analysis using a strain controlled computation scheme. Each total strain increment is composed of an elastic part ($d\varepsilon_{ij}^{e}$) and a plastic part ($d\varepsilon_{ij}^{p}$) as given below:

$$d\varepsilon_{ij} = d\varepsilon_{ij}^{e} + d\varepsilon_{ij}^{p} \tag{4.9}$$

The incremental relations for the elastic part are given by:

$$d\sigma_{ij} = E_{ijkl} d\varepsilon_{kl}^{e} \tag{4.10}$$

where E_{ijkl} is a function of the elastic shear modulus G_e and Poisson's ratio ν:

$$E_{ijkl} = \frac{2G_e\nu}{1-2\nu}\delta_{ij}\delta_{kl} + G_e(\delta_{ik}\delta_{jl} + \delta_{il}\delta_{jk}) \tag{4.11}$$

The elastic shear modulus G_e is defined as

$$G_e = Ap_a \frac{(2.17-e)^2}{1+e}\left(\frac{p}{p_a}\right)^n \tag{4.12}$$

where A is a dimensionless material parameter, p is the mean normal stress, p_a is the atmospheric pressure, e is the void ratio and n is a dimensionless material parameter that determines the rate of variation of G_e with p.

The magnitude of the plastic strain increment ($d\varepsilon_{ij}^{p}$) is calculated as a function of the plastic modulus H_P, given by

$$H_p = \left\{ G_N - f \frac{\varepsilon_q^p}{0.01}(G_N - G_{N,\min}) \right\} p \left\{ 1 - \frac{\eta}{\eta_{\max}} \right\}^2 \qquad (4.13)$$

where η is the stress ratio τ/p as given by Equation 2.

4.3.4 Material parameters

The SDM requires four groups of parameters to be determined:

1. Reference lines (UR and QSS lines)
2. Stress-strain parameters (a_1, a_2, a_3, b_1, b_2, b_3, f)
3. Dilatancy parameters (μ_0, M, S_c)
4. Elastic parameters (A, ν, n)

These parameters are determined by a series of laboratory triaxial tests, generally 12-15 tests are considered sufficient.

Reference lines

The reference lines refer to the upper reference line and quasi steady state line in the *e-p* plot shown in Figure 4.1. These are determined from the results of several monotonic undrained strain controlled tests on loose samples having different void ratios. For these tests the quasi steady state line can be defined by plotting the *e-p* states where a drop in shear stress occurs and drawing a line between them.

Stress – strain parameters

The stress-strain parameters of the model are determined from drained *p*-constant tests on samples with distinctive relative initial states (different values of I_s). The peak stress ratio $(\tau/p)_{max}$, can be directly read off the measured normalised stress-strain curve and the initial plastic moduli $G_{N,\max}$ and $G_{N,\min}$ are determined by fitting the values to the experimental curves. Then for each test the state index is calculated using the reference lines and the initial *e-p* state, and the values of $(\tau/p)_{max}$, $G_{N,\max}$ and $G_{N,\min}$ are plotted against I_s; linear correlations with I_s are used to evaluate the linear coefficients a_1, a_2, a_3 and b_1, b_2, b_3. The value of f is generally greater than 3 and increases with any increase in the relative size of the difference ($G_{N,\max} - G_{N,\min}$) with respect to the value of $G_{N,\min}$.

Dilatancy parameters

The dilatancy parameter, M, can be estimated from $M = (\tau/p)_{cs,}$ stress ratio at the critical state obtained in the monotonic undrained tests. Alternatively it can be approximated by the peak stress ratio obtained in a drained p-constant test with $I_s = 0$. The parameter μ_0 is defined by simulating the initial part of the effective stress path of the undrained test; values of μ_0 are typically between 0.10 and 0.25, where a larger value indicates more contractive behaviour.

The dilatancy parameter S_c controls the pore pressure development and hence has a large influence on the liquefaction resistance of the soil. This parameter is therefore determined by simulating a given cyclic strength versus number of cycles curve. This curve, known as the liquefaction resistance curve and shown in Figure 4.3 for Toyoura sand, plots the results of cyclic undrained tests where a soil sample is subjected to uniform cycles of loading at a constant stress ratio, τ/p. The stress ratio is plotted against the number of cycles required to develop 3%, 5% or 7.5% double amplitude shear strain. As shown in Figure 4.3, in this study a double amplitude shear strain of 3% was used. The process of determining S_c consists of identifying the value which provides the best fit curve to the experimental data. Figure 4.3a shows that the modelled cyclic strength moves upward with increasing S_c. This is because S_c represents the shear strain at which the average value of the dilatancy parameter, μ, is obtained. Thus a larger value of S_c represents smaller μ at a given strain, resulting in less contractive behaviour and a greater liquefaction resistance. Figure 4.3b shows simulated liquefaction resistance curves for Toyoura sand at different densities; the liquefaction resistance increases with increasing density and the model simulations fit well with the experimental results over a wide range of densities.

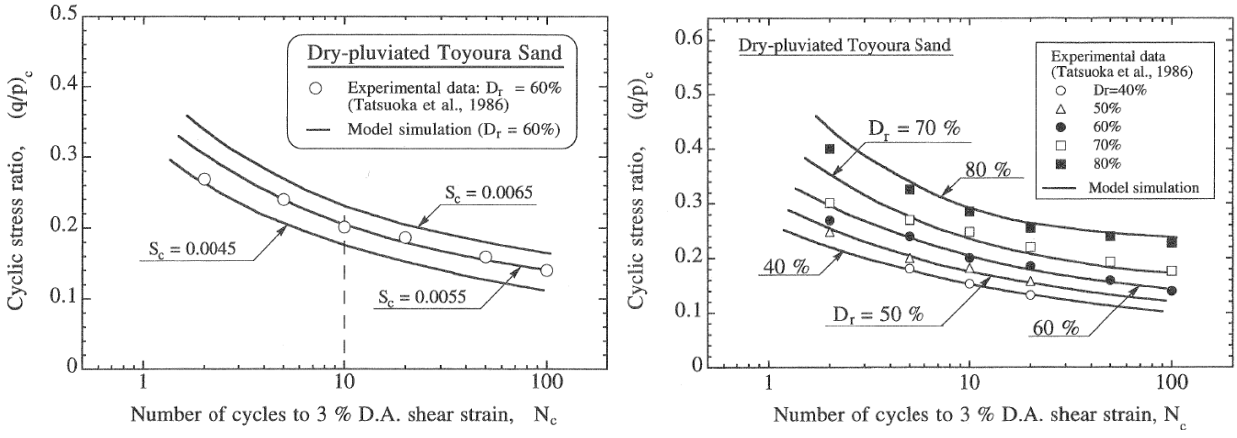

Figure 4.3 Liquefaction resistance curves for Toyoura sand; (a) determination of dilatancy parameter S_c by fitting to experimental data, (b) simulation of liquefaction resistance for different relative densities (Cubrinovski and Ishihara 1998b)

Elastic parameters

The elastic parameter A can be calculated from a known value of the elastic shear modulus G_e, and the Poisson's ratio (ν) and the exponent (n) can be assumed fixed values in the range of 0.2-0.3 and 0.5-0.6 respectively.

4.4 Application to a case study

4.4.1 Fitzgerald Avenue Bridges

The Fitzgerald Avenue Twin Bridges, described in Chapter 3, are again used as a case study. Here the effective stress analysis procedure is applied to examine the seismic response of the central pier of the east bridge. The central pier was modelled as a two dimensional cross section running through the central pier in the east-west direction. It was assumed the central pier is situated on level ground, thus the analysis considers the level ground or cyclic phase of the response. Key considerations here are the inertial effects of the bridge deck above and the cyclic ground displacements.

4.4.2 Soil profile

For the purposes of the effective stress analysis the soil profile at the north-east corner was conservatively adopted due to the lack of site investigation data in the middle of the river. The soil profile described in Chapter 3 is further simplified into four layers, as shown in Figure 4.4, consisting of three liquefiable layers above a non-liquefiable base layer. The 2m thick top layer has a corrected SPT blow count of N_1 = 10, and overlies a 6.5m thick stronger liquefiable layer with N_1 = 15 and a 6.5m thick weaker layer with N_1 = 10. The base layer is non-liquefiable with N_1 = 30.

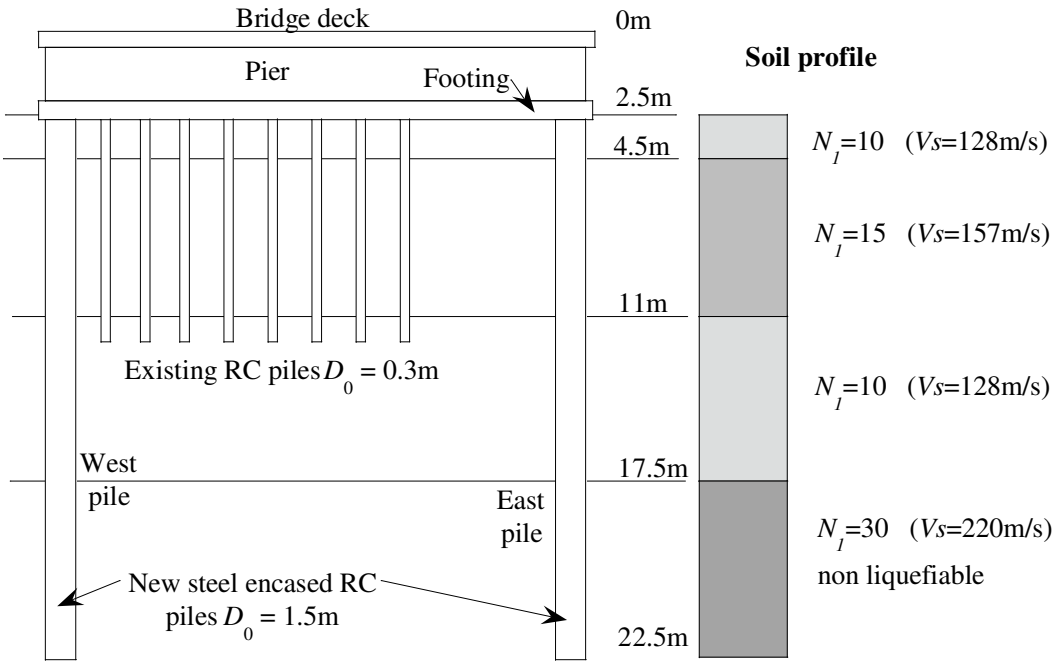

Figure 4.4 Central pier of bridge: (a) Foundation layout, (b) soil properties used in analysis

4.4.3 Bridge foundations

The existing bridge pier is founded on eight reinforced concrete piles, 0.3m in diameter and 9m long. The proposed retrofit involves installation of two new bored piles 1.5m in diameter at each end of the pile cap, as shown in Figure 4.4. Both the existing piles and the new piles were modelled using a hyperbolic moment curvature relationship. This relationship was determined by fitting a hyperbolic curve with parameters *EI* and M_{max} to a non-linear relationship calculated using the program MPHI described in Chapter 3. *EI* and M_{max} represent the initial stiffness and ultimate moment respectively.

The moment curvature relationship for the existing piles were calculated assuming f'_c = 25MPa and f_y = 300MPa, with an axial load of 150kN. For the new piles concrete with f_c' = 30MPa, steel reinforcement at a 0.8% longitudinal reinforcement ratio with a yield strength of f_y = 500MPa and a 10mm thick steel casing with f_y = 250MPa were assumed. Figure 4.5a shows the tri-linear M-ϕ curves calculated assuming axial loads corresponding to both the serviceability limit state (N=2800kN) and the ultimate limit state (N=4100kN). Figure 4.5b shows the fitted hyperbolic curve fitted to the non-linear M-ϕ relationship of the pile and its tri-linear moment curvature relationship calculated assuming an axial load of N=3000kN. The initial stiffness and ultimate moment used to define the hyperbolic M-ϕ relationships of both the existing and new piles is shown in Table 4.1.

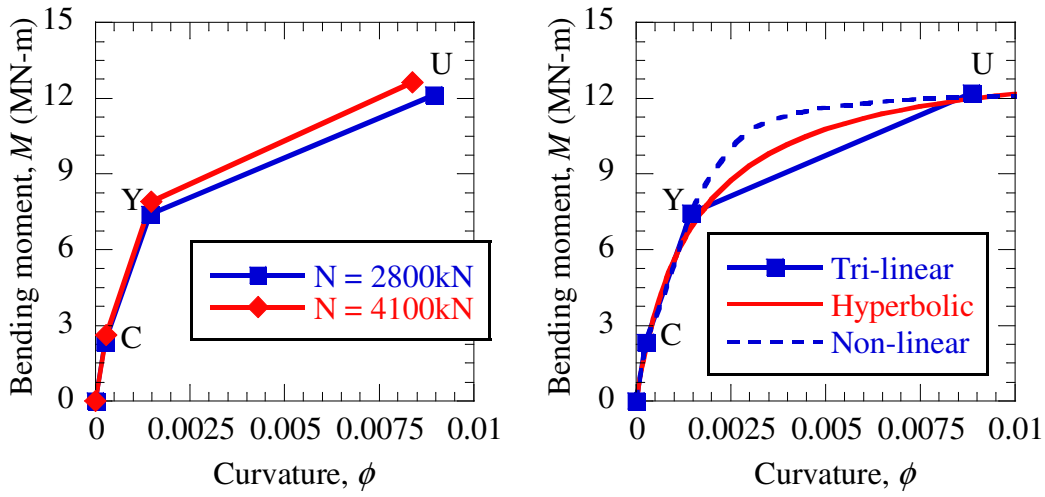

Figure 4.5 Moment curvature relationships for D_0 *= 1.5m pile: (a) effect of axial load on M-*ϕ *curve, (b) fitting hyperbolic curve to tri-linear relationship*

Table 4.1 Parameters for hyperbolic moment curvature relationships for the existing and new piles

D_0 = 0.3m Existing pile		D_0 = 1.5m New pile	
Initial stiffness EI (MN-m^2)	Ultimate moment, M_u (MN-m)	Initial stiffness EI (MN-m^2)	Ultimate moment, M_u (MN-m)
9.73	0.0337	934.7	14.0

4.4.4 Ground motion

Previous seismic hazard studies for Christchurch indicate that the most significant contribution to the ground shaking is a rupture event on the Porters Pass fault in North Canterbury. Both Howard *et al.* (2005) and Pettinga *et al.* (2001) indicate that the rupture on the strike-slip Porters Pass fault would produce an earthquake of magnitude 7.2-7.4. The fault is 40-60km from the site, and probabilistic seismic hazard studies such as Stirling et al. (2001) give peak ground acceleration values of 0.37g in a 475yr event and 0.47g in a 1000yr event.

Having all this in mind, a ground motion with similar attributes as above was chosen as the base input motion for the analysis. A motion recorded during the 1995 Kobe earthquake (M=7.2) was used; this motion was recorded at a depth of 25m in a down-hole array. The motion was scaled to have a peak acceleration of 0.4g, as shown in Figure 4.6.

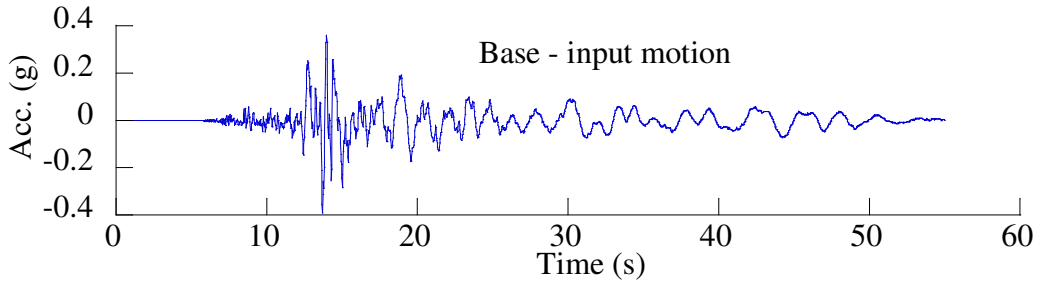

Figure 4.6 *Base input motion used in the effective stress analysis*

4.5 Dynamic analysis

4.5.1 Determination of constitutive model parameters

In the absence of detailed laboratory tests, the constitutive model parameters were determined by largely adopting the parameters of Toyoura sand and modifying some of the key parameters as described below. The parameters of Toyoura sand were established based on a previous study (Cubrinovski and Ishihara 1998a; Cubrinovski and Ishihara 1998b) where a comprehensive set of torsional tests including monotonic drained *p*'-constant tests, monotonic undrained tests and cyclic undrained (liquefaction) tests. The parameters were modified for the Fitzgerald Bridge analysis by determining key parameters, such as the dilatancy parameter S_c, using empirical correlations with the SPT blow count. The initial void ratios of the soil layers were determined in this way, using the correlation of Cubrinovski and Ishihara (1999):

$$\frac{N_1}{D_r^{\,2}} = C_D \qquad (4.14)$$

Where N_1 is the normalised SPT blow count, D_r is the relative density and C_D is a parameter that reflects the grain size properties of the soil. The value of C_D is assumed to be 41 for sands; this is equivalent to the well known expression of Meyerhof (1957). The void ratio *e* is then calculated from D_r.

The value of S_c was determined by simulation of the liquefaction resistance curves shown in Figure 4.7. The two lines represent the simulated liquefaction resistance curves for the N_1 = 10 and N_1 = 15 soil layers. The relative position of these curves was determined by changing the value of S_c to match the target cyclic stress ratio at N_c = 20 cycles (shown by the black circles in Figure 4.7). The target cyclic stress ratio was evaluated using the Seed and Idriss procedure (Youd et al. 2001) for evaluation of liquefaction resistance. The occurrence of liquefaction as plotted with the lines in the CSR / $(N_1)_{60}$ chart (Figure 4.8) was taken to

represent, for a magnitude 7.5 earthquake, the cyclic stress ratio causing liquefaction after 20 uniform cycles of motion. Therefore cyclic stress ratios of 0.15 and 0.22 were calculated for the N_1 = 10 and N_1 = 15 soil layers respectively, assuming a fines content of 10%.

The elastic shear constant, A, was determined by calculating the elastic shear modulus, G_e, using the relationship

$$G_e = \rho \cdot V_s^{\,2} \tag{4.15}$$

Where ρ is the mass density of the soil and V_s is the shear wave velocity. The value of V_s was assumed based on the results of the SPT and CPT testing, the assumed values for each layer are shown in Figure 4.4. The value of A was then back calculated using Equation (11). Table 4.2 shows the material parameters used in the analysis.

Table 4.2 Material parameters used in analysis

Material parameter	Value
Elastic parameters	
Shear constant, A	250 for N_1=10, 350 for N_1=15
Poisson's ratio, v	0.15
Exponent, n	0.6
State index parameters	
UR-line (void ratio, normal stress in kPa)	(0.895, ≤ 400)
QSS-line	(0.873, 30)
	(0.870, 50)
	(0.860, 100)
	(0.850, 200)
	(0.833, 400)
Stress strain parameters	
Peak stress ratio coefficients a_1, b_1	0.021, 0.592
Max. shear modulus coefficients a_2, b_2	13.0, 98.0
Min. shear modulus coefficients a_3, b_3	55.0, 291.0
Degradation constant, f	4
Dilatancy parameters	
Dilatancy coefficient (small strains), μ_0	0.20
Critical state stress ratio, M	0.60
Dilatancy strain, S_c	0.005

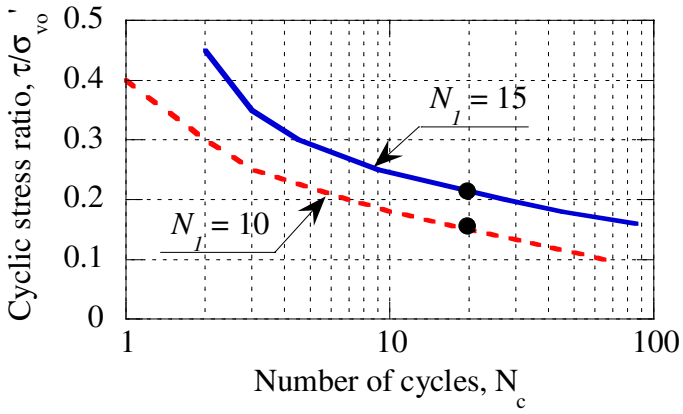

Figure 4.7 *Simulated liquefaction resistance curves for N_1 =10 and N_1 =15 soil layers*

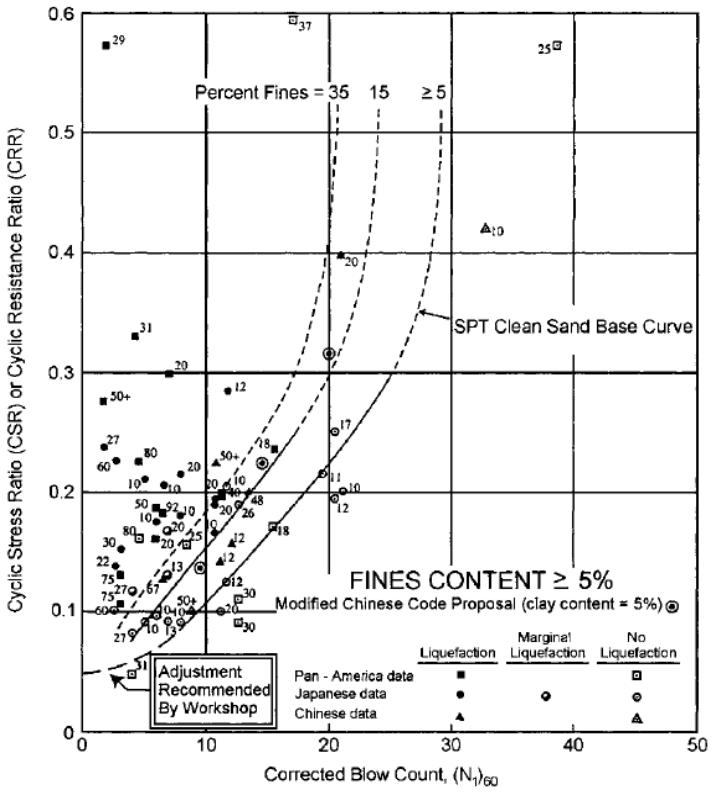

Figure 4.8 *Empirical chart used to evaluate the occurrence of liquefaction using the SPT blow count (Youd et al. 2001)*

4.5.2 Numerical model

The 2D numerical model used in the analysis is shown in Figure 4.9, where solid elements are employed for the soil and bridge superstructure, while beam elements are used for the piles and footing. The model is 160m x 30m in size. The soil elements were modelled using the stress-density constitutive model; the piles were modelled as nonlinear members with a moment-curvature relationship approximated using the hyperbolic model. The footing, bridge deck and pier were all modelled as elastic materials with an appropriate tributary mass to simulate inertial effects of the weight of the bridge deck above.

In keeping with the level ground assumption of the model, the nodes on the lateral boundaries on each side of the model are constrained to have the same displacements. This was to ensure that a free field motion of a level ground site occurs near the lateral boundary of the model. Along the soil-pile interface, the piles and the adjacent soil were connected at the nodes and were forced to share identical displacements.

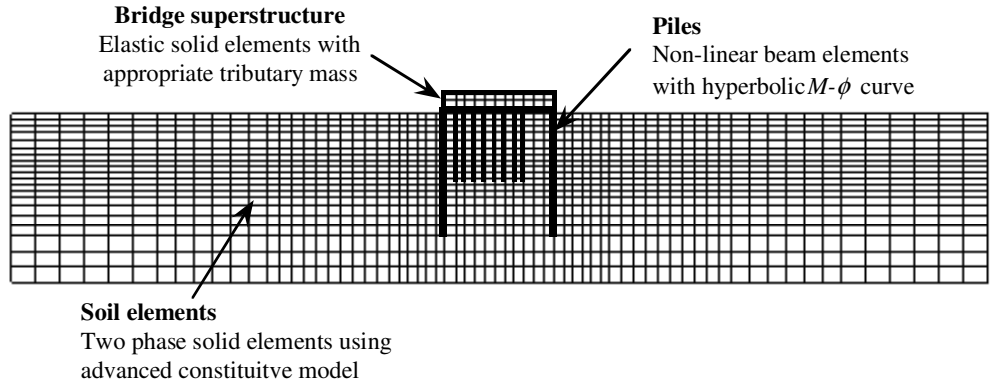

Figure 4.9 Numerical model used in the analysis

4.5.3 Dynamic parameters

The duration of the time history in the analysis was 55 seconds; the response was calculated using a time increment of 0.005 seconds giving 11000 calculation steps. Rayleigh numerical damping was used with parameters $\alpha = 0$ and $\beta = 0.005$.

4.6 Results

4.6.1 Observed behaviour

Figure 4.10 shows the reduction in the mean effective stress caused by the excess pore pressure build-up throughout the model, at different times throughout the shaking. In the weaker (N_1=10) layer the pore water pressure builds up suddenly after the first cycle of strong shaking at t =13.5s, liquefaction starts at the top of the layer and spreads downwards. At t -=14.5 the weaker layer has completely liquefied in the free field. The free field behaviour in the stronger (N_1=15) layer is different, here the pore water pressure build up is much slower and spreads outwards from the piles. In the weaker (N_1=10) layer of foundation soil the pore water pressure builds up in the in-between the two large piles and at the bottom of the layer. Liquefaction spreads upwards in the weaker soil and is fully liquefied at t =17.5s. The stronger (N_1=15) layer of foundation soil does not liquefy and retains some stiffness even at the end of the shaking.

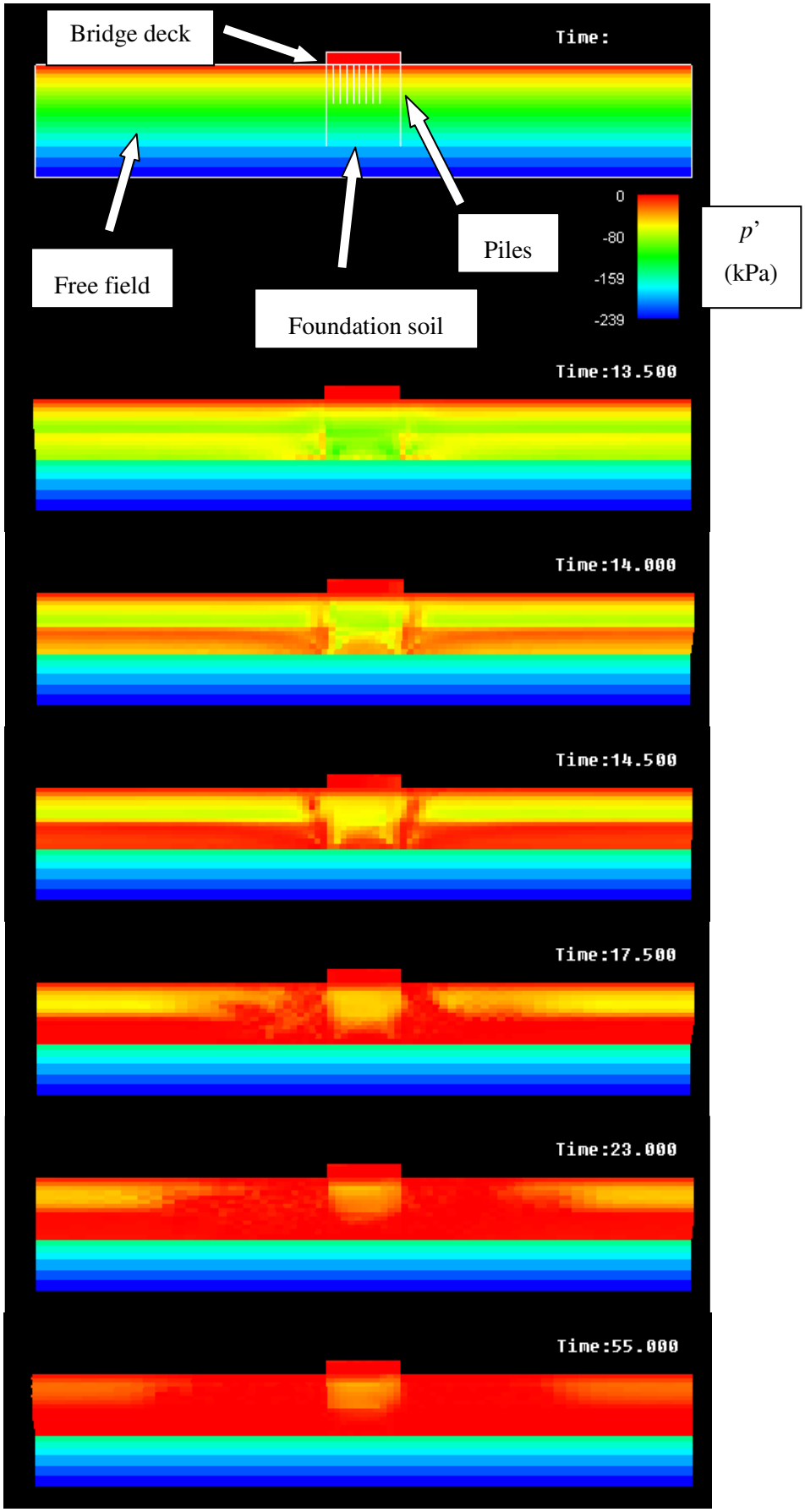

Figure 4.10 Development of liquefaction throughout the model illustrated by reduction in the mean effective stress p'

4.6.2 Free field response

Figure 4.11a shows computed excess pore water pressure time histories at different depths throughout the soil profile. In the weaker layer (N_1=10) liquefaction occurs straight after the first cycle of strong shaking while in the stronger layer (N_1=15) liquefaction doesn't fully develop and the excess pore pressures build up gradually. Figure 4.11b illustrates this feature, giving snapshots of the extent of liquefaction at different stages of the shaking. Note that here a pore pressure ratio of unity indicates complete liquefaction.

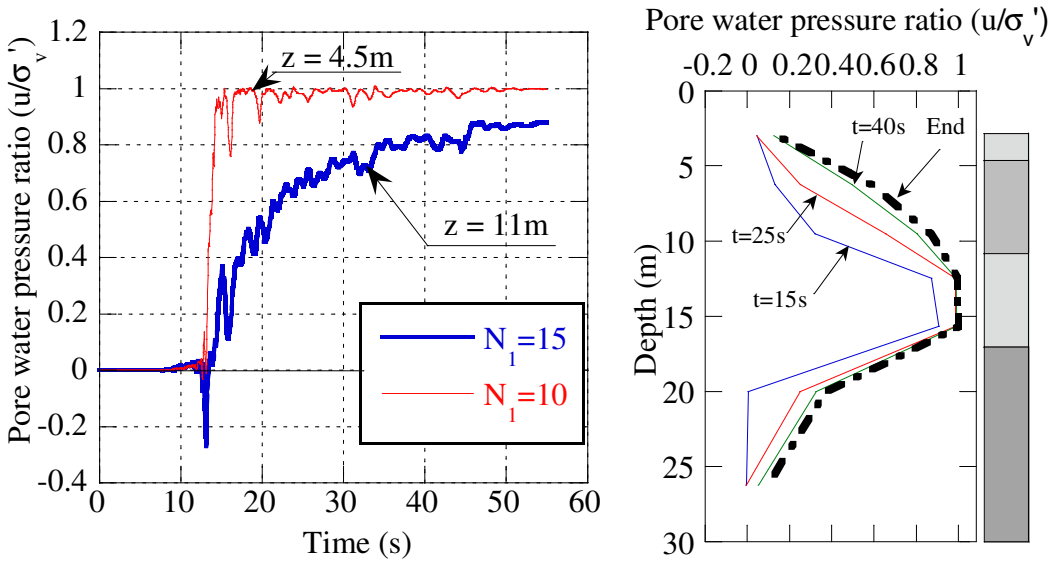

Figure 4.11 Free field excess pore water pressures; (a) time histories, showing the progression of liquefaction at different depths, (b) excess pore water pressure ratio as a function of depth at different times of the response

Effects of liquefaction on the ground response are evident in Figure 4.12 where acceleration time histories at three different depths are shown. Following the complete liquefaction in the mid layer at about 13-14 seconds, the accelerations above the liquefied layer decrease significantly and the ground motion shows elongation of the vibration period and loss of high frequencies. This diminished ground shaking and consequent reduction in the shear stress can explain the slower gradual build-up of the excess pore water pressure in the layers above the liquefied layer. This trend is continued to the response at the ground surface; the response of the weaker layer controls the response of the layers above.

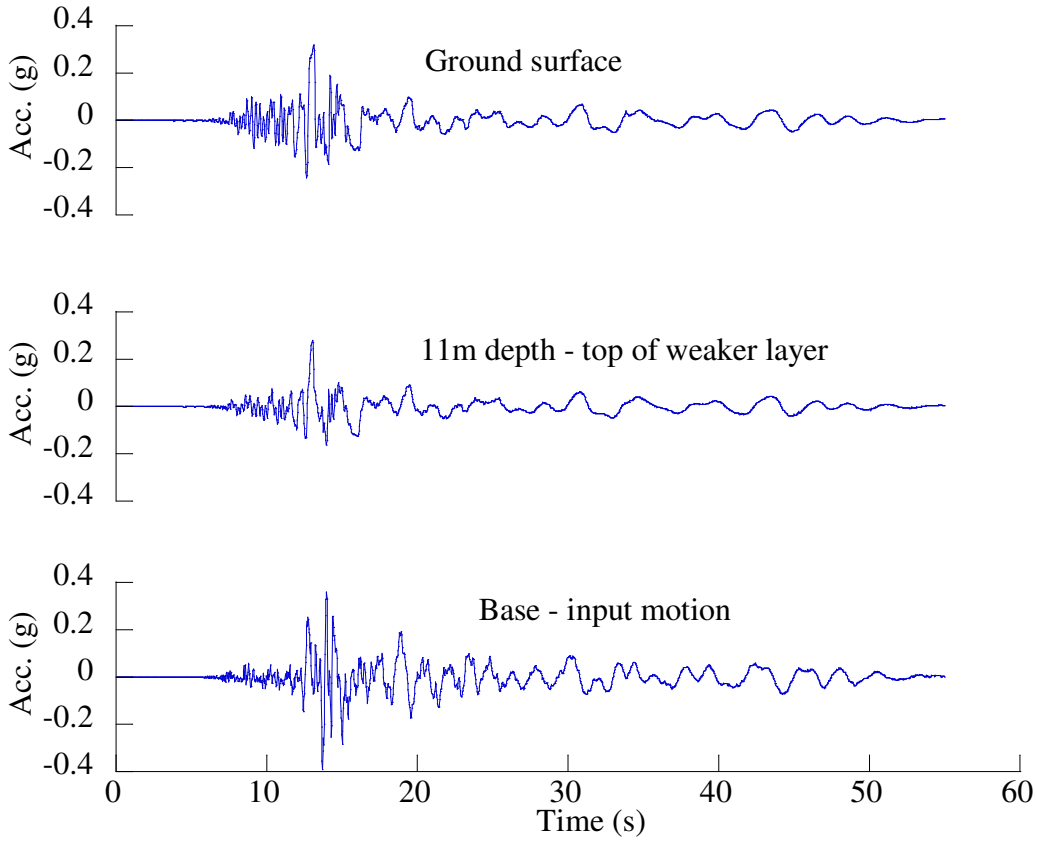

Figure 4.12 *Free field acceleration time histories for different depths of the soil profile*

The maximum values of the ground acceleration, shear strain and ground displacement, plotted in Figure 4.13, clearly display the effects of liquefaction on the free field ground response. Figure 4.13a shows a decrease in acceleration above the weaker layer which liquefied suddenly; this phenomenon has been observed in down-hole arrays during the 1995 Kobe earthquake and in many experimental tests. Figure 4.13b and 4.13c show that the majority of the ground deformation occurs in the mid layer with N_1=10, where the peak shear strains reach about 4%. The strains in the shallow part of the deposit are well below 1%. This is reasonable as the effects of shaking above this layer have been diminished as previously described.

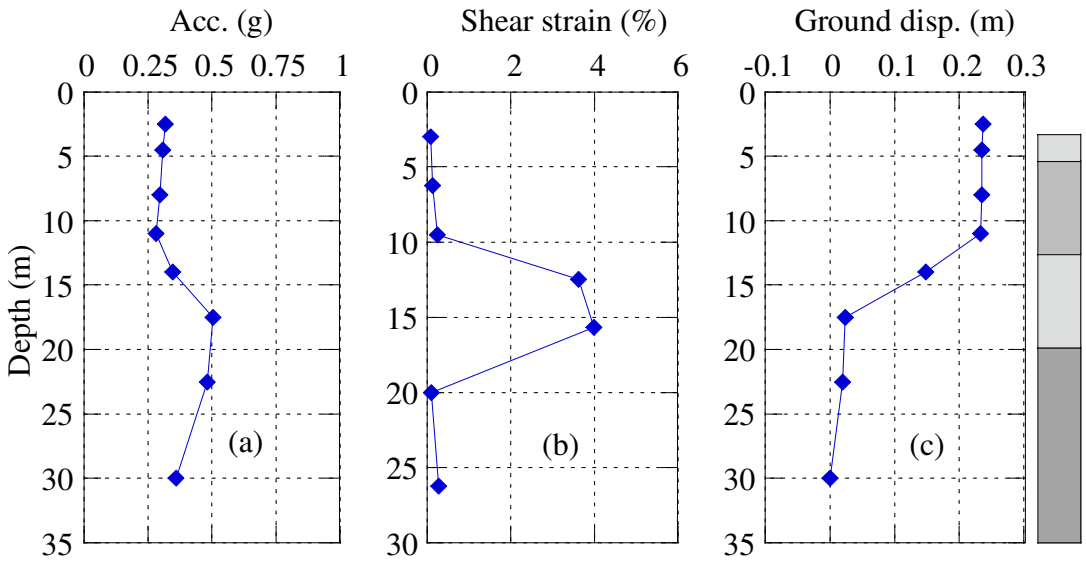

Figure 4.13 *Maximum free field response: (a) accelerations, (b) shear strains, (c) ground displacements*

4.6.3 Foundation soil

In general terms, the pile foundation provides a stiffening effect to the surrounding soil. This is illustrated in Figure 4.14, which compares the ground response at the free field and in between the piles. Despite large increases in pore water pressure, the soil retains some stiffness and the fluid-like behaviour of the free field with filtering effects is not observed. The stiffening effect of the foundation on the response of the soil is further shown in Figure 4.15, with a large decrease in ground displacement for soil amongst the piles.

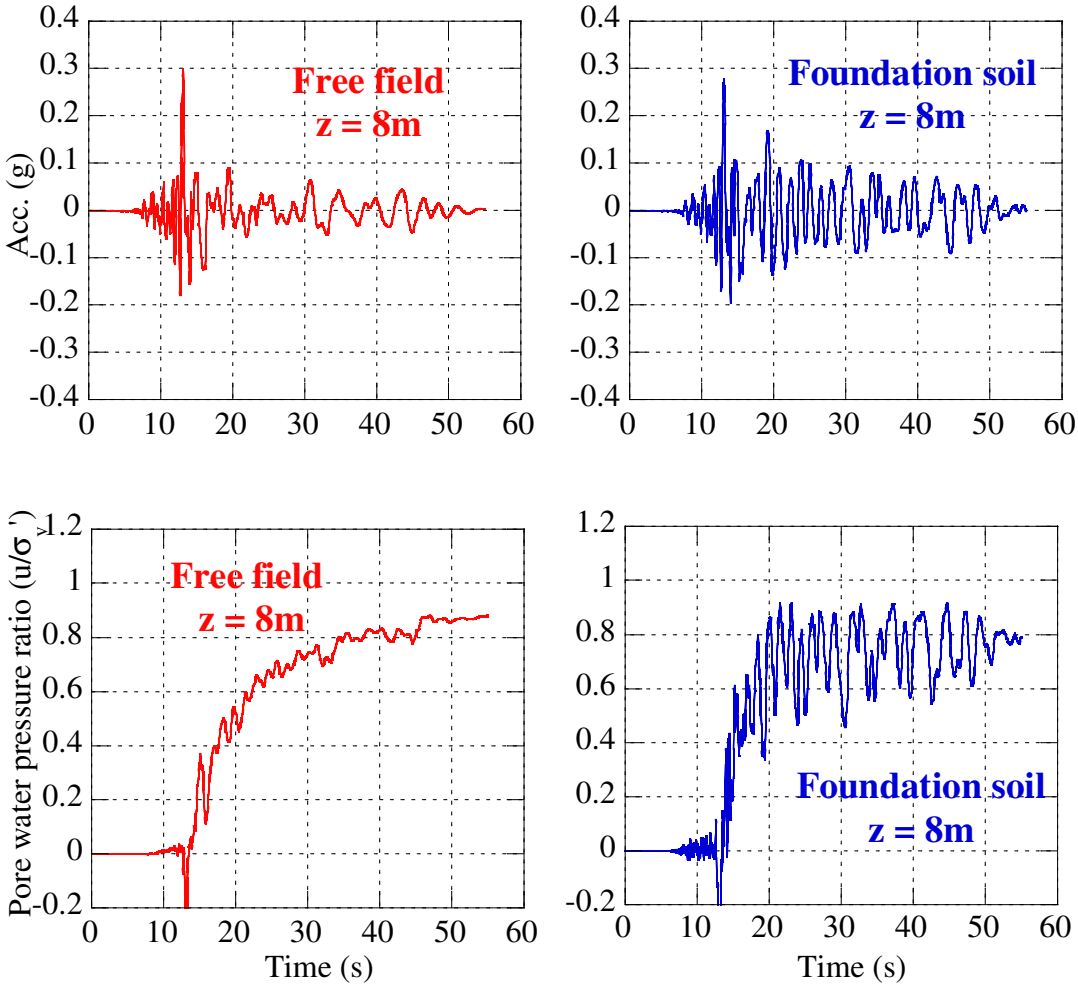

Figure 4.14 *Time histories of acceleration and excess pore water pressure in the stronger liquefied soil (N_1=15 at z =8m) for locations (a) in the free field; and (b) in the foundation soil*

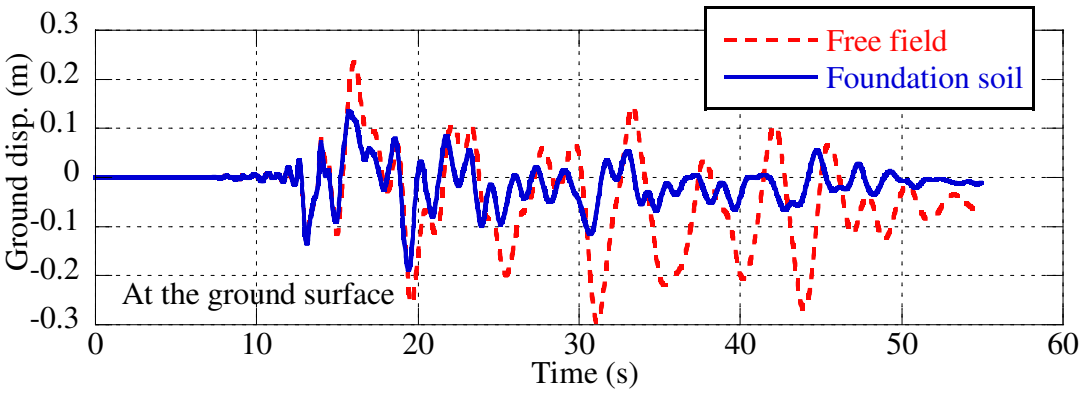

Figure 4.15 *Comparison of the horizontal displacement at the ground surface for locations in the free field and in between the piles*

4.6.4 Pile response

The modelling of the non-liquefied base layer has a large effect on the pile response. With this in mind three analyses were conducted with different base layer properties; the first analysis used a base layer with non-linear stress-strain properties calculated using the procedure described in Section 4.5.1. Then two further analyses were conducted using base layers with equivalent linear stress-strain relationships. In the equivalent linear cases a degraded shear modulus *G* was used, this was to account for the effects of pore pressure build-up and the non-linear behaviour of the soil at large strains. In this study the modulus was degraded relative to its initial value by factors of 0.3 and 0.5. Figure 4.16 shows the stress-strain curves for the three cases computed during the time history analysis for a free field soil element in the base layer at a depth of 20m.

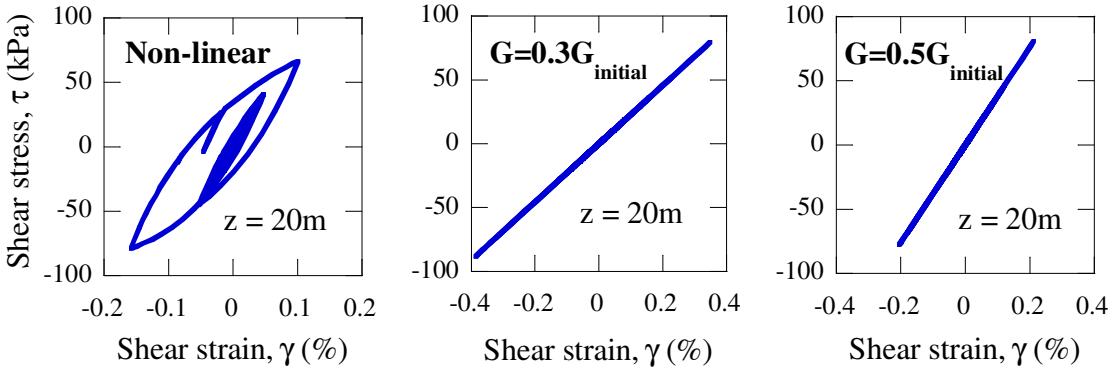

Figure 4.16 Computed stress-strain relationships in the non-liquefied base layer for three different analyses: non-linear case, equivalent linear case with $G=0.3G_{initual}$ and equivalent linear case with $G=0.5G_{initial}$

Figure 4.17a shows the bending moment distribution with depth for the west pile calculated using the non-linear base layer soil, plotted for the time when the maximum bending moment was reached at the pile head. The pile exhibits behaviour typical of piles in liquefied soils, with the largest bending moments occurring at the pile head and at the interface between the liquefied and base layers. It can be seen that the bending moment exceeds the pile cracking moment in the top 10m of the pile; the largest moments occur at the pile head but do not exceed the pile yield moment. Figure 4.17b shows the displacement of the pile relative to the maximum free field ground displacement, indicating that below 16m depth the pile is pushing the soil, whereas above 16m the soil is pushing the pile. Figure 4.20 shows a time history of the bending moment at the pile head for the west pile.

Figure 4.18 shows the computed pile response for the two equivalent linear cases. Both cases show much larger bending moments at the interface between the liquefied and base layers than the non-linear base layer. The equivalent linear case with the stiffer $G = 0.5G_{initial}$ base layer shows larger bending moments at the interface but lower bending moments at the pile head. The bending moments calculated using the equivalent linear case with $G = 0.3G_{initial}$ in the base layer exceed the yield moment in the top 5m of the pile. Figure 4.18b shows that both equivalent linear cases exhibit more flexible pile behaviour than the non-linear case. The pile displacement of the stiffer $G = 0.5G_{initial}$ base layer case is less than the $G = 0.3G_{initial}$ case.

To examine the cause of these differences Figure 4.19 shows the computed response at the interface between the liquefied and base layer in more detail. Comparison of the free field soil displacements in Figure 4.17b and Figure 4.18b show that in the non-linear case relatively large ground displacements occur in the base layer, which are much larger than the equivalent linear cases. Also, it can be seen in Figure 4.19 that the pile tip displacement is virtually zero for the equivalent linear cases, but it is about 7mm in the non-linear case. This indicates that the pile is not fixed at the pile tip. As it is assumed in the pile design that the pile is embedded in a stiff bearing stratum the non-linear base layer model may be unconservative, as pile fixity at the pile tip increases the pile bending moments. Figure 4.19 shows that the $G = 0.5G_{initial}$ case has the largest curvature at the interface; this is reflected in the bending moments. The non-linear base layer soil case has very little pile curvature; this explains the low bending moment at the interface.

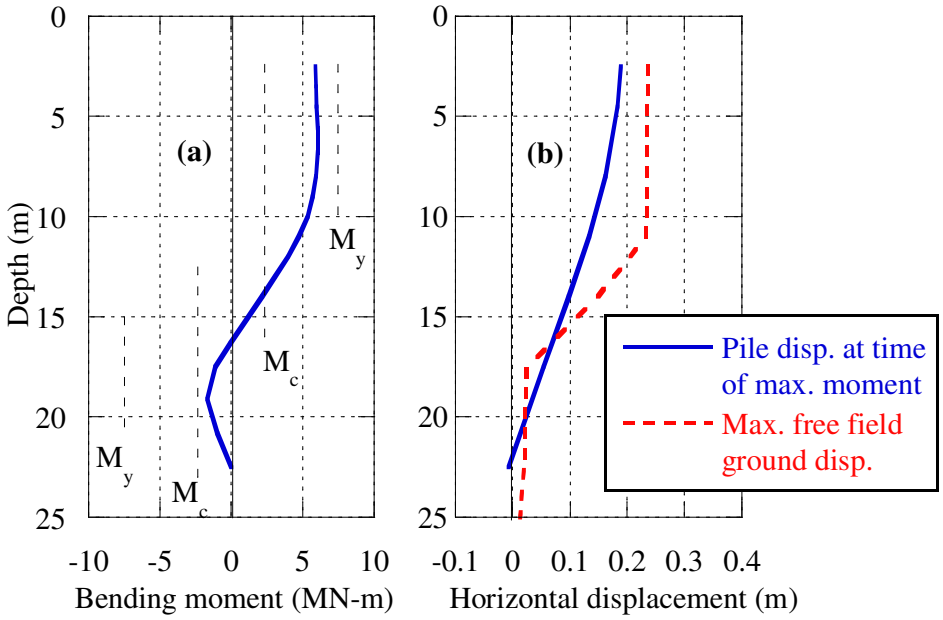

Figure 4.17 *Computed pile response with non-linear base layer soil: (a) Maximum pile bending moment, (b) pile displacement profile at the time of the maximum moment*

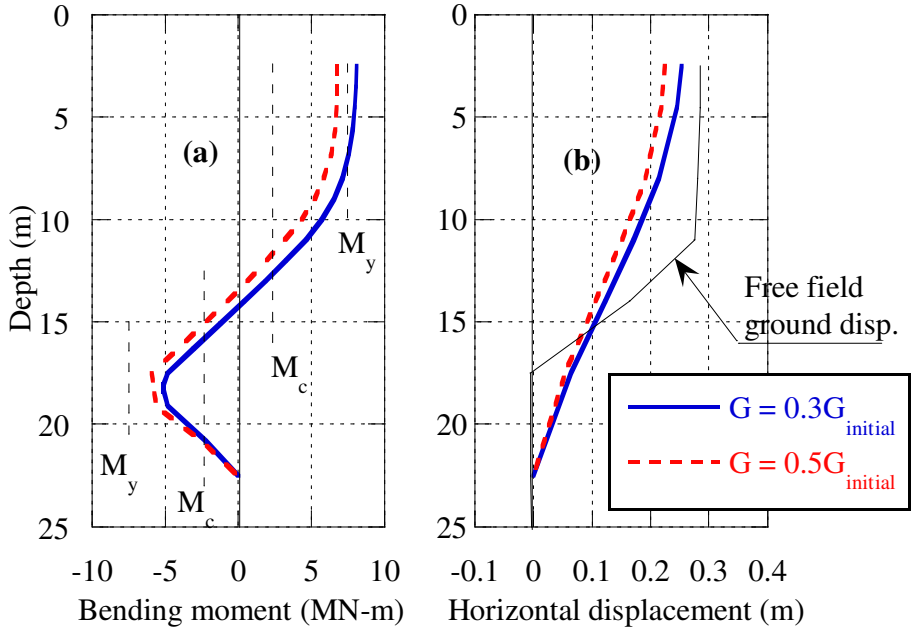

Figure 4.18 *Computed pile response using equivalent linear base layer soil: (a) Maximum pile bending moment, (b) pile displacement profile at the time of the maximum moment*

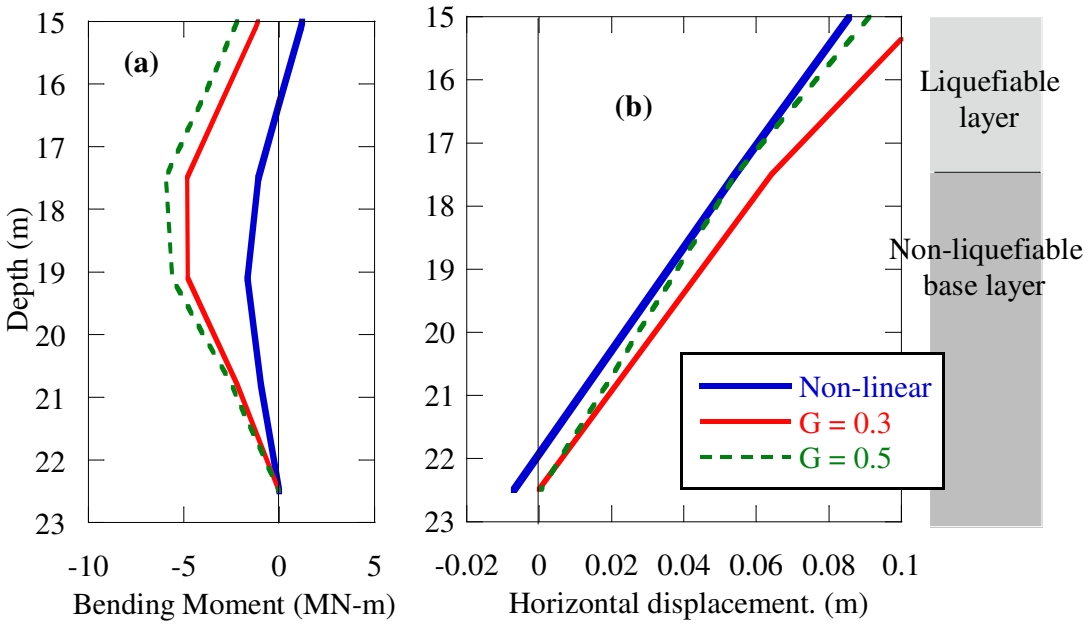

Figure 4.19 *Computed pile response in the base layer (a) Maximum pile bending moment, (b) pile displacement profile at the time of the maximum moment*

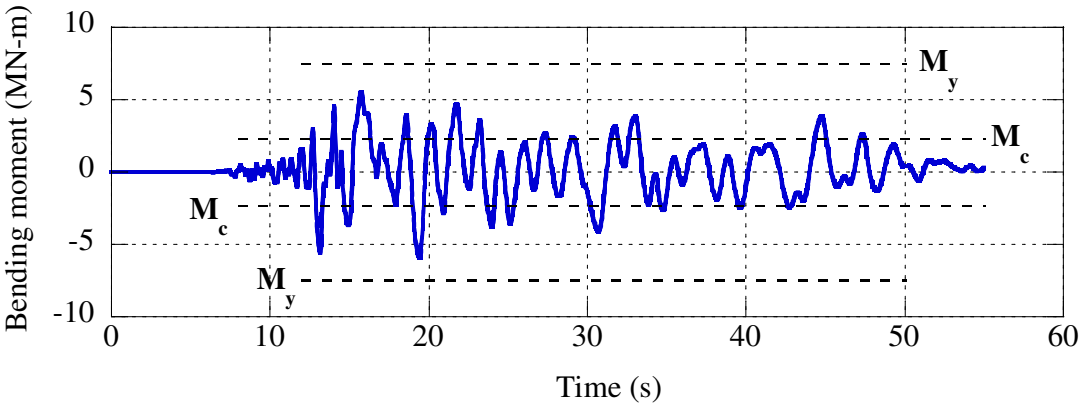

Figure 4.20 *Bending moment time history at the pile head calculated using the non-linear base layer model*

4.6.5 Performance levels

The preliminary design of the new piles was conducted following the Transit Bridge Manual which refers the designer to the earthquake loadings code NZS 1170.5. With regard to the high importance level of the bridge, the code requires that two serviceability limit states and

an ultimate limit state must be considered. These cases correspond to events with annual probabilities of exceedance of 1/25, 1/500 and 1/2500 years respectively. Using NZS 1170.5 the design peak ground accelerations for these cases were determined as 0.06g, 0.25g and 0.44g. The strengthened foundation was designed to achieve certain performance levels for each case; these are given in Table 4.3.

Table 4.3 Design performance philosophy for seismic cases

Case	Event	PGA (g)	Desired performance
SLS1	1/25yr	0.06	Minor, easily repairable damage, no traffic disruption
SLS2	1/500yr	0.25	Bridge passable for emergency services only, yielding of piles OK. Significant repairs needed before bridge reopens.
ULS	1/2500yr	0.44	With some repairs bridge is passable for emergency services, piles may approach ultimate capacity. Replacement might be necessary for long term.

With this in mind three analysis cases were conducted to analyse the performance of the central pier in the three events described above. These events were modelled using the numerical model described above but with the peak ground acceleration scaled to 0.06g, 0.25g and 0.44g. Figure 4.21 shows the results of the three analysis cases, it can be seen that both the ground and pile responses are very small for the SLS1 case and the pile bending moment is well below the cracking moment of the new piles. The SLS2 and ULS cases have much larger ground displacements and bending moments however in both cases the bending moment does not reach the yield level, indicating that the new piles of the central pier satisfy the performance objectives identified in Table 4.3.

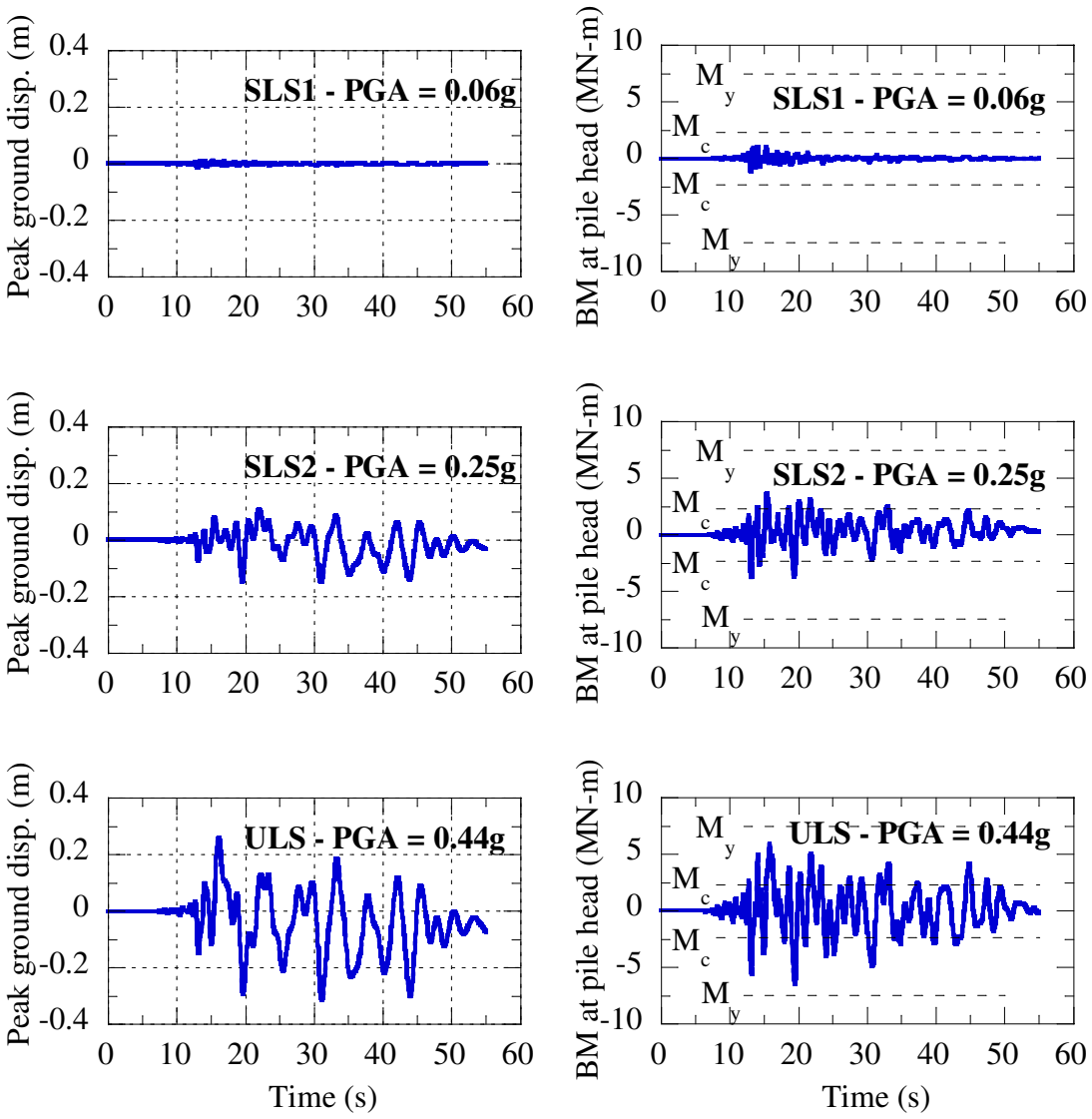

Figure 4.21 Time histories of peak ground displacement and bending moment at the pile head for three seismic cases corresponding to peak ground accelerations of 0.06g, 0.25g and 0.44g

Thus the effective stress analysis methodology is able to give a performance based assessment of the likely bridge performance at different levels of ground motion intensity. Such detailed results are only possible using an advanced analysis, and provide detailed and comprehensive information on the pile response.

4.7 Comparison with pseudo – static analysis

4.7.1 Free field

It is interesting to compare the results of the effective stress analysis with those obtained using a more conventional pseudo-static approach. In the latter approach, as described in Chapter 3, the complex dynamic forces are approximated by two static loads. Kinematic loads from the soil movement are applied through free-field ground displacements acting on a series of soil springs. In addition, inertial loads from the superstructure are modelled with a lateral force applied to the pile head. The stiffness of the soil springs, ultimate pressure from the soil and the free field ground displacement are calculated using simple empirical methods based on SPT blow counts.

Figure 4.22 compares the free field ground response predicted by the effective stress analysis to that predicted by the simplified empirical method for cyclic shaking cases described in Chapter 3. In Figure 4.22a, the maximum cyclic shear strains from the effective stress analysis are compared to the values obtained from a simple correlation with SPT blow count (Tokimatsu and Asaka 1998). In the simplified procedure, the free field ground displacement that is applied to the pile is calculated by integrating the shear strains throughout the soil profile. Figure 4.22b shows that this approach is conservative when compared to the more rigorous effective stress analysis, predicting a much larger displacement at the pile head. In the effective stress analysis, large strains only occur in the mid liquefied layer with N_1=10, so most of the ground deformation occurs in this layer. The simplified procedure is unable to capture these complex characteristics of the response.

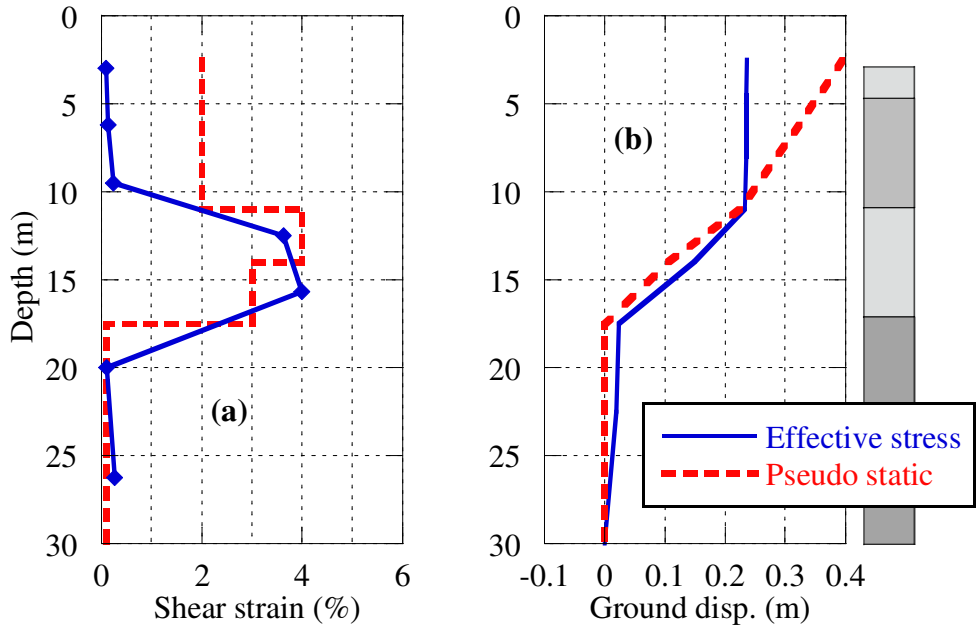

Figure 4.22 Comparison between the free field ground response calculated from the effective stress and psuedo static methods; (a) maximum cyclic shear strain, (b) ground displacement

4.7.2 Pile response

Due to the uncertainty regarding the stiffness of liquefied soils, two simplified analyses were performed using different stiffness for the liquefied soil using a degradation factor of 1/20, and 1/50 respectively. Both analyses used an inertial load corresponding to 0.44g ground acceleration.

The pile behaviour predicted by both simplified analysis cases (dashed lines) and the effective stress analysis (solid lines representing the two equivalent linear cases) is compared in Figure 4.23. The maximum bending moment distributions are compared in Figure 4.23a, and it can be seen that the distribution predicted by the effective stress analysis is similar to the pseudo static results. The bending moment at the interface between the liquefied and base soil layers is slightly lower, and the bending moment flattens out above the mid liquefied layer. In the pseudo-static analysis the base layer is rigid; this results in more of a contrast in stiffness between the liquefied and base layers and hence higher bending moment. The second observation is also expected as the effects of widespread liquefaction occurring in the mid layer before the layers above cannot be captured in the pseudo static analysis.

Figure 4.23b shows that the pile displacement profile is different between the two methods. The pile is more flexible at the base in the effective stress analysis, due to the different modelling of the base layer as described above. The displacement at the pile head predicted

by the pseudo static analysis varies considerably as the stiffness of the liquefied soil is varied. The more rigorous effective stress analysis predicts a displacement in between the upper and lower bounds predicted in the simplified analysis. By and large, the results of the effective stress analysis and pseudo-static analysis are in good agreement and consistent with the assumptions made and details of modelling.

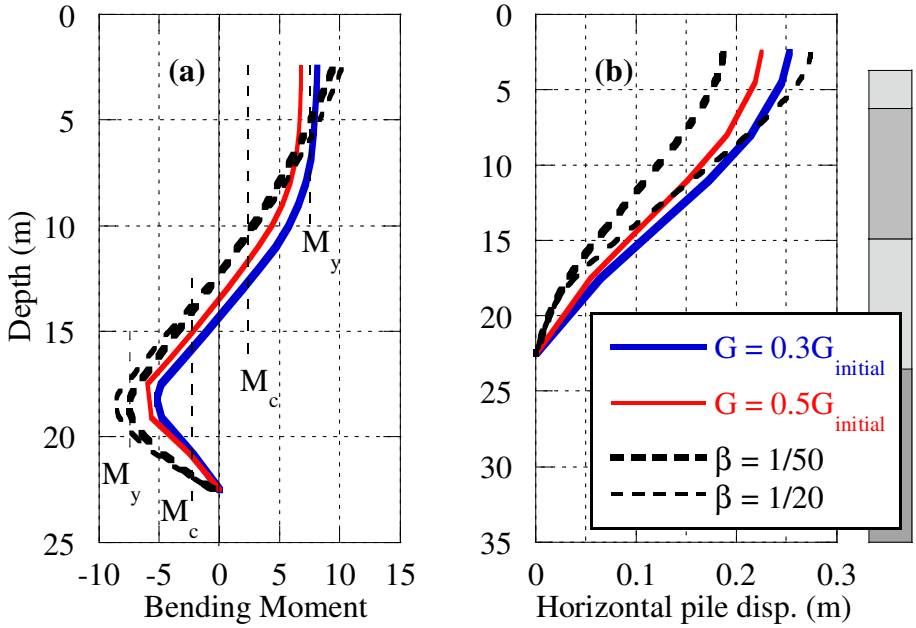

Figure 4.23 *Comparison of pile behaviour between the two methods; (a) maximum bending moment distribution. (b) maximum pile displacement*

4.8 Conclusions

An advanced dynamic analysis based on the effective stress principle has been performed to evaluate the seismic performance of foundation piles of a bridge pier founded in liquefiable soils. This case study demonstrated the capability of the effective stress analysis to capture important features of the complex soil-pile interaction in liquefying soils including:

- Detailed development of excess pore water pressure through time and space including effects of soil density and complex interaction between intensity of shaking, pore pressures and associated ground deformation. Typical effects of liquefaction on the ground motion such as loss of high-frequency content and elongation of the period were also observed.

- The soil-pile interaction significantly affected both the response of the foundation soil and piles. The presence of piles increased the stiffness of the foundation soil and consequently reduced its deformability as compared to the free field ground. The peak ground displacements were about 18 cm and 28 cm in the soil in-between piles and the free field soil respectively.
- The seismic performance of piles was rigorously evaluated by taking into account the highly complex dynamic nature of loads and soil-pile interaction. The horizontal displacement of the piles reached about 18 cm and bending moments reached yield level at the top of the pile. Hence, the analysis provided very detailed information on the performance of the piles including development, variation and duration of loads and consequent damage level to piles.

For the above reasons, the advanced effective stress analysis is suitable for a rigorous evaluation of the seismic performance of pile foundations of important structures. It can explain complex features of the response and verify design assumptions, and hence, it provides confidence in the design of the piles.

5. 2-D modelling of 3-D effects

5.1 Introduction

Effective stress analysis techniques such as the method described in Chapter 4 can be formulated in two or three dimensions. The response of pile foundations in liquefied soil is clearly a three dimensional (3-D) problem; three dimensional effects arise from:

(a) The geometry of the soil-pile-structure system,

(b) Multi-directionality of earthquake motion, and

(c) The 3-D stress strain behaviour of soil.

Whilst full 3-D analysis methods are desirable, the application of these methods in practice is constrained by large computation demands, the high level of user knowledge and time required to set up the model and process the results. 2-D finite element simulations can give sufficient accuracy and have been verified by many studies; however it is difficult in 2-D models with stiff pile groups to model the effects of large lateral ground displacements typical of lateral spreading. For example, consider the case of a pile group embedded next to a quay wall or riverbank. In a conventional 2-D model the seaward soil is separated from the landward soil by a stiff pile group, thus large lateral ground displacements are unable to develop. Also, each pile in the group experiences the same ground displacement.

This chapter presents a modelling concept where the 2-D finite element method is extended by overlapping a secondary mesh layer to account for the effects of three-dimensional geometry. The concept is first applied to the simulation of the seismic performance of deep-soil-mixing walls; the concept is then extended to the more complex case of pile groups undergoing lateral spreading.

5.2 Modelling concept

5.2.1 Two layer mesh

Figure 5.1 shows three types of 2-D finite element models. Conventional 2-D plane models (Figure 5.1a) can be extended by adding an out-of-plane thickness (Figure 5.1b) to account for the width of the finite element mesh in the z- direction. Shown in Figure 5.1c is a two layer model; here the two layers of different stiffness are attached to each other. The combined thickness of the two layers sums to unity.

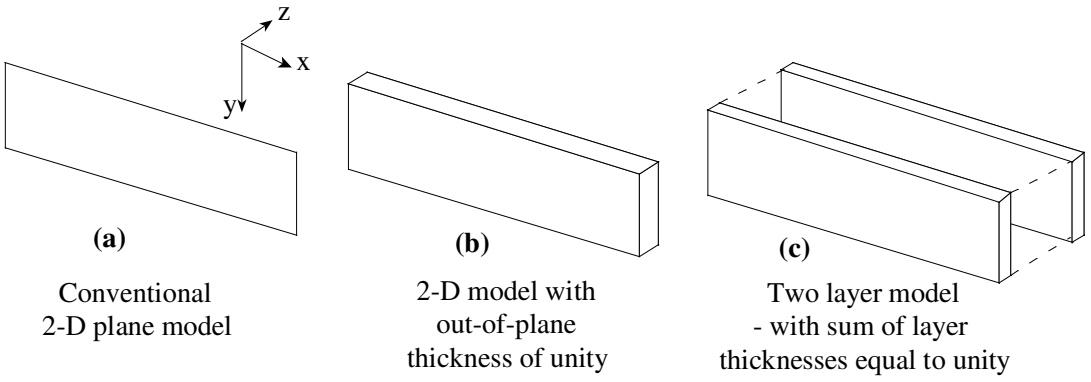

Figure 5.1 Finite element modelling techniques: (a) conventional plane model with no out-of-plane thickness, (b) one layer model with out-of plane thickness, (c) two layer model with layers of different thicknesses

It is proposed that by overlapping two 2-D finite element meshes, linked by appropriate boundary conditions, certain characteristics of 3-D behaviour can modelled. For example to model the lateral spread of liquefied soil past a pile group, a 2-D finite element mesh representing the pile group is overlain by another mesh representing the free field soil. The relative contributions of these two meshes can be controlled by altering the out-of-plane thicknesses of the two meshes. It was found that the most effective modelling technique was to model the stiffer layer (i.e. the layer containing the piles) as a secondary layer attached to a primary layer of free field soil. The most appropriate way to connect the two layers was by constraining the nodal displacements of the edges of the secondary layer to those of the corresponding nodes on the primary layer.

This is shown schematically in Figure 5.2 for a deep-soil-mixing (DSM) wall. Here the primary layer represents a cross section through the centre of the DSM-wall cell and the secondary layer represents the wall stiffness. The nodes of the two layers are connected on both sides and throughout the depth of the wall.

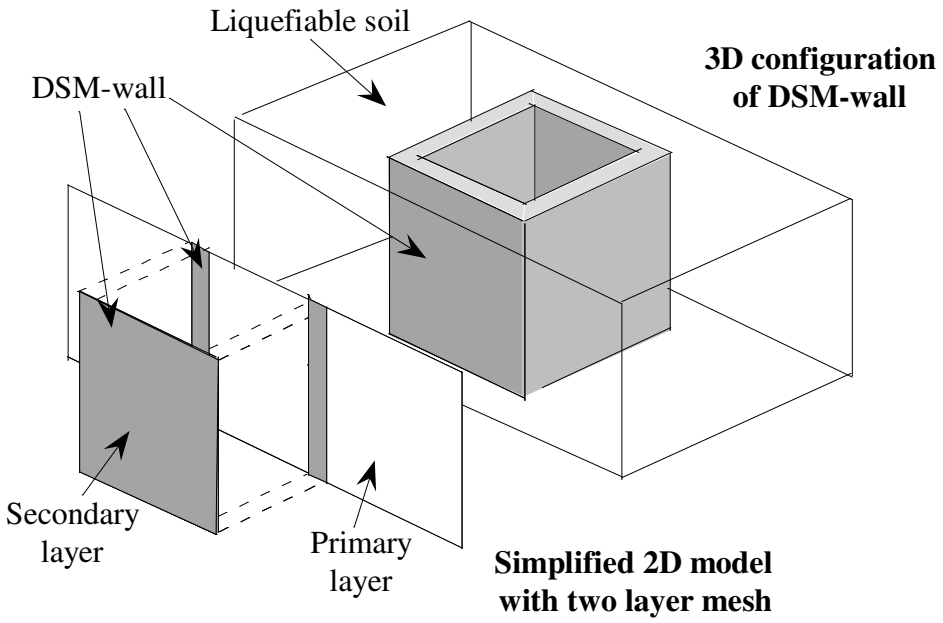

Figure 5.2 Simplified 2-D modelling of the 3-D configuration of a DSM-wall using a two layer mesh

5.2.2 Verification with simple model

To verify the modelling concept a simplified model was created of a point load on a cantilever beam. The model consisted of two layers of elastic solid elements, one layer has a stiffness of $k = EI$ and the other layer has a stiffness of $k = 2EI$. The layers were connected at both the fixed and free ends of the beam. A point load was applied at the free end; the magnitude of the load was kept at a constant value.

The out-of-plane thicknesses of the two layers were varied; this was done for three reasons:

- To verify that two layer meshes can be modelled successfully
- To verify that the total stiffness of a two layer model can be controlled by varying the out-of-plane thicknesses of the two layers
- To verify that the two layer model is consistent with an equivalent conventional one layer model

Figure 5.3 shows a plot of displacement calculated at the free end of the beam against the out of plane thickness of Layer No. 2, which has twice the stiffness of Layer No. 1. The y- axis is the displacement relative to the displacement of one layer model with a stiffness of $k = EI$. The thicknesses of the two layers were varied from zero to one; however the sum of the two thicknesses always summed to unity. For example when Layer No. 2 has thickness of 0.6

Layer No. 1 has a thickness of 0.4. The results of the two layer cases are plotted as points in Figure 5.3, these results are compared with a conventional one layer model (solid line) with an equivalent stiffness.

When the thickness of Layer No. 2 is 1.0 and the thickness of Layer No. 1 is 0, the relative displacement is 0.5. This is expected as the stiffness of the model has doubled. Figure 5.3 shows that the total stiffness of a two layer model can be appropriately modelled by changing the layer thickness. Note that both the one and two layers cases do not quite match the straight line predicted by theory. It is assumed that this is due to the relatively coarse finite element mesh.

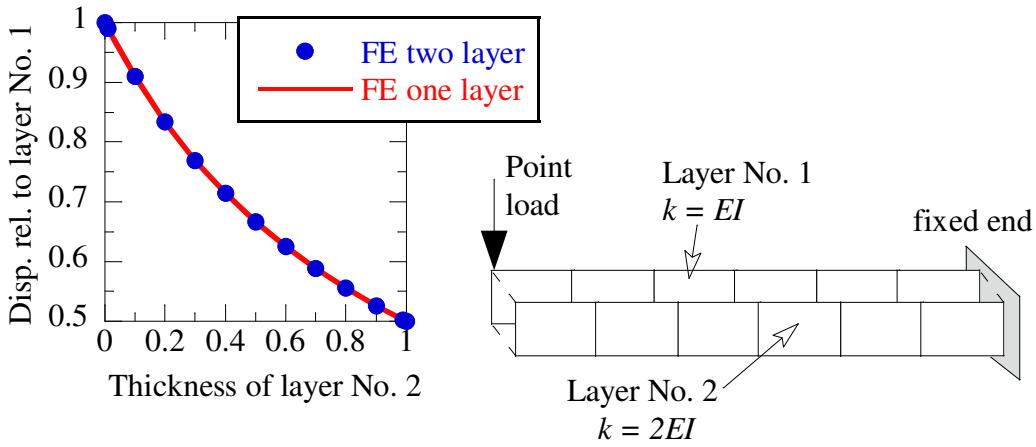

Figure 5.3 Comparison of theoretical and two layer cantilever beam results

5.2.3 Effect of layer thickness

The simplified method described above was extended to incorporate non-linear materials and more complicated loadings. A similar series of analyses were conducted on two layer models with varying thicknesses. The models consisted of a primary layer of liquefiable soil enclosed between two stiff elastic DSM-walls. A secondary layer consisting of a DSM wall was connected to each end of the model as shown in Figure 5.4b. Two different loading cases, shown in Figure 5.4c, were applied to the model. In the static case, a point load was applied at the top of the wall; the dynamic case was subjected to earthquake excitation.

Figure 5.4a shows how the calculated displacement of the model varies with the thickness of the secondary layer for both loading cases. The relative wall displacement is plotted on the y-axis. Here this represents the displacement at the top left node of the model divided by the

corresponding displacement of a model with the secondary layer only. The thickness of the secondary DSM-wall layer is plotted on the x- axis. It can be seen that both loading cases show similar trends and that as the thickness of the wall increases the wall displacement decreases. This indicates that the modelling concept can be applied to complex materials such as liquefiable soil and complex loadings such as earthquake excitation.

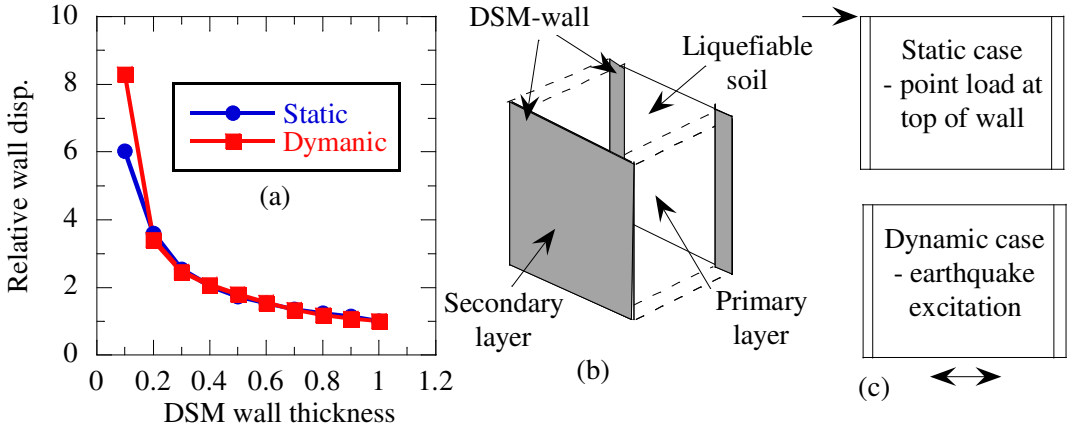

Figure 5.4 Relative displacement of wall as a function of DSM-wall thickness

5.3 Simulation of DSM walls

5.3.1 DSM walls

Deep-soil-mixing (DSM) is a ground improvement technique where cement is mixed *in situ* with native soil to increase its strength and stiffness. Typically a grid of DSM walls is created in the ground, constraining the development of shear strains in the enclosed liquefiable soil. This results in reduced pore pressures and ground displacements inside the enclosed soil. This method was successful in preventing liquefaction in the foundation soils of the Oriental Hotel during the 1995 Kobe earthquake (Porbaha et al. 1999).

The seismic response of DSM walls is dependent on the size and geometry of the enclosing cell. Therefore in the design of DSM walls it is necessary to consider these effects to determine the optimal layout and dimensions of the cells. The proposed two layer model is applied to a hypothetical model of DSM cell to examine how shortcomings in traditional 2-D analyses can be overcome. The two layer model is then used to examine the effects of cell size on the ground response.

5.3.2 Numerical model

Figure 5.5 shows the primary mesh layer of the 2-D numerical model used for a 10x10x10m DSM-wall cell (C-10). The soil profile consists of a non-liquefiable base layer of 6m thickness and a 10m thick upper layer of liquefiable saturated loose sand. The DSM-wall is modelled as a linear, elastic material with a shear modulus of G = 400MPa. The primary mesh layer consisting of the soil and two one-metre width walls is connected to a secondary DSM-wall layer, as indicated in Figure 5.2.

In addition to the C-10 case, analysis was also performed on smaller (5x5m) and larger (20x20m) DSM cells, referred to as C-5 and C-20 respectively. Plan views of all DSM wall configurations are shown in Figure 5.6. The C-5 model was analysed assuming a configuration of four cells joined together; this is considered more representative of a practical application of the DSM wall method. All three models are 16m deep, with 1m thick DSM-walls extending to a depth of 10m. The out-of-plane thicknesses of the two mesh layers were determined as a proportion of tributary area, i.e. for the C-10 case the secondary layer thickness was calculated as 0.167 (= 2m thickness of wall/12m width of enclosed soil plus wall thickness). The out-of-plane thicknesses of the model sum to unity, therefore where the two layers overlap the primary layer has an out-of-plane thickness of 0.833 in the C-10 case.

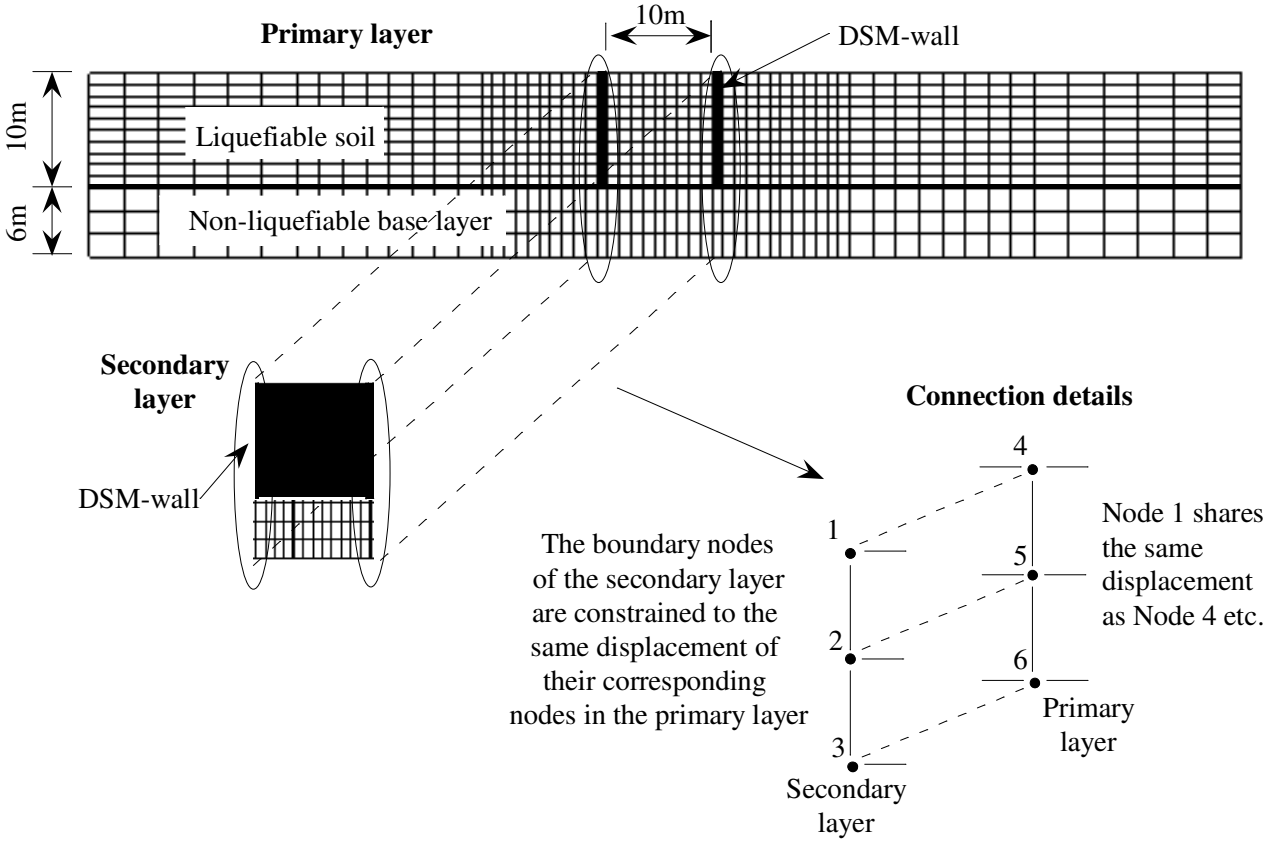

Figure 5.5 Numerical model used in the analysis for the C-10 case

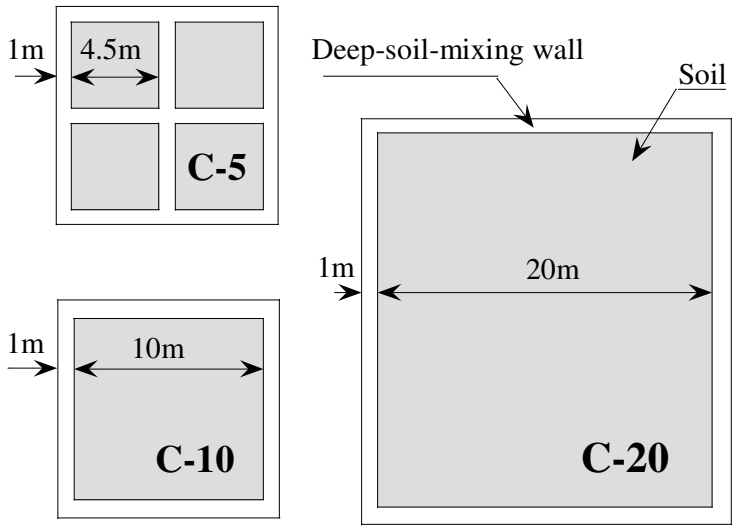

Figure 5.6 Plan view of the three DSM-wall models

The N-S accelerations recorded at 32m depth in a down-hole array at Port Island during the 1995 Kobe earthquake were used as input motion. The time history of this record is shown in Figure 5.7.

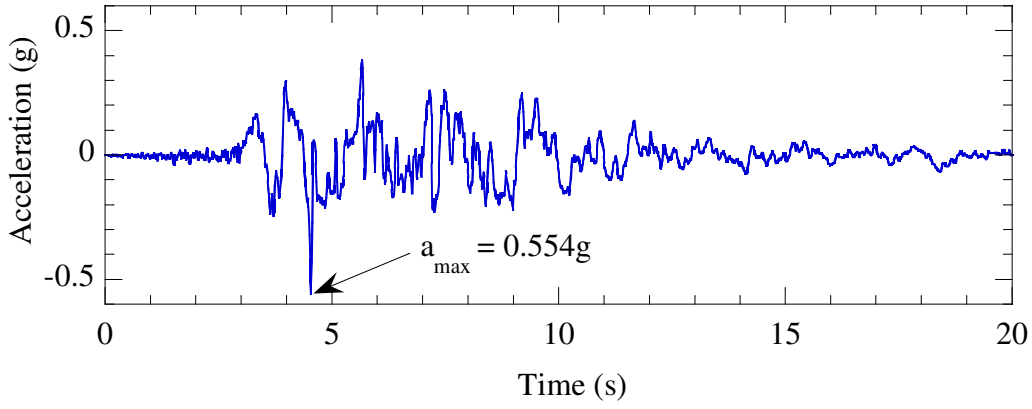

Figure 5.7 Base input motion used in the analysis

5.3.3 Comparison with conventional models

The goal of performing the two layer analysis is to be able to model 3-D effects of DSM-walls. With this in mind Figure 5.8 and Figure 5.9 compare the computed maximum pore pressure ratios, shear strains and ground displacements throughout the depth of the liquefiable soil for the one-layer (conventional) and two-layer cases respectively. The one-layer-mesh model is unable to capture the stiffening effects of the DSM cell, with the ground response in the middle of the cell nearly identical to that of the free field (unimproved) soil. Similar

results were obtained with the one-layer models of the C-5 and C-20 cases. The two-layer case shows a reduction in excess pore pressures and shear strains throughout the liquefied soil, this is reflected in significant reduction in ground displacement. Clearly the two-layer case is a more appropriate model to simulate the seismic response of the DSM-wall cell.

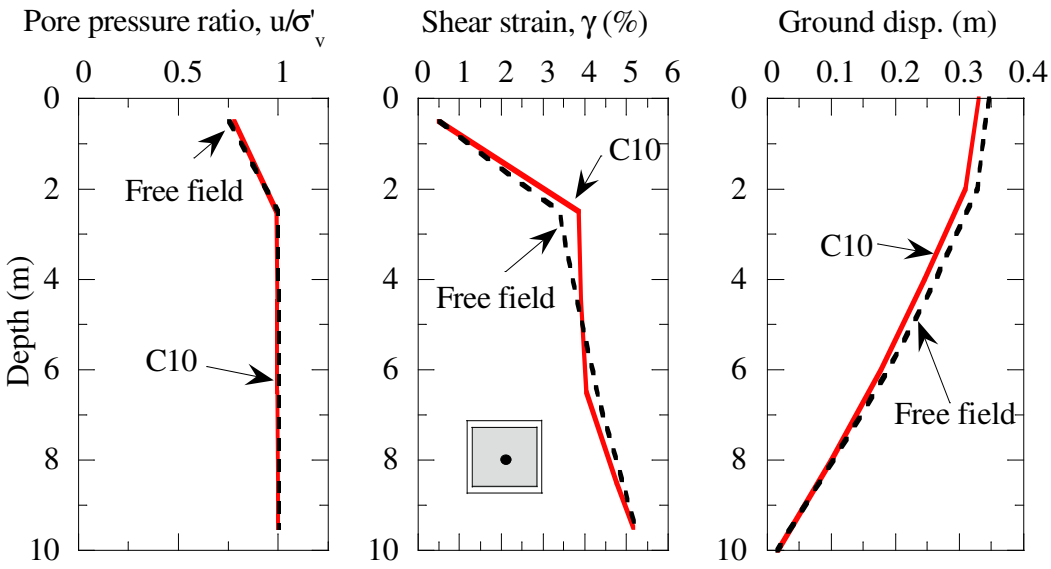

Figure 5.8 *Computed response of soil inside the C-10 DSM-wall using a single layer mesh (conventional 2D model)*

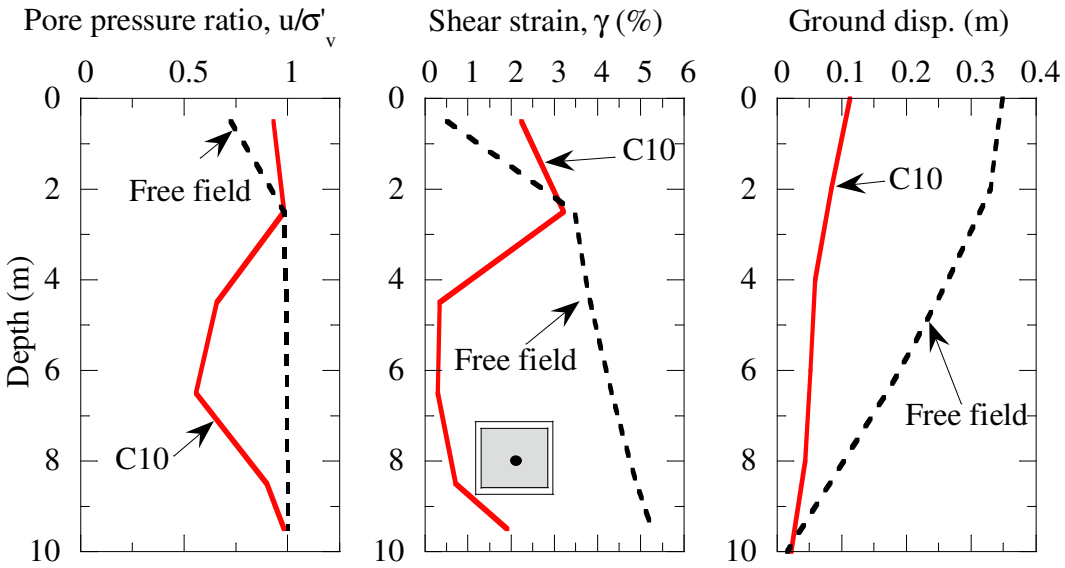

Figure 5.9 *Computed response of soil inside the C-10 DSM-wall using a double layer mesh*

5.3.4 3D geometry effects

The two-layer model was used to calculate the response of the soil enclosed in the C-5, C-10 and C-20 cases. The results indicate that the pore pressure build up and ground response depend strongly on the size of the DSM cell. The pore pressure build up calculated using the two-layer model for the three model configurations are shown in Figure 5.10, Figure 5.11 and Figure 5.12 for the C-5, C-10 and C-20 cases respectively. The dark colours show the development of liquefaction; it can be seen that the C-5 case the close spacing of the DSM-walls has reduced the excess pore pressures inside the cell, whereas liquefaction fully develops inside the C-20 cell. Figure 5.13 compares the excess pore pressure time histories at a depth of 6.5m for the three models. The soil in the largest cell, C-20, liquefies; however as the size of the cell decreases the excess pore pressure decreases due to the stiffening effects imposed by the walls.

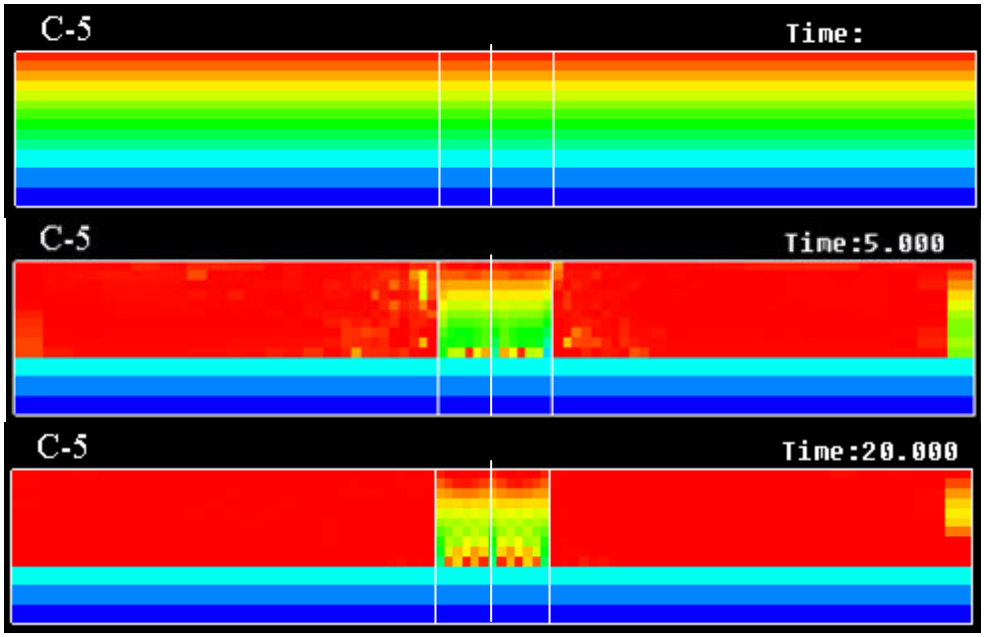

Figure 5.10 Development of liquefaction throughout C-5 the model illustrated by reduction in the mean effective stress p'

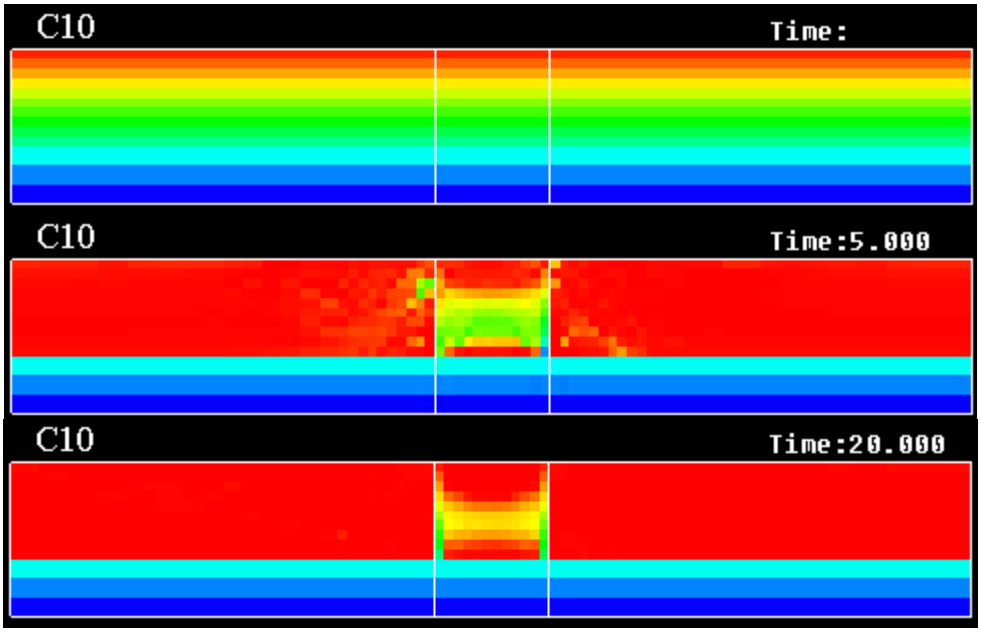

Figure 5.11 *Development of liquefaction throughout C-10 the model illustrated by reduction in the mean effective stress* p'

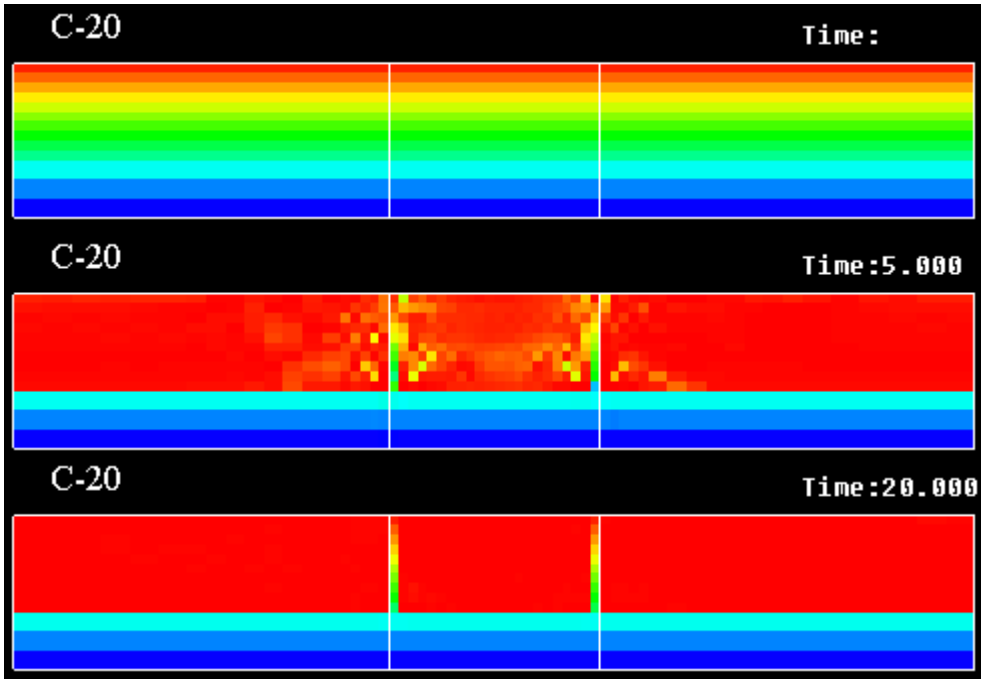

Figure 5.12 *Development of liquefaction throughout C-20 the model illustrated by reduction in the mean effective stress* p'

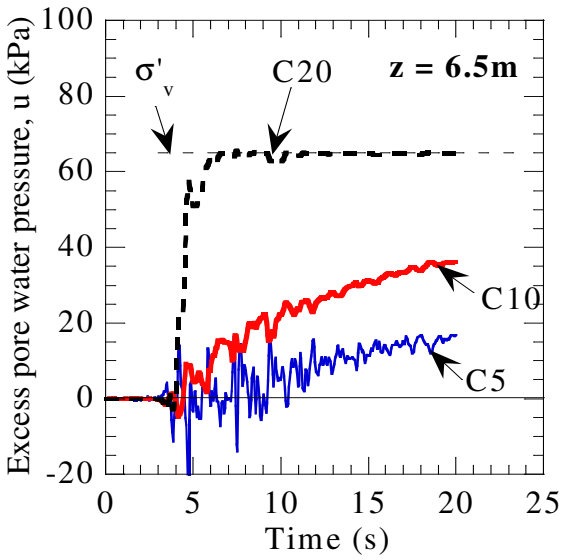

Figure 5.13 *Pore pressure time histories at 6.5m depth at the centre of the soil inside the DSM wall calculated using the two layer method*

Figure 5.14 shows the maximum values of pore pressure ratio, shear strain and ground displacement for the three models calculated using the two-layer model. The decrease in cell size and corresponding reduction in pore pressure result in lower shear strains and ground displacements. The C-5 case had the smallest ground displacement; here the pore pressure ratio was lower throughout the depth and the shear strains were practically zero throughout much of the depth. In the C-10 case liquefaction occurred in the top 3m of soil, below this depth the pore pressures were lower and the shear strains were much less. The C-20 case showed liquefaction to a depth of 10m, the shear strains were much higher than the C-5 and C-10 cases. It is interesting to note that the ground displacement of the C-20 case is significantly smaller than that of the free field, indicating that the large cell was successful in constraining the ground deformation despite the development of liquefaction. It should be noted that a relatively coarse mesh was used; in general a node spacing of 1m was used. For the C-5 case in particular this may have a large effect on the model stiffness, as there are only five soil elements in between the DSM-walls, with the two of those attached to the walls. This coarse mesh probably resulted in an under-prediction of the pore pressure build up and ground deformation.

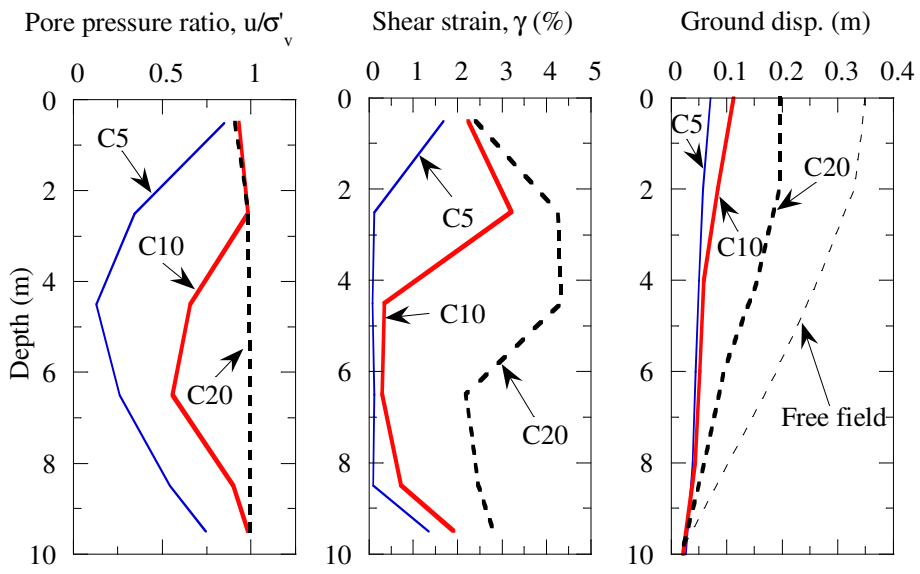

Figure 5.14 Maximum response along the centre line of the soil inside the DSM wall: (a) pore pressure ratios, (b) shear strains, (c) horizontal ground displacements

5.3.5 Effect of DSM-wall stiffness

The response of soil within the DSM cell is affected by both the geometry and the stiffness of the walls. To quantify the effects of wall stiffness Figure 5.15 shows the results of two analyses with two different values of shear modulus G. The C-10 case is analysed with the original G value of 400MPa and then with a value of G = 200MPa. It can be seen that the G = 200MPa model provides less of a stiffening effect than the G = 400MPa case with increases in pore pressure, shear strain and ground displacement. However the effects are relatively minor compared with the effects of reducing the size of the DSM cell.

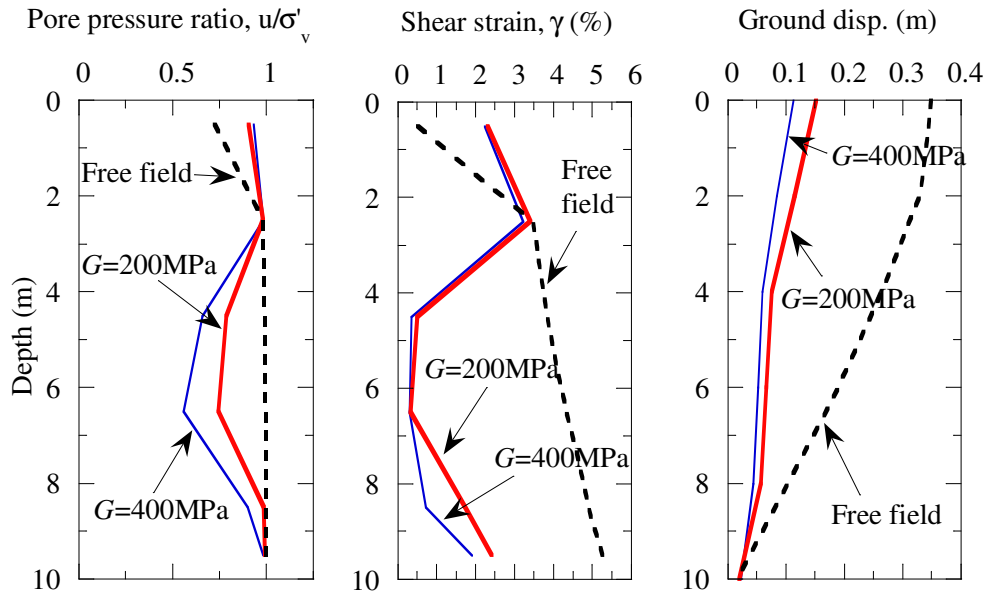

Figure 5.15 *Effect of changing the DSM-wall stiffness for the C10 analysis case*

5.3.6 Verification with 3D analysis and centrifuge tests

The trends observed using the two-layer 2-D analysis method are consistent with those observed in centrifuge tests and 3-D analysis. Figure 5.16 shows the maximum pore pressure ratio plotted against the length of the DSM-cell. This plot effectively shows the effects of size of the DSM-wall cell on the maximum pore pressure response. The results of the 3-D analysis (Cubrinovski et al. 2003), where a simplified 2-D formulation of the constitutive model was extended to a 3-D finite element mesh, are shown with the dashed lines and open points. The results of centrifuge tests (O'Rourke and Goh 1996) are shown by the shaded area. In general the trend observed with the 2-D two-layer analyses is consistent with both the more rigorous analysis and the experimental data. However the C-5 case predicts pore pressures slightly less than those observed in the experimental tests. This is possibly due to the coarse mesh used in the C-5 case.

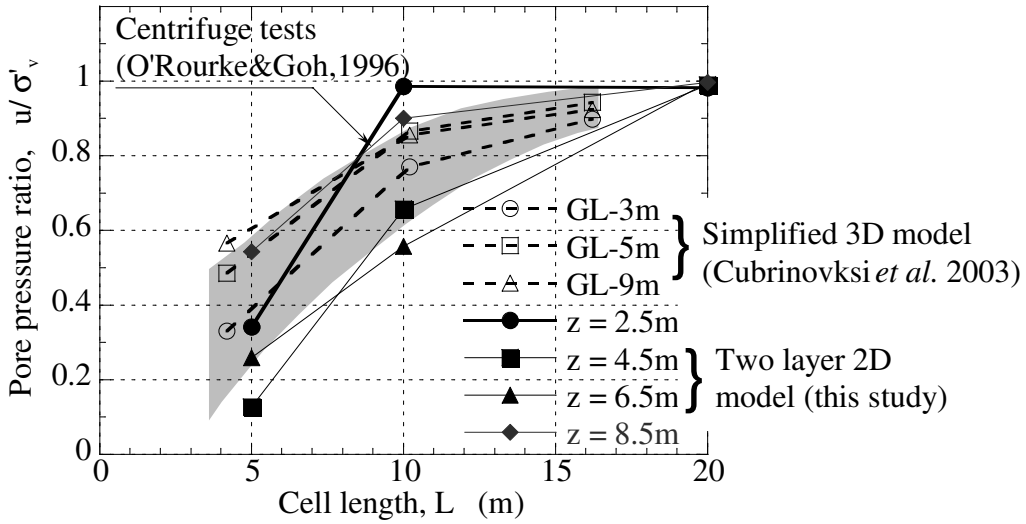

Figure 5.16 Effects of size of the DSM-wall cell on the maximum pore pressure response (solid lines) as compared to centrifuge tests (shaded area) and 3-D simulations (dashed lines)

5.4 Simulation of pile groups

Conventional 2-D finite element methods are unable to model certain 3-D geometrical issues present when analysing pile groups in liquefied soil. These issues include the flow of liquefied soil past stiff piles and the influence of pile location within a pile group. Here the two layer model is applied to address these issues; however unlike the DSM-wall models the interaction between the out-of-plane layer thickness and ground response is not straightforward in this case. A large scale shaking table experiment is simulated using the two-layer model to determine its effectiveness in modelling these issues.

5.4.1 PWRI experiment

Figure 5.17 shows the layout of large-scale shaking table experiment conducted at the Public Works Research Institute (PWRI) in Tsukuba, Japan. It consists of a 3x3 pile group embedded in a liquefiable sand deposit in the vicinity of a sheet pile wall representing a waterfront. The pile foundation consists of 9 steel piles arranged in a 3x3 group at 2.5*D* spacing. The piles were 1.45m long, 50.8mm in diameter, 1.5mm thick, had a flexural rigidity of EI=12.8kNm^2 and were fixed at the base and rigidly connected to a pile cap with a mass of 21.6kg. The sheet pile was a relatively rigid steel plate with a thickness of 6mm, it was free to move horizontally and fixed at the base.

The piles were embedded in a 1.8m thick sand deposit which had three distinct layers. A crust layer of coarse sand above the water table overlies a loose saturated layer of Toyoura sand with a relative density D_r = 35% and a base layer of dense Toyoura sand with D_r = 90%. The thicknesses of the three layers are 0.4m, 0.9m and 0.5m respectively. The submerged sand in front of the sheet pile wall is also loose Toyoura sand with D_r = 35%.

The model was built in a rigid container which was fixed at the bottom to the shake table. The model was shaken with a horizontal base excitation in the longitudinal direction (perpendicular to the wall). The shake table motion consisted of 20 uniform cycles with a frequency of 5 Hz and peak amplitude of 0.48g, as shown in Figure 5.18. A large number of accelerometers, pore pressure transducers and displacement gauges were used to measure the response of the piles and the ground. Pairs of strain gauges were installed at 12 locations along the length of the piles for measuring bending strains.

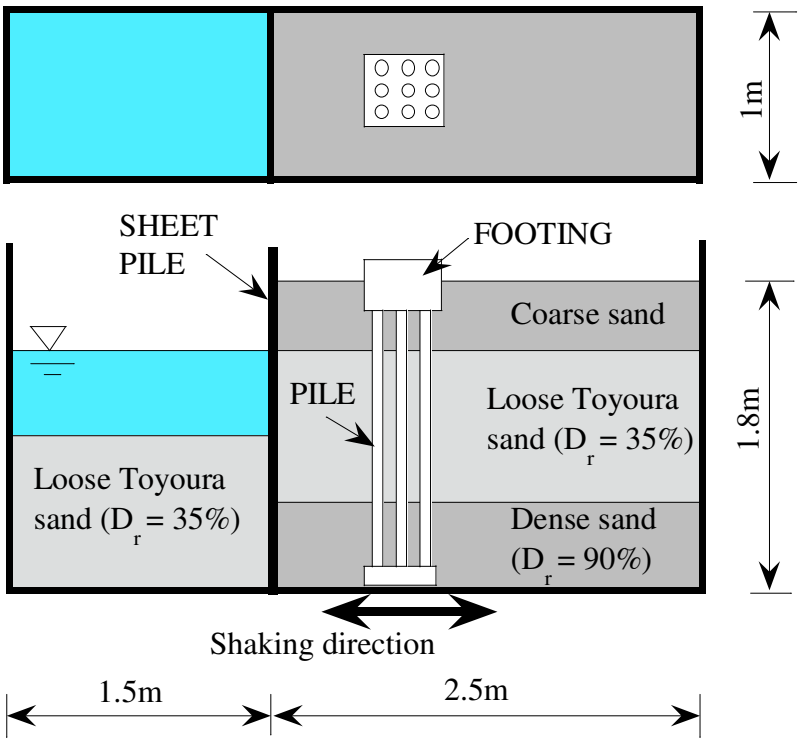

Figure 5.17 Schematic plot and plan and side view of the soil pile model used in the experiment (after Cubrinovski et al. 2005)

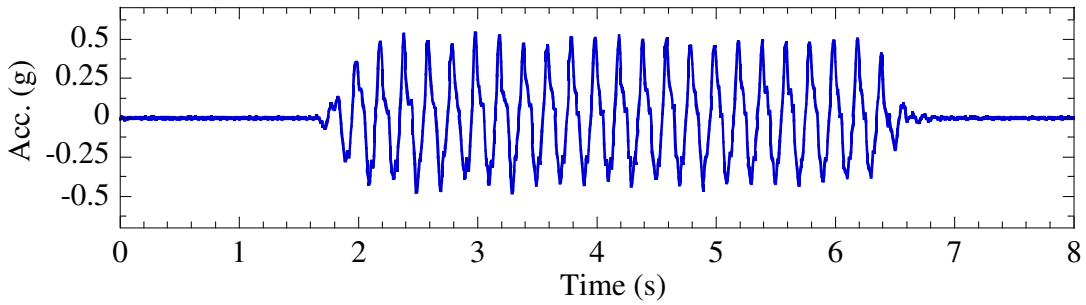

Figure 5.18 Horizontal accelerations recorded at the shake table

5.4.2 Experimental results

In the experiment liquefaction developed in the loose layers within the first few cycles of shaking. A large lateral movement of the sheet pile wall occurred, accompanied with spreading of the liquefied backfill soils. The lateral displacement of the sheet pile wall was about 380mm at the end of the shaking. Despite this large ground movement the piles showed stiff behaviour; the peak lateral displacement of the piles was 12mm during the cyclic shaking and 4mm at the end of the test.

5.4.3 Numerical analysis

Effective stress analyses simulating the experiment were conducted using both the one-layer and two-layer cases to determine the effectiveness of the two-layer model to model 3-D effects.

Material parameters

The soil was modelled as a two phase material using the stress density model as described in Chapter 4 used as a constitutive model. The elastic, state index and stress-strain material parameters for Toyoura sand given in Table 4.2 were used; however the dilatancy parameters of the model were determined by fitting the liquefaction resistance to specific tests at low confining pressure. Due to the scaled down nature of the experiment the effective overburden stress in the loose sand is in the range between 6kPa and 14kPa. Since low confining stresses are known to affect the liquefaction resistance of sands the dilatancy parameters were determined by simulating the liquefaction resistance observed in element tests conducted by Cubrinovski *et al*. (2005) on samples with low confining pressures (10-20kPa). The dilatancy parameters used for this model are given in Table 5.1.

The material parameters of the coarse sand surface layer sand were determined using the results of drained triaxial compression tests. The test conducted at the lowest confining stress (20kPa) was used as target curve in the evaluation of the model parameters. The piles were modelled as non-linear beam elements with a hyperbolic $M=\phi$ curve, and the footing and sheet pile wall were modelled as elastic solid elements.

Table 5.1 Dilatancy parameters for Toyoura sand determined from element tests on samples with low confining stress

Parameter	Symbol	Value
Dilatancy coefficient (small strains)	μ_0	0.20
Critical state stress ratio	M	0.60
Dilatancy strain	S_c	0.005

Initial stress state

When driving stresses are present in soil, lateral spreading may be triggered when the soil loses stiffness and strength due to liquefaction. The resistance of the liquefied soil is unable to resist the driving stresses and lateral spreading occurs. Therefore for lateral spreading analyses it is critical to consider the initial stress state of the soil.

During the soil deposition phase of the experimental model preparation the sheet pile wall was supported by horizontal struts. Prior to the shaking the struts were removed, subjecting the sheet pile wall to an unbalanced earth pressure from the backfill soil which caused lateral movement of the sheet pile wall towards the water. This caused a significant change of stress in the soil. An initial stress analysis was conducted that considered the two phases in the model preparation: first it was assumed that initially the soil underwent K_0-consolidation and the horizontal and vertical stresses were approximated as $\sigma'_v = \gamma h$ and $\sigma'_h = K_0\ \sigma'_v$ respectively, where it was assumed $K_0 = 0.5$ for the loose soil and $K_0 = 0.4$ for the crust and dense soil layers. Next, using the post consolidation stress states as initial states, a distributed lateral load representing the resultant earth pressure after removing the struts was applied to the sheet pile wall, as shown in Figure 5.19.

The results of the initial stress analysis showed that in the backfill soil a relaxation of the lateral stresses occurred, $K = \sigma'_h / \sigma'_v$ was mostly around 0.3 near the sheet pile wall and increased to about 0.5 away from the wall. The stress ratios in the submerged sand approached the passive state with K values from about 3 near the wall decreasing to 1 with distance from the wall. The horizontal shear stress ratios τ_{hv} / σ'_v were in the range 0.02 to 0.20. The calculated stresses were used as the initial stresses in the analysis.

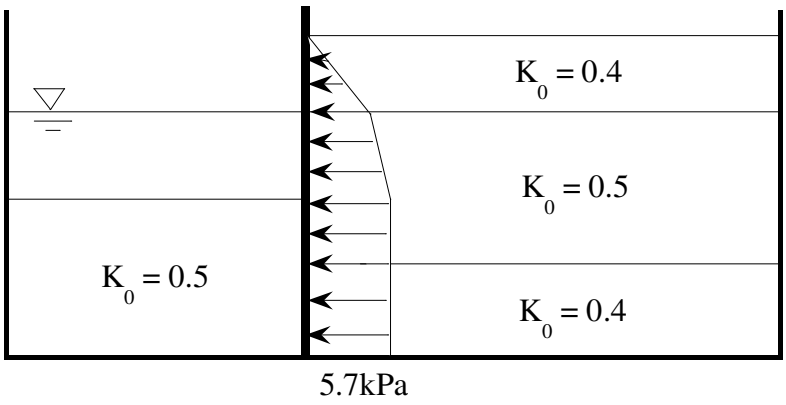

Figure 5.19 Illustration of the initial stress analysis showing the assumed K_o values for the post-consolidation stress and the applied lateral load simulating the resulting soil pressure induced upon removal of the struts (after Cubrinovski et al. 2005)

Finite element mesh

Figure 5.20 shows the finite element mesh used in the one-layer model, with the piles connected directly to the soil elements. Figure 5.21 shows the two finite element meshes used in the two-layer model, here the primary layer consists of the free field soil and sheet pile wall only. The secondary layer consists of the piles and soil elements next to the piles. It is connected to the primary layer by constraining the nodes of the edge of the secondary layer to have the same displacement as the corresponding nodes in the primary layer as shown in Figure 5.21.

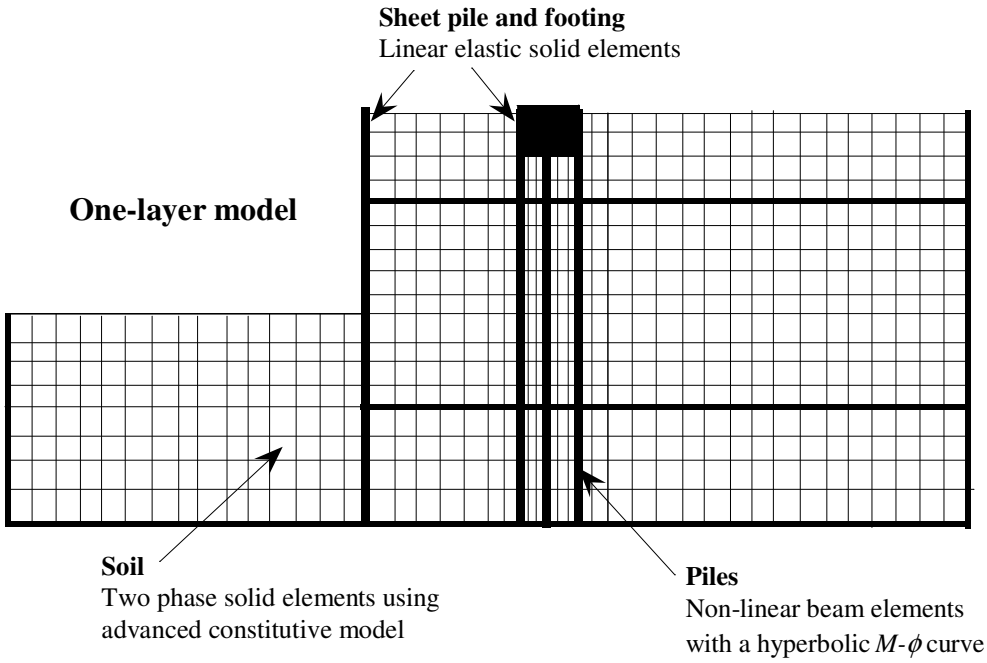

Figure 5.20 Finite element mesh used in the one-layer effective stress analysis

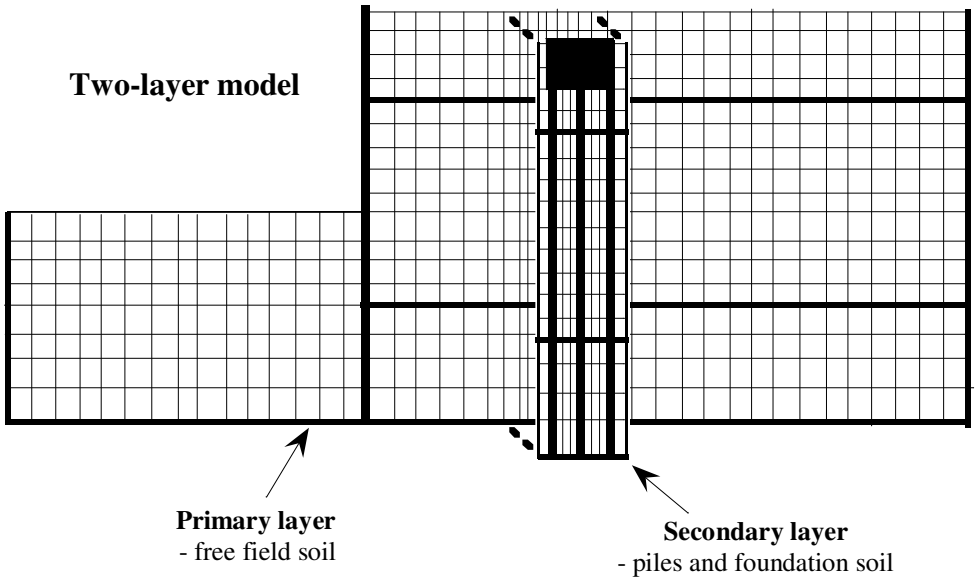

Figure 5.21 Finite element mesh used in the two-layer effective stress analysis

Dynamic properties

The duration of the analysis was 10 seconds; the response was calculated every 0.001 seconds giving 10000 calculation steps. The acceleration values were specified every 0.005 seconds,

linear interpolation was used for intermediate time steps. Rayleigh numerical damping was used with $\alpha = 0$ and $\beta = 0.005$ in the liquefiable soil.

5.4.4 Flow of soil past piles

Cubrinovski *et al.* (2005) performed both 2-D and 3-D simulations of this experiment. As expected the conventional 2-D analysis was unable to correctly model the flow of soil around the footing that was observed in the experiment. A conventional one layer 2-D analysis predicted a sheet pile wall displacement that was 75% less than that predicted using a 2-D free field analysis without the piles.

Figure 5.22a shows that in the one layer analysis the ground deformation only occurs on the waterfront side of the foundation, the soil behind the foundation is restrained by the stiffness of the piles and footing. The same soil displacement is applied to all three piles.

Also shown in Figure 5.22b is the result of a two layer 2-D analysis, where a secondary layer containing the foundation soil, three piles and the footing are connected to a free field layer. The secondary layer, which has a length slightly longer than the footing width, is connected to the primary layer by constraining the nodal displacements at the ends of the secondary layer with their corresponding nodes in the primary layer. The layers were connected on the both sides of the footing. The lateral sheet pile displacement predicted by the two layer 2-D analysis was twice that of the one layer model. Figure 5.22b shows that the lateral ground displacement starts to develop on the landward side of the pile foundation, this suggests that the two layer model can be useful in predicting the effects of different ground displacements on different sides of a pile group.

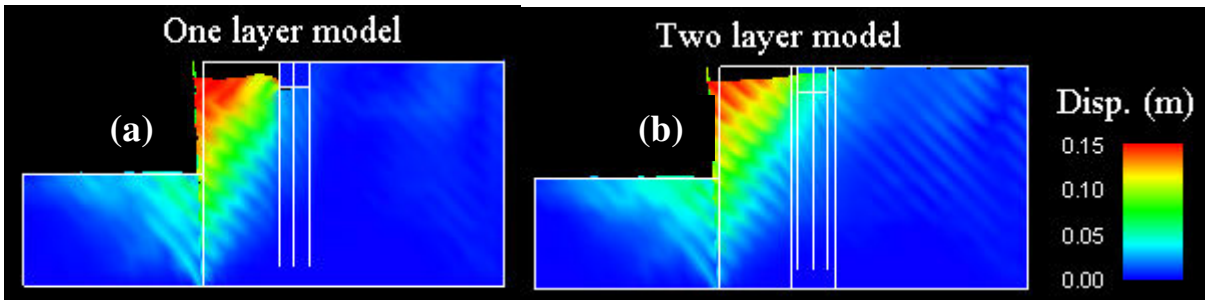

Figure 5.22 Deformation of one and two layer models

5.4.5 Pile groups

When analysing pile groups subjected to lateral spreading, determining the out-of-plane thicknesses of the two layers is not obvious. In general, three approaches can be considered, depending on the pile group geometry. The first approach considers the pile foundation and footing acting as a whole; the secondary layer thickness is calculated as the footing width B divided by the total width of the laminar box containing the soil and piles L. Each pile in the secondary layer was modelled having the stiffness of three piles. This approach is more appropriate for closely spaced piles where it is assumed that the piles and foundation soil act together as a block.

The second approach is to consider a single row of piles. Here the thickness of the secondary layer was calculated as the pile diameter D divided by the total width L. This approach is more appropriate for piles at larger spacing. Similarly a third approach can be used, which considers three rows of piles with a stiffness equivalent to three piles and a secondary layer thickness of $3D/L$.

Figure 5.23 shows the first two approaches applied to the simulation of the PWRI experiment. The calculated secondary layer thicknesses using the two approaches were B/L = 0.35m/1.0m = 0.35 and D/L = 0.05m/1.0m = 0.05. Figure 5.24 shows the peak bending moments computed using both two layer models with the different thicknesses. It can be seen that the two approaches yield very similar pile responses. Both approaches fit well with the bending moments observed in the experiment.

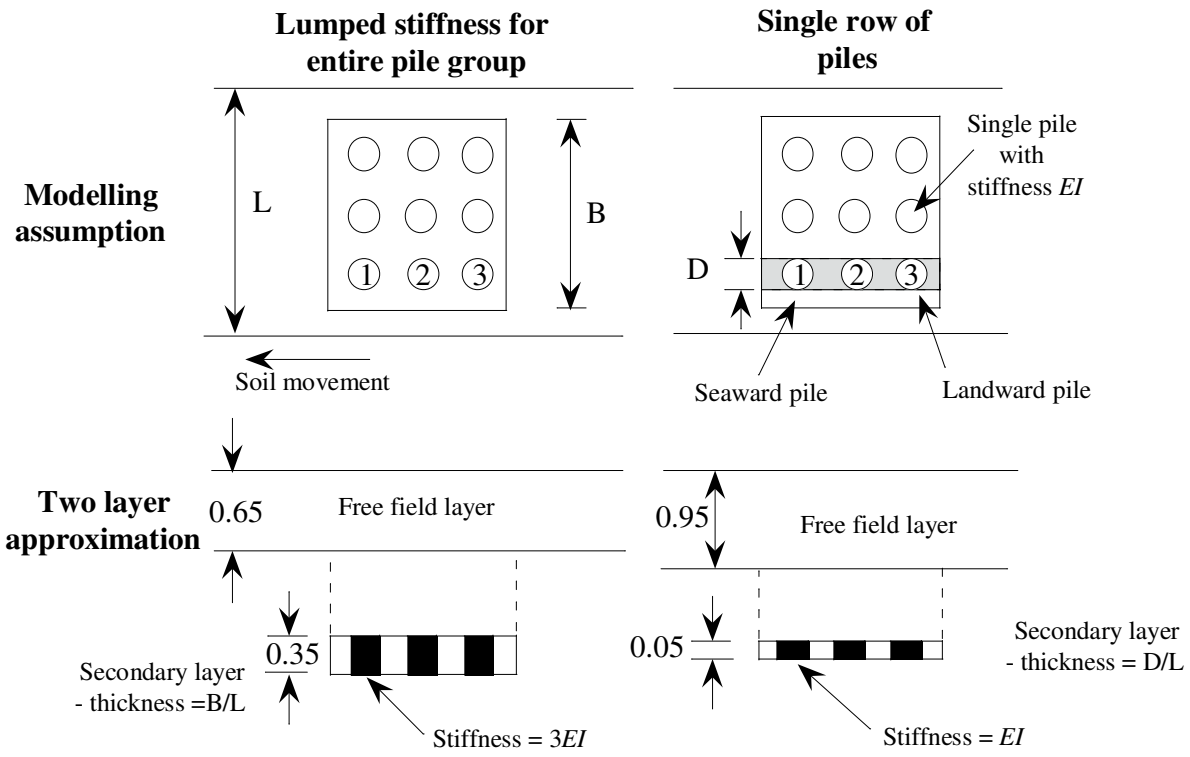

Figure 5.23 *Concepts for modelling pile groups using two layers*

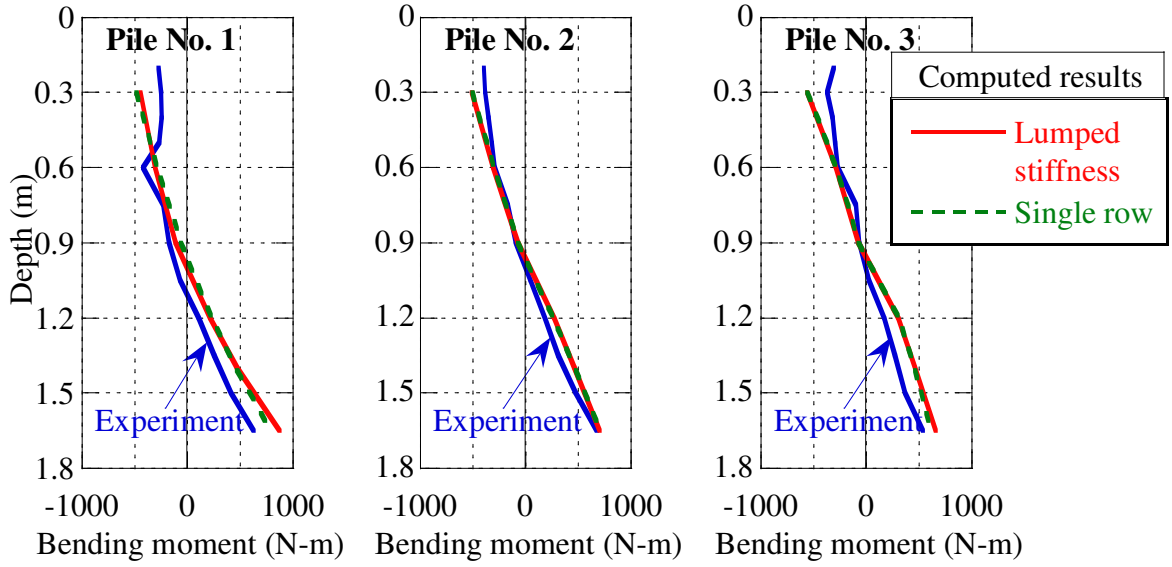

Figure 5.24 *Comparison of experimental and computed pile bending moments using both two layer modelling concepts*

5.4.6 Effect of pile location

It has been noted in previous earthquakes that for large pile groups contrasting deformation and damage characteristics were observed between the seaward piles and the landward piles, despite the piles having the same pile head displacement (Cubrinovski and Ishihara 2006; Tokimatsu et al. 1997). The differences can be explained by the different ground displacements on the seaward and landward sides and cross-interaction effects through the pile cap / foundation beams.

To examine whether the two layer modelling technique can model this phenomenon the finite element model described above was elongated by a factor of five in the x- direction (as shown in Figure 5.25. The model was lengthened to simulate two piles on either side of a large pile group in a case where the seaward piles near the sheet pile wall are subjected to a larger ground displacement than the landward piles. The soil deformation of the elongated model was similar to the simulations of the original model shown in Figure 5.22; however the larger distance between the piles increased the influence of the two layer model.

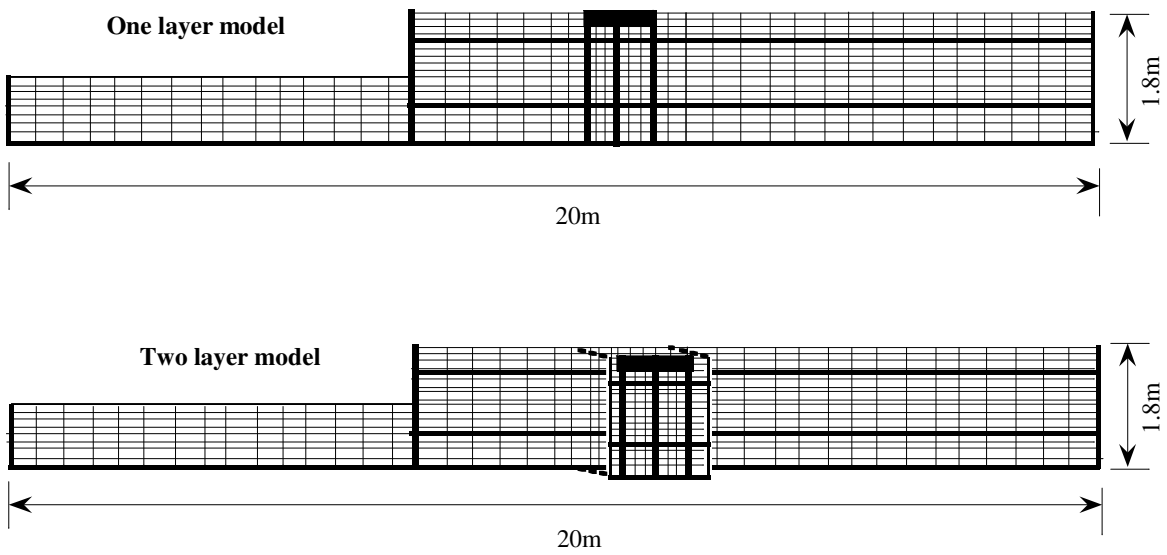

Figure 5.25 Finite element mesh for one and two layer cases of the elongated model

The computed pile responses are shown in Figure 5.26 and Figure 5.27 for the one layer and two layer mesh models respectively. In the one layer case the seaward pile (Pile No. 1) has the same displacement and bending moment as the landward pile (Pile No. 3). This is because the pile nodes are rigidly connected to the soil nodes; the soil must move with the pile. The stiffness of the piles and the footing result in the foundation moving as one block; all piles of the group experience the same soil displacement. The two layer case however shows some differences in the behaviour of the seaward and landward piles. The two piles are restrained to have the same deformation at the pile cap; however the seaward pile shows slightly larger displacement throughout its depth. This is because at the seaward pile the corresponding soil displacement in the free field layer is larger than at the landward pile. The change in pile deformation is reflected in the maximum pile bending moment distribution with depth. These results have been observed in case histories of damaged piles during recent earthquakes, as discussed in Chapter 2.

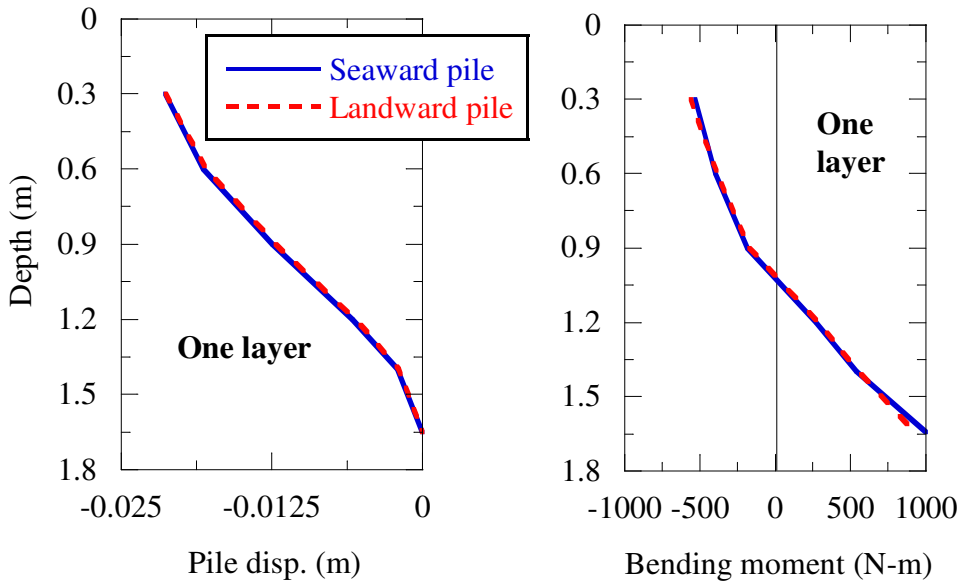

Figure 5.26 *Pile response for the elongated model using a single layer analysis; (a) peak lateral pile displacement, (b) peak bending moment*

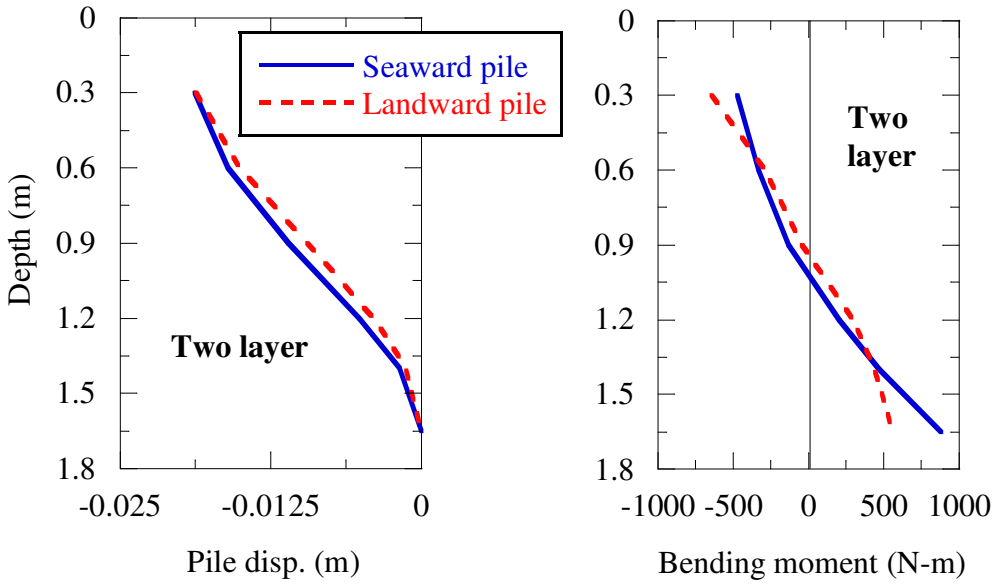

Figure 5.27 *Pile response for the elongated model using a double layer analysis; (a) peak lateral pile displacement, (b) peak pile bending moment*

5.5 Conclusions

In this chapter an extension of conventional two dimensional finite element methods used for the analysis of liquefaction problems has been presented. The theory and verification of the modelling technique has been described through consideration of simplified models. The method was able to successfully predict certain aspects of the three dimensional response of both DSM-walls and pile groups in liquefiable soil. Key conclusions include:

- The two-layer mesh method was able to successfully predict the stiffening effect of DSM-walls on the enclosed soil indicating effects on excess pore water pressure, development of shear strains and lateral ground displacements. The soil response inside the DSM-wall was shown to depend on the size of the DSM cell. Conventional (one-layer mesh) 2-D finite element methods are unable to model these features.
- The two-layer model predicted the same trends as those observed in centrifuge tests and 3-D analyses, indicating the validity of the modelling concept.
- To some extent the two layer model was able to consider the 3-D aspects of a pile group in laterally spreading soils that cannot be modelled using conventional models. The flow of soil past piles was better simulated using the two layer model than the conventional one layer model.

- This enabled the two layer model to consider the effects of pile location in a large pile group; differences in the response between landward and seaward piles were observed. These differences are consistent with case history observations and cannot be simulated using conventional one-layer models.

6. Concluding remarks

6.1 Summary

6.1.1 Pile behaviour

Investigations into the behaviour of pile foundations in liquefied soil observed in both case histories from previous earthquakes and from experimental studies using large scale shake tables and seismic centrifuges revealed the key features influencing pile response. It was found that the loads on piles during earthquakes arise from both soil displacement and inertial loads from the superstructure. The occurrence of liquefaction results in a degradation of soil stiffness and an increase in soil displacement. It was found that in liquefied soil two distinct phases occur in the pile response: a cyclic phase and a lateral spreading phase. For both cases the pile response depends on the pile stiffness, the stiffness and strength of the liquefied soil throughout the shaking, the level of fixity at both the head and tip of the pile, the interaction effects in pile groups and the presence of a non-liquefied crust layer. In general, the most severe damage occurred at the pile head and at interfaces between liquefied and non-liquefied soil.

6.1.2 Simplified analysis methods

Existing simplified analysis methods were reviewed; the most appropriate were *seismic displacement* methods. One such method was described in detail and applied to a case study of a bridge foundation. On this case study a parametric study was performed where the key parameters in the analysis, namely the stiffness and strength of the liquefied soil, the magnitude of the lateral ground displacement, the ultimate pressure from the crust load and the magnitude of inertial load, were varied to identify key features of the response. It was found that for stiff piles the choice of liquefied soil properties has a large effect on the response. Also, for stiff piles undergoing lateral spreading, it was found that a threshold ground displacement exists. Once this threshold value has been reached any further increases in ground displacement have no further effect on the pile response. Increasing loads at the pile head due to a combination of a non-liquefied crust layer and inertial loads leads to a transition from stiff to flexible pile behaviour.

6.1.3 Advanced analysis methods

Advanced, time history analysis methods were discussed in terms of theory and application. One technique, which used an advanced constitutive model for soil based on the state

concept, was described in detail and applied to the same case study. The analysis results gave detailed information on the free field ground response, including the effects of soil density and the interaction between shaking intensity, excess pore water pressure development and ground deformation. The performance of the piles was rigorously evaluated by taking into account the highly complex nature of the loads and soil – pile interaction.

6.1.4 Two layer finite element modelling

In order to improve the capabilities of 2-D finite element modelling, a new two-layer finite element analysis technique was presented. The two-layer method was applied to two cases: first the effects of deep-soil-mixing walls on liquefaction remediation were evaluated and then the simulation of pile groups in laterally spreading soil was considered. In both cases the new two-layer model was able to model features of the response that conventional one-layer models cannot. The simulation of the deep-soil-mixing walls showed a decrease in pore pressures and ground deformation inside a DSM cell, this decrease depended on the size of the cell and the analytical trends agreed with experimental results and more rigorous 3-D simulations. The simulation of the pile groups showed that the flow of soil past a pile group can be simulated using the two-layer model; conventional one-layer models are unable to do so. This enabled the two-layer model to predict different pile deformations depending on the location of a pile within a pile group.

6.2 Conclusions

The characteristics of damage to piles in liquefied soil during strong earthquakes have been identified through investigation of experimental tests on full-size shake tables and seismic centrifuges and back-calculations from well-documented case studies. The key damage features and factors influencing the pile response have been summarised.

Regarding seismic assessment of pile foundations in liquefied soil, two levels of assessment have been studied; a simplified design-orientated method and an advanced time history method. In the simplified method the effects of varying key parameters have been evaluated and summarised, this provides guidance to designers on how to choose these key parameters. Use of the described beam-spring analysis method is recommended in practice as it captures the key features of the response but is based upon readily available site investigation data. It is recommended that for the identified key parameters a range of values should be used in design. The description of the advanced effective stress analysis provides guidance its application to practice and illustrates its advantages and disadvantages when compared to

simplified analysis. It can be concluded that the effective stress analysis is appropriate for special or important structures and can be used to give an accurate, performance based assessment of pile response in liquefied soil.

Finally, a two-dimensional, two-layer finite element modelling technique was developed. This technique was successful in predicting three dimensional aspects of deep-soil-mixing walls and pile groups in liquefied soil. For cases where such aspects are important to the overall response of the foundation, this method is an alternative to the exhaustive demands of full 3-D analysis.

6.3 Recommendations for further research

To further develop simplified analysis methods more research is needed not on the modelling itself but in identifying the key parameters more accurately and providing better correlations of these parameters with *in-situ* site investigation data. Back-calculations of soil properties (such as β, p_{max} and S_U) from experimental tests and case histories are very valuable; such studies have been done previously but there is a need to consider data from all sources in a rigorous way using a consistent methodology. Similarly, the interaction between the kinematic loads from the ground displacement and inertial loads from the superstructure can be studied in greater detail. This can be conducted by calculated back-calculating the loads from experimental tests or by using advanced time history analysis; information on the phasing and magnitude of these loads would be of great benefit.

In order to provide more guidance on the application of effective stress analysis to practice, more case studies need to be considered. For these case studies, detailed laboratory tests should be conducted on the soil to obtain the model parameters more accurately. The two-layer model should be further verified using experimental tests and case histories.

References

Abdoun, T., and Dobry, R. (2002). "Evaluation of pile foundation response to lateral spreading." *Soil Dynamics and Earthquake Engineering*, 22(9-12), 1051-1058.

Abdoun, T., Dobry, R., Zimmie, T. F., and Zeghal, M. (2005). "Centrifuge research of countermeasures to protect pile foundations against liquefaction-induced lateral spreading." *Journal of Earthquake Engineering*, 9(SPEC. ISS.), 105-125.

Architectural Institute of Japan. (2001). *Recommendations for the Design of Building Foundations*.

Arulanandan, K., and Scott, R. F. (1994). *Verification of numerical procedures for the analysis of soil liquefaction problems*, A. A. Balkema, Rotterdam.

Berrill, J., and Yasuda, S. (2002). "Liquefaction and piled foundations: Some issues." *Journal of Earthquake Engineering*, 6(SPEC. ISS. 1), 1-41.

Berrill, J. B., Christensen, S. A., Keenan, R. P., Okada, W., and Pettinga, J. R. (2001). "Case study of lateral spreading forces on a piled foundation." *Geotechnique*, 51(6), 501-517.

Bhattacharya, S., Madabhushi, S. P. G., and Bolton, M. D. (2004). "An alternative mechanism of pile failure in liquefiable deposits during earthquakes." *Geotechnique*, 54(3), 203-213.

Biot, M. A. (1962). "Mechanics of deformation and acoustic propagation in porous media." *Journal of Applied Physics*, 33, 1482-1492.

Boulanger, R. W., Wilson, D. W., Kutter, B. L., Brandenberg, S. J., and Chang, D. (2004). "Nonlinear FE analyses of soil-pile interaction in liquefying sand." *ASCE Geotechnical Special Publication 126*, 403-410.

Brandenberg, S. J., Boulanger, R. W., Kutter, B. L., and Chang, D. (2005). "Behavior of pile foundations in laterally spreading ground during centrifuge tests." *Journal of Geotechnical and Geoenvironmental Engineering*, 131(11), 1378-1391.

Chang, D., Boulanger, R. W., Brandenberg, S. J., and Kutter, B. L. (2005). "Dynamic analysis of soil-pile-structure interaction in laterally spreading ground during earthquake shaking." *ASCE Geotechnical Special Publication 145*, pp 218-229.

Cubrinovski, M., and Ishihara, K. (1998a). "Modelling of sand behaviour based on state concept." *Soils and Foundations*, 38(3), 115-127.

Cubrinovski, M., and Ishihara, K. (1998b). "State concept and modified elastoplasticity for sand modelling." *Soils and Foundations*, 38(4), 213-225.

Cubrinovski, M., and Ishihara, K. (1999). "Empirical correlation between SPT N-value and relative density for sandy soils." *Soils and Foundations*, 39(5), 61-71.

Cubrinovski, M., and Ishihara, K. (2004). "Simplifed method for analysis of piles undergoing lateral spreading in liquefied soils." *Soils and Foundations*, 44(5), 119-133.

Cubrinovski, M., and Ishihara, K. (2006). "Assessment of pile group response to lateral spreading by single pile analysis." *ASCE Geotechnical Special Publication 145*, 242-254.

Cubrinovski, M., Ishihara, K., and Furukawazono, K. (1999). "Analysis of full-scale tests on piles in deposits subjected to liquefaction." *Second International Conference on Earthquake Geotechnical Engineering*, 567-572.

Cubrinovski, M., Ishihara, K., and Kijima, T. (2001). "Effects of liquefaction on seismic response of a storage tank on pile foundations." *Fourth International Conference on Recent Advances in Geotechnical Earthquake Engineering and Soil Dynamics*.

Cubrinovski, M., Ishihara, K., and Poulos, H. (2006a). "Psuedo static analysis of piles subjected to lateral spreading." *NZ Workshop on Geotechnical Engineering*, Christchurch 2006, pp337-350.

Cubrinovski, M., Ishihara, K., and Shibayama, T. (2003). "Seismic 3-D effective stress analysis: constitutive modelling and application." *Proc. 3rd Int. Conf. Deformation Characteristics of Geomaterials*, S-Lyon-03.

Cubrinovski, M., Ishihara, K., and Tanizawa. (1996). "Numerical simulation of Kobe Port Island liquefaction." *11th World Conference on Earthquake Engineering*, Acapulco, Mexico (Paper No. 330).

Cubrinovski, M., Kokusho, T., and Ishihara, K. (2006b). "Interpretation from large-scale shake table tests on piles undergoing lateral spreading in liquefied soils." *Soils Dynamics and Earthquake Engineering*, Vol. 26, 275-286.

Cubrinovski, M., Sugita, H., Tokimatsu, K., Sato, M., Ishihara, K., Tsukamoto, Y., and Kamata, T. (2005). "3-D Numerical simulation of shake-table tests on piles subjected to lateral spreading." *Proc. TC4 Satellite Conf. on Recent Developments in Earthquake Geotechnical Engineering*.

Dowrick, D. J., Berryman, K. R., McVerry, G. H., and Zhao, J. X. (1998). "Earthquake hazard in Christchurch." *Bulletin of the New Zealand National Society for Earthquake Engineering*, 31(1), 1-22.

Finn, W. D. L., and Fujita, N. (2002). "Piles in liquefiable soils: Seismic analysis and design issues." *Soil Dynamics and Earthquake Engineering*, 22(9-12), 731-742.

Fujii, S., Cubrinovski, M., Tokimatsu, K., and Hayashi, T. (1998). "Analyses of damaged and undamaged pile foundations in liquefied soils during the 1995 Kobe Earthquake." *Geotechnical Special Publication*, 2, 1187-1198.

Hamada, M., and O'Rourke, T. D. (1992). "Case studies of liquefaction and lifeline performance during past earthquakes." M. Hamada and T. D. O'Rourke, eds., National Center for Earthquake Engineering Research, Buffalo, NY.

Horikoshi, K., Tateishi, A., and Ohtsu, H. (2000). "Detailed Investigation of piles damaged by Hyogoken Nambu Earthquake." *12th World Conference on Earthquake Engineering*, CD ROM Paper No. 2477.

Howard, M., Nicol, A., Campbell, L., and Pettinga, J. (2005). "Holocene paleoearthquakes on the strike-slip Porters Pass Fault, Canterbury, New Zealand." *New Zealand Journal of Geology and Geophysics*, 48, 59-74.

Idriss, I. M., and Boulanger, R. W. (2007). "SPT- and CPT-Based Relationships for The Residual Shear Strength of Liquefied Soils." *4th International Conference on Earthquake Geotechnical Engineering - Invited Lectures*.

Ishihara, K., and Cubrinovski, M. (1998). "Performance of large-diameter piles subjected to lateral spreading of liquefied deposits." *13th Southeast Asian Geotechnical Conference*.

Ishihara, K., and Cubrinovski, M. (2004). "Case studies of pile foundations undergoing lateral spreading in liquefied deposits." *Fifth International Conference on Case Histories in Geotechnical Engineering*.

Ishihara, K., Yoshida, K., and Kato, M. (1997). "Characteristics of lateral spreading in liquefied deposits during the 1995 Hanshin-Awaji Earthquake." *Journal of Earthquake Engineering*, 1(1), 23-55.

Liao, S., and Whitman, R. V. (1986). "Overburden correction factors for SPT in sand." *Journal of Geotechnical Engineering - ASCE*, 112(3), 373-377.

Liyanapathirana, D. S., and Poulos, H. G. (2005). "Pseudostatic approach for seismic analysis of piles in liquefying soil." *Journal of Geotechnical and Geoenvironmental Engineering*, 131(12), 1480-1487.

O'Rourke, T. D., and Goh, S. H. (1996). "Reduction of liquefaction hazards by deep soil mixing." *NCEDE Workshop, Buffalo*.

O'Rourke, T. D., Meyersohn, W. D., Shiba, Y., and Chaudhuri, D. (1994). "Evaluation of pile response to liquefaction-induced lateral spread." Tech. Report NCEER-94-0026.

Oh-Oka, H., Onishi, K., Nanba, S., Mori, T., Ishikawa, K., Koyama, S., and Shimazu, S.-i. (1997). "Liquefaction induced failure of piles in the 1995 Kobe Earthquake." *Proceedings of the Third Kansai International Geotechnical Forum (KIG-Forum'97)*, pp.265-274.

Olson, S. M., and Stark, T. D. (2002). "Liquefied strength ratio from liquefaction flow failure case histories." *Canadian Geotechnical Journal*, 39(3), 629-647.

Orense, R., Ishihara, K., Yasuda, S., Morimoto, I., and Takagi, M. (2000). "Soil spring constants during lateral flow of liquefied ground." *12th World Conference on Earthquake Engineering*, CD ROM Paper No. 2099.

Pettinga, J., Yetton, M., Van Dissen, R. J., and Downes, G. (2001). "Earthquake source identification and characteristation for the Canterbury Region, South Island, New Zealand." *Bulletin of the New Zealand Society for Earthquake Engineering*, 34(4), 282-316.

Porbaha, A., Zen, K., and Kobayashi, M. (1999). "Deep mixing technology for liquefaction mitigation." *Journal of Infrastructure Systems*, 5(1), 21-34.

Seed, H. B. (1987). "Design problems in soil liquefaction." *Journal of Geotechnical Engineering - ASCE*, 113(8), 827-845.

Seed, R. B., and Harder, L. F. (1990). "SPT based analysis of cyclic pore pressure generation and undrained residual strength." *H. Bolton Seed Memorial Symposium Proceedings*, 2, pp 351-376.

Stirling, M., Pettinga, J., Berryman, K., and Yetton, M. (2001). "Probabilistic seismic hazard assessment of the Canterbury region, New Zealand." *Bulletin of the New Zealand Society for Earthquake Engineering*, 34(4), 318-334.

Tamura, S., Suzuki, Y., Tsuchiya, T., Fujii, S., and Kagawa, T. (2000). "Dynamic response and failure mechanisms of a pile foundation during soil liquefaction by shaking table test with a large-scale laminar shear box." *12th World Conference on Earthquake Engineering*, CD ROM Paper No. 0903.

Tokimatsu, K., and Asaka, Y. (1998). "Effects of liquefaction induced ground displacements on pile performance in the 1995 Hyogoken-Nambu Earthquake." *Soils and Foundations*(Special Issue), 163-177.

Tokimatsu, K., Oh-Oka, H., Shamoto, Y., Nakazawa, A., and Asaka, Y. (1997). "Failure and deformation modes of piles caused by liquefaction induced lateral spreading in the 1995 Hyogoken-Nambu Earthquake." *3rd Kansai Int. Geotech. Forum on Comparative Geotech. Engrg.*, pp. 239-248.

Tokimatsu, K., Suzuki, H., and Sato, M. (2005). "Effects of inertial and kinematic interaction on seismic behavior of pile with embedded foundation." *Soil Dynamics and Earthquake Engineering*, 25(7-10), 753-762.

Uchida, A., and Tokimatsu, K. (2006). "Comparison of current Japanese design specifications for pile foundations in liquefiable and laterally spreading ground." *ASCE Geotechnical Special Publication 145*, 61-70.

Uzuoka, R., Cubrinovski, M., Zhang, F., Yashima, A., and Oka, F. (2006). "Accuracy of prediction with effective stress analysis for liquefaction-induced earth pressure on a pile group." *New Zealand Workshop on Geotechnical Earthquake Engineering*, pp120-132.

Uzuoka, R., Sento, N., Kazama, M., Zhang, F., Yashima, A., and Oka, F. (2007). "Three-dimensional numerical simulation of earthquake damage to group-piles in a liquefied ground." *Soil Dynamics and Earthquake Engineering*, 27(5), 395-413.

Wang, S.-T., and Reese, L. C. (1998). "Design of pile foundations in liquefied soils." *ASCE Geotechnical Special Publication No. 75*, pp. 1331-1343.

Yasuda, S., and Berrill, J. B. (2000). "Observations of the earthquake response of foundations in soil profiles containing saturated sands." *GeoEng2000*.

Yasuda, S., Ishihara, K., Morimoto, I., Orense, R., Ikeda, M., and Tamura, S. (2000). "Large-scale shaking table tests on pile foundations in liquefied ground." *12th World Conference on Earthquake Engineering*, Paper No. 1474/5/A.

Yoshida, N., and Hamada, M. (1991). "Damage to foundation piles and deformation pattern of ground due to liquefaction induced permanent ground deformations." *Tech. Rep. NCEER 91-0001*, NCEER, Buffalo, N.Y.

Youd, T. L., Hansen, C. M., and Bartlett, S. F. (2002). "Revised multilinear regression equations for prediction of lateral spread displacement." *Journal of Geotechnical and Geoenvironmental Engineering*, 128(12), 1007-1017.

Youd, T. L., Idriss, I. M., Andrus, R. D., Arango, I., Castro, G., Christian, J. T., Dobry, R., Liam Finn, W. D., Harder L.F, Jr., Hynes, M. E., Ishihara, K., Koester, J. P., Liao, S. S. C., Marcuson Iii, W. F., Martin, G. R., Mitchell, J. K., Moriwaki, Y., Power, M. S., Robertson, P. K., Seed, R. B., and Stokoe Ii, K. H. (2001). "Liquefaction resistance of soils: Summary report from the 1996 NCEER and 1998 NCEER/NSF workshops on evaluation of liquefaction resistance of soils." *Journal of Geotechnical and Geoenvironmental Engineering*, 127(10), 817-833.

Zienkiewicz, O. C., and Shiomi, T. (1984). "Dynamic Behaviour of Saturated Porous Media: the Generalised Biot Formulation and its Numerical Solution." *International Journal for Numerical and Analytical Methods in Geomechanics*, 8(1), 71-96.